HIGH PRESSURE CRYOCOOLING
FOR MACROMOLECULAR CRYSTALLOGRAPHY

A Dissertation

Presented to the Faculty of the Graduate School

of Cornell University

In Partial Fulfillment of the Requirements for the Degree of

Doctor of Philosophy

by

Chae Un Kim

January 2008

HIGH PRESSURE CRYOCOOLING FOR MACROMOLECULAR CRYSTALLOGRAPHY

Chae Un Kim, Ph. D.

Cornell University 2008

A novel high-pressure cryocooling technique to reduce radiation damage in macromolecular crystallography is developed and explored. The method involves cooling macromolecular crystals to cryogenic temperatures (~ 77 K) in high pressure Helium gas (up to 200 MPa). Several different kinds of macromolecular crystals have been successfully high-pressure cryocooled and excellent crystal diffraction has been obtained without adding any penetrating cryoprotectants. This new method has great potential for structural biology and high-throughput crystallography.

This dissertation details technical aspects of high pressure cryocooling. Recent experimental results are presented, including crystal cryoprotection, extension of the method to Krypton/Xenon single-wavelength anomalous dispersion (SAD) phasing, capillary sample cryoprotection and native sulfur SAD phasing. Finally, a mechanism involving high density amorphous (HDA) ice is proposed to explain why the method works.

BIOGRAPHICAL SKETCH

Chae Un Kim was born on the August 18th, 1976 in Seoul, Korea. He graduated from Pusan Science High School and continued his education in Seoul National University (SNU) majoring in Physics. After achieving his B.S. degree in 1999, he spent 26 months in Korean Army as a medic. Then he entered biophysics program at Cornell University in 2002. After one-year rotation, he joined Prof. Sol M. Gruner's lab, where he studied high pressure cryocooling for macromolecular crystallography as a Ph.D. research project. Upon the completion of Ph.D. in 2007, he will continue his research in the Gruner lab as a postdoctoral research associate.

To my family for their love and support

ACKNOWLEDGMENTS

This work would not have been possible without the support of my research advisor, Professor Sol M. Gruner. His intriguing ideas always inspired me to pursue something new and his support and patience were essential to the completion of my graduate study. I thank all the Gruner group members including Mark W. Take, Marty Novak, Gil Toombes, Rafael Kapfer, Buz Barstow, Nozomi Ando, Yi-fan Chen and would like to show special thanks to Sang-Youn Park and Seong Anthony Kang from the Brian Crane lab for their kind help in my early study.

I thank the Cornell High Energy Synchrotron Source (CHESS) and Macromolecular Crystallography at CHESS (MacCHESS) staff and scientists for help and support. Their help and assistance were crucial for the high quality data collection and successful data analysis. I would like to especially thank Quan Hao and Qun Liu for their helpful advice and discussions on the macromolecular crystallographic phasing.

I am grateful for financial support from the US Department of Energy (grant DE-FG02-97ER62443), National Science Foundation (award DMR-0225180), and National Institutes of Health (RR-001646 & GM-074899)

Finally, I thank my loving parents. My parents have always been wonderful source of love, patience and encouragement. I am sincerely thankful for what they have done for me. Without them, all my academic accomplishments would not have been possible. I also thank my sister and brother for their encouragement.

TABLE OF CONTENTS

LIST OF TABLES

LIST OF FIGURES

CHAPTER ONE
INTRODUCTION

1.1 Radiation damage in X-ray crystallography

As of June 2007, approximately 85 % of the all deposited structures (37500 out of 44300) in Protein Data Bank were determined by X-ray crystallography. To understand the biochemical functions of a macromolecule, its three-dimensional structure solved by X-ray crystallography has played an essential role.

Since the beginning of macromolecular x-ray crystallography, radiation damage has been a major concern because it dramatically limits the useful information that can be obtained from a single crystal (Nave & Garman, 2005; Ravelli & Garman, 2006). The first X-ray damage study on the macromolecular crystal was reported by Blake and Phillips (1962). They carried out X-ray dose experiment on myoglobin at room temperature and concluded that the damage was proportional to absorbed dose (measured in Gray, Gy = J/kg): it was calculated that each 8 keV photon disrupted ~ 70 molecules and disordered another 90. More interestingly, they found that some reflections increased in intensity with X-ray exposure, indicating that there might be some specific sites of damage. Since then, numerous studies have been carried out to understand the effects of radiation damage on macromolecular crystals. The typical symptoms of radiation damage are several: (i) decrease in diffraction resolution, (ii) increase in temperature factor (Wilson B-factor) & unit cell volume and (iii) site-specific damage, such as the breakage of disulfide bonds.

The mechanism behind radiation damage is complex and involves both the primary and the secondary effects (Kmetko *et al*., 2006). The primary radiation damage involves inelastic scattering of an X-ray photon with an electron in the crystal and the photo-electric effect. Each photoelectron was estimated to produce up to 500

secondary lower energy electrons, which cause further damage. The secondary radiation damage involves thermal diffusion and subsequent reaction of atomic and molecular free radicals produced by X-ray radiation.

As long as X-rays are used, the primary damage cannot be avoided. However, it turned out that the secondary damage could be dramatically reduced or delayed if the crystal is kept under cryogenic conditions. When a protein crystal is properly cryocooled, the molecular motions of both the polypeptide chains and the solvent in the crystal are damped to below the glass transition and the diffusion of harmful free radicals is drastically reduced, allowing a typical 50–300 μm crystal to survive 10^2 - 10^3 higher doses during the X-ray diffraction data collection. For a crystal held at 77 K, the theoretical X-ray dose limit, where the crystal loses roughly half of its diffraction power, was estimated to be 2×10^7 Gy (Henderson, 1990), which is equivalent to about 2.5 years of X-ray exposure on a Cu rotating anode beamline.

1.2 Cryocrystallography

Owing to the prolonged lifetime of crystals held at cryogenic conditions, most of the macromolecular diffraction data are currently being collected at cryogenic temperatures.

Because protein crystals can have a high solvent content (average of ~ 50 %), cryocooling them to near 100 K requires particular techniques to avoid the formation of water crystalline ice (Garman & Owen, 2006). The extension of the small-molecule techniques to protein crystals by Hope (1988) facilitated a number of subsequent experimentation. Currently, a loop-mounting method, which was originally developed by Teng (1990), is most widely used. In the method, the crystal is first soaked in a cryo-solution containing cryoprotectants (antifreeze agents). The crystal is then scooped into a loop made of thin (~ 20 μm diameter) fiber (e.g. nylon). After that, it is

immediately flash-cooled by plunging into a cryogen such as gaseous nitrogen cold stream or liquid nitrogen at temperatures around 100 K or below.

During flash cooling, crystalline ice should be avoided because it yields spurious diffraction that obscures useful protein diffraction. The formation of amorphous ice, which requires exceedingly rapid temperature drops, is usually limited by the time it takes heat to diffuse out of a typical 50–300 μm diameter crystal (Kriminski *et al*., 2003). To facilitate amorphous ice formation, soaking crystals into cryo-solutions containing chemical cryoprotectants such as glycerol or polyethylene glycol is usually required (Garman & Schneider, 1997). Another problem with flash cooling is that even with fully amorphous ice, the differential volume changes of the mother liquor, protein, and unit cell upon cooling degrades or totally deteriorates the crystal diffraction (Kriminski *et al*., 2002; Juers & Matthews, 2004). A second important benefit of a properly chosen cryoprotectant is that it limits this volume-related damage.

However, it has been noticed that protein crystals are very often deteriorated by the chosen cryo-solution itself by either surface attack or osmotic shock. A number of chemicals often need to be tested at various concentrations in order to find suitable cryoprotectant conditions (Fig. 1.1), which can be a very time-consuming process. The best and easiest case is when the mother liquor already contains a high enough concentration of cryoprotecting agents for flash-cooling. But it has been observed that adding cryoprotectant sometimes dramatically affects protein crystallization, which makes crystallization difficult. Even in cases where a suitable cryoprotectant is found, care has to taken due to unwanted interactions between cryoprotectants and crystallization additives, ligands and substrates. For example, it was suggested that the ligand occupancy in the RCK domain of a K+ transporter was perturbed by the cryoprotectant additives, hampering the study of ligand-protein interaction (Albright *et al*., 2006).

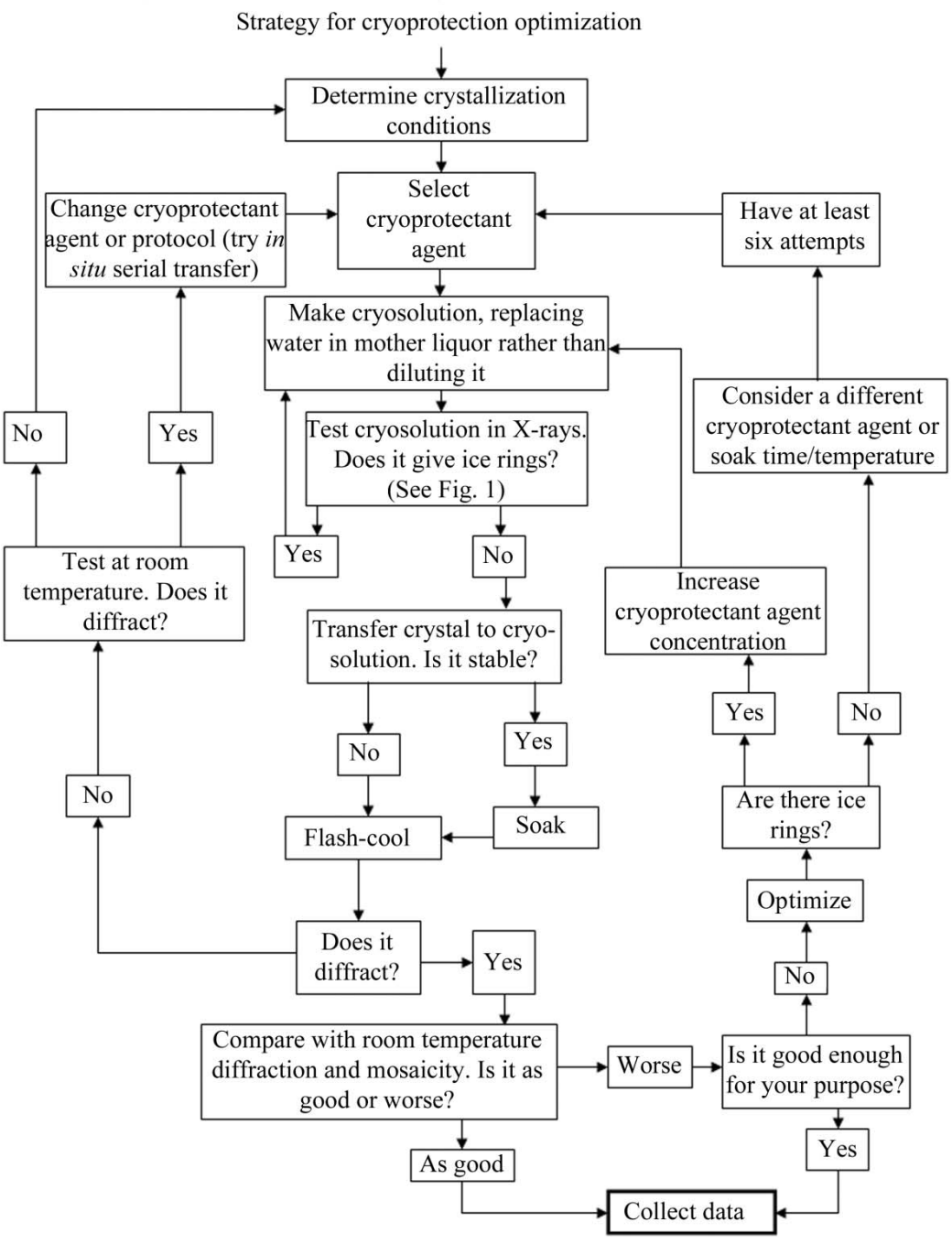

Figure 1.1. Flow diagram showing a possible strategy for optimizing the cryoprotocol (adapted from Garman & Owen, 2006; Reproduced with permission from International Union of Crystallography).

1.3 High pressure cryocooling

An alternative crystal cryocooling method was suggested by Thomanek *et al*. (1973). They pressurized myoglobin crystals to 250 MPa prior to cooling, reasoning that the pressurized water would freeze as ice III (density of 1.14 g/cm^3) instead of ice I (density of 0.92 g/cm^3). Since water contracts during the formation of ice III, the volume-expansion related damage associated with ice I would not occur. In order to prevent the ice formation around the crystal, they chose the water-immiscible liquid isopentane as a pressure medium. Prior to pressurization, mother liquor around the crystal was carefully removed. Decent precession diffraction patterns could be obtained from the myoglobin crystals and it was observed that a number of reflections changed their diffraction intensities, indicating that some structural arrangement had occurred under pressure. However, to the best of our knowledge there was no further development of the technique or structure report of the high pressure cryocooled myoglobin. Almost 30 years later, Urayama *et al*. (2002) used a slightly modified version of this technique to study pressure-induced changes in the myoglobin structure.

The modified method involved pressurizing a protein crystal at room temperature, cryocooling to below the glass transition temperature, removing the pressure at cryogenic temperatures. Because this method still used liquid isopentane as a pressure medium, crystal samples had to be specially loaded into a pressure cell as describe in Fig. 1.2. Though successful, this method had a few major disadvantages. First, the freezing rate of the crystal sample was highly limited by the large thermal mass of the metal pressure tube. The resultant freezing rate was around 1 to 2 K/s, which was approximately 100 times slower than the typical freezing rate during conventional flash cooling. Another challenge was that small and colorless crystals were hardly visible in the liquid isopentane so that they were easily lost during removal from the pressurizing medium. The tedium of removing the pressure-cryocooled crystal from

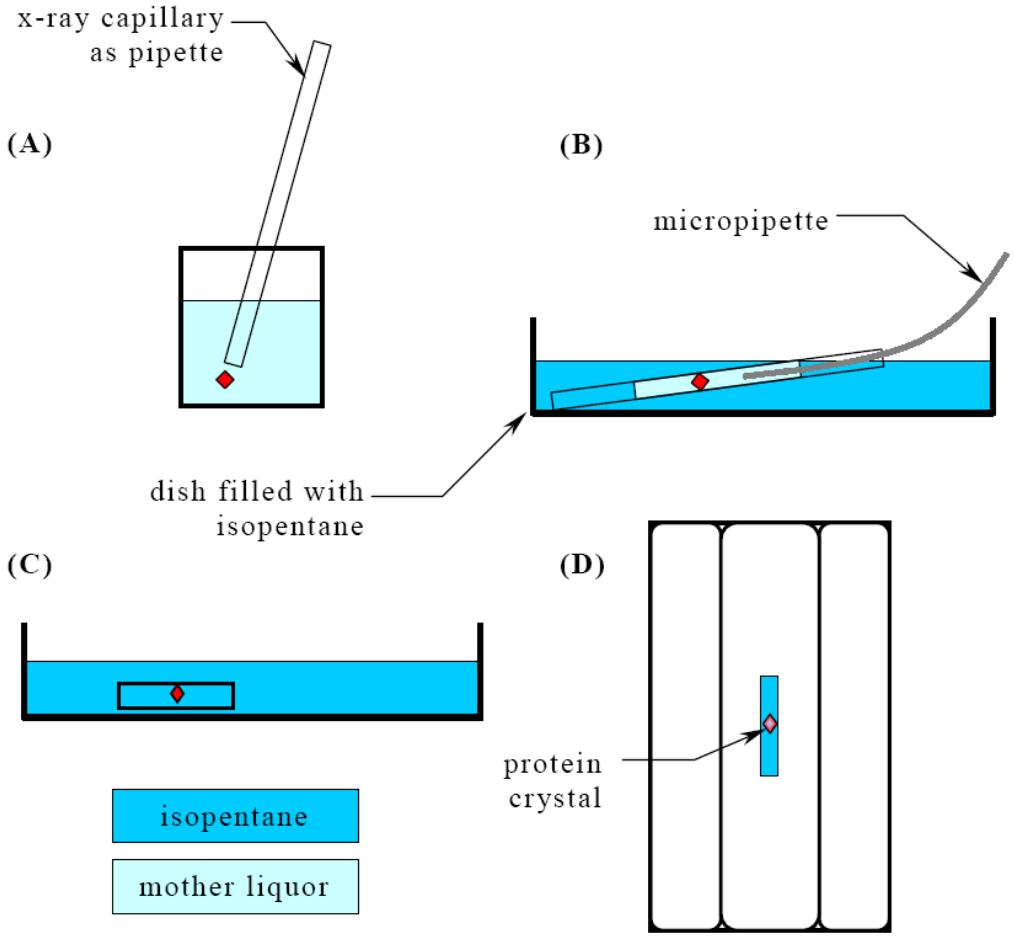

Figure 1.2. Loading Cell for High Pressure Cooling (adapted from Urayama, 2001) (A) Use an x-ray capillary as a pipette to draw in a crystal. (B) Submerge the capillary in isopentane. Draw out mother liquor with micropipette. (C) Trim down capillary to fit pressure cell. (D) Capillary sample inserted into a stainless steel pressure cell (High Pressure Equipment Comapny, Catalog No. 60-21HF2HF4)

isopentane at liquid-nitrogen temperature led the development of a more convenient method of pressure-cryocooling in a gas medium.

For the gas high pressure cryocooling, helium has been selected as a pressure medium for several reasons. First, helium stays in a gaseous phase at liquid nitrogen temperature (77 K), which makes it easier to control pressures. Secondly, helium is an inert gas, which interacts with proteins mainly with low energy interactions such as Van der Waals forces. Finally, helium is a mono atomic element and has the smallest Van der Waals radius (1.4 Å) of any element except for hydrogen, which minimizes the protein structural perturbation when it diffuses into protein molecules.

This modified high pressure cryocooling has dramatically reduced the time for sample preparation and improved the success rate of sample recovery after the high pressure treatment. It has become typical that three or more crystals are prepared in an hour by high pressure cryocooling. Furthermore, the method is compatible with the cryoloop technique (Garman & Schneider, 1997) which means that no special skills are required to handle high pressure cryocooled crystal samples.

To date, the modified high pressure cryocooling has been successfully cryocooled various different kinds of samples including water soluble protein crystals such as citrine, membrane crystals such as Kv1.2 K+ ion channel, ligand-protein complexes such as RCK domain of K+ transporter, large complexes such as ribosome, and catalytic RNA, ribozyme. The method has been extended to the diffraction phasing by the incorporation of heavier noble gases, krypton and xenon. More interestingly, capillary samples have been successfully vitrified by the high pressure cryocooling and it has been demonstrated that sulfur single anomalous dispersion (SAD) phasing is possible with the diffraction data obtained from the high pressure cryocooled capillary sample.

These results imply that high pressure cryocooling has great potential for the structural determination of proteins and, especially, for high throughput protein crystallography. On the other hand, it has been demonstrated that high pressure cryocooling can successfully capture the pressure effects in the protein structures (Urayama *et al*, 2002). Therefore, the method can be a very powerful tool to study functional changes of proteins under pressure, which has been usually carried out in solution states without the detailed three-dimensional structural information.

In the following chapters, I am describing the recent research achievements on the high pressure cryocooling.

In chapter 2, the procedure of high pressure cryocooling is described to cryocool protein crystals in high-pressure helium gas without the need for penetrative cryoprotectants. Three different kinds of water soluble protein crystals, glucose isomerase, thaumatin and L-amino acid oxidase, are treated by the method. A dramatic improvement in diffraction quality in terms of diffraction resolution and crystal mosaicity is observed in all cases. It is demonstrated that the structural change induced by high pressure cryocooling is small, on the order of a few tenths of an angstrom. A mechanism for the pressure cryocooling is proposed involving high-density amorphous (HDA) ice which is produced at high pressure and is metastable at room pressure and 110 K. It is proposed that the density of HDA ice (1.17 g/cm^3), which is significantly higher than that of pure water, may reduce the crystal damage related to solvent volume expansion upon cryocooling.

In chapter 3, the high pressure cryocooling is extended to the diffraction phasing by the incorporation of heavier noble gas, krypton. A modified Kr–He high pressure cyrocooling procedure is described wherein crystals are first pressurized with krypton gas to 10 MPa for 1 h. The krypton pressure is then released and the crystals are repressurized with helium over 150 MPa and cooled to liquid-nitrogen temperatures.

Porcine pancreas elastase (PPE; 240 residues, 26 kDa) is selected as a test case for this study. Excellent diffraction is achieved by the modified high-pressure cryocooling without penetrating cryoprotectants. And a single 0.31 occupied krypton site in a PPE molecule [Bijvoet amplitude ratio ($<|\Delta F|>/<F>$) of 0.53%] is sufficient for SAD phasing at 1.3 Å. Surprisingly, 6 out of 10 sulfurs naturally present in elastase are clearly visible in the anomalous difference map which is created with the experimental phases. Because sulfur has the anomalous strength of only 0.18 e at the data collection wavelength, 0.86 Å, this result reflects the quality of the diffraction produced by the high-pressure cryocooling.

In chapter 4, two new developments of the high pressure cryocooling are presented. First, the method is modified for xenon incorporation. An elastase crystal is Xe-He high pressure cryocooled and xenon SAD phasing is successfully carried out at long wavelength (1.75 Å). Compared to the krypton SAD phasing, stronger anomalous signal is obtained from the incorporated xenon and all 10 sulfur atoms in elastase are clearly visible at higher signal level. Secondly, cryopreservation of thaumatin crystals in a thick-walled capillary without additional cryoprotectants other than the native mother liquor is demonstrated. The crystal diffraction was excellent in terms of diffraction resolution and crystal mosaicity. Furthermore, sulfur SAD phasing is successfully carried out with the diffraction collected at the wavelength of 1.74 Å.

In chapter 5, X-ray diffraction studies are described which confirm the presence of high density amorphous (HDA) ice in the high-pressure cryocooled protein crystallization solution and protein crystals analyzed at room pressure. Diffuse scattering with a spacing characteristic of HDA ice is observed at low temperatures. This scattering then converts successively to low density amorphous (LDA), cubic, and hexagonal ice phases as the temperature is gradually raised from 80 K to 230 K. It is noticed that the ice phase in the high pressure cryocooled protein crystals is highly

correlated to the diffraction quality of crystals. During the phase transition from HDA ice to LDA ice, the resolution limit of crystal diffraction slightly decreased and crystal mosaicity increased by ~ 150 %. Upon formation of crystalline cubic ice from LDA ice, the crystal diffraction from the protein became even more degraded. The protein crystal diffraction entirely disappeared upon the formation of hexagonal ice. These results support the proposed mechanism of high pressure cryocooling, where HDA ice plays a key role for the superior diffraction quality of the high pressure cryocooled crystals.

REFERENCES

Albright, R. A., Vazquez Ibar, J.-L., Kim, C. U., Gruner, S. M. & Morais Cabral, J. H. (2006). *Cell*, **126**, 1147-1159.

Blake, C. C. F. & Phillips, D. C. (1962). *Biological Effects of Ionizing Radiation at the Molecular Level*, pp. 183–191. Vienna: International Atomic Energy Agency.

Garman, E. F. & Schneider, T. R. (1997). *J. Appl. Cryst*. **30**, 211-237.

Garman, E. F. & Owen, R. L. (2006), *Acta Cryst*. D**62**, 32-47.

Henderson, R. (1990). *Proc. R. Soc. London*, B**241**, 6–8.

Hope, H. (1988). *Acta Cryst.* B**44**, 22–26.

Juers, D. H. & Matthews, B. W. (2004). *Q. Rev. Biophys*. **37**, 1-15.

Kmetko, K., Husseini, N. S., Naides, M., Kalinin, Y. & Thorne, R. E. (2006). *Acta Cryst*. D**62**, 1030-1038.

Kriminski, S., Caylor, C. L., Nonato, M. C., Finkelstein, K. D. & Thorne, R. E. (2002). *Acta Cryst*. D**58**, 459-471.

Kriminski, S., Kazmierczak, M. & Thorne, R. E. (2003). *Acta Cryst*. D**59**, 697-708.

Nave, C. & Garman, E. F. (2005). *J. Sync. Rad*. **12**, 257-260.

Ravelli, R. B.G. & Garman, E. F. (2006). *Curr. Opin. Struc. Biol.* **16**, 624-629

Teng, T.-Y. (1990). *J. Appl. Cryst.* **23**, 387–391.

Thomanek, U. F., Parak, F., Mössbauer, R. L., Formanek, H., Schwager, P. & Hoppe, W. (1973). *Acta Cryst*. A**29**, 263-265.

Urayama, P. (2001). PhD thesis, Cornell University, USA

Urayama, P., George, N. P. & Gruner, S. M. (2002). *Structure*, **10**, 51-60.

CHAPTER TWO
HIGH-PRESSURE COOLING OF PROTEIN CRYSTALS WITHOUT CRYOPROTECTANTS*

2.1 Introduction

A typical protein crystal at room temperature only survives a fraction of the X-ray dose required for a complete high resolution data set before it becomes irrevocably radiation damaged. The mechanism of radiation damage is complex and includes both direct damage to protein molecules and secondary chemical degradation by the highly reactive free radicals created when water or other chemical additives are exposed to X-rays (Garman & Schneider, 1997). When a protein crystal is properly cryocooled, the molecular motions of both the polypeptide chains and the solvent in the crystal are damped to well below the glass transition and the diffusion of harmful free radicals is drastically reduced, allowing a typical 50–300 μm crystal to survive long enough in the X-ray beam to collect a complete high-resolution data set using a single crystal (Hope, 1988, 1990; Young *et al*., 1993; Rodgers, 1994; Watowich *et al*., 1995; Chayen *et al*., 1996; Garman & Schneider, 1997; Garman, 1999).

The primary goal of cryocooling is to turn the water surrounding and inside the crystal into amorphous ice. Amorphous ice is necessary because crystalline ice yields spurious diffraction that obscures useful protein diffraction. The formation of amorphous ice, which requires exceedingly rapid temperature drops, is usually limited by the time it takes heat to diffuse out of a typical 50–300 μm diameter crystal (Kriminski *et al*., 2003). To facilitate amorphous ice formation, chemical cryoprotectants such as glycerol or polyethylene glycol are usually added to the mother liquor (Garman & Schneider, 1997). Another problem with cryocooling is that

* Reproduced with permission from Kim, C. U., Kapfer, R. & Gruner, S. M. (2005). *Acta Cryst*. D**61**, 881-890. Copyright 2005 International Union of Crystallography.

even with fully amorphous ice, the differential volume change of the mother liquor, protein and unit cell upon cooling degrades or totally destroys the diffraction quality of the crystal (Kriminski *et al*., 2002; Juers & Matthews, 2004). A second benefit of a properly chosen cryoprotectant is that it limits this volume-related damage. In practice, cryoprotectants that work with one protein do not work with another, requiring a trial-and-error search for suitable cryoprotectant conditions. Unfortunately, there are few rules to guide this search; indeed, some crystals, such as crystals of viruses and large complexes, have never been successfully cryocooled. Even in cases where a suitable cryoprotectant is found, cooling usually degrades the crystal quality and increases the mosaic spread, thereby limiting the quality of the data set (Juers & Matthews, 2004). Moreover, the chemical reactions between cryoprotectants and molecules within the crystal cannot always be ruled out. Hence, care has to be taken in choosing a proper cryoprotectant agent for a specific protein crystal to minimize unwanted side effects such as cryoprotectant binding to the protein active site (Garman & Schneider, 1997).

An alternative cooling method was suggested by Thomanek *et al*. (1973). They pressurized myoglobin crystals to 250 MPa in isopentane prior to cooling, reasoning that such pressures would freeze water to ice III which contracts, in contrast to ice I which expands, thus protecting the crystal from damage. Although decent diffraction patterns were obtained from crystals removed from the isopentane using this procedure, to the best of our knowledge there was no further development of the technique. Almost 30 years later, Urayama *et al*. (2002) used a slightly modified version of this technique to study pressure-induced changes in the myoglobin structure. It was shown that the magnitude of the structural changes induced by pressure-cooling followed by cryocrystallography was comparable to the changes arising from flash-cooling at ambient pressure. The tedium of removing the pressure-cooled crystal from isopentane at liquid-nitrogen temperature led us to develop a more convenient method

of pressure cooling in helium gas. We now report on tests of this system using several protein crystals. In almost all cases, we observed a significant improvement in diffraction quality in terms of both mosaicity and resolution without any permeable cryoprotectants. A mechanism is proposed to explain why the method works.

2.2 Experimental

2.2.1 Cooling methods: flash-cooling at room pressure versus high-pressure cooling

2.2.1.1 Flash-cooling at room pressure

Crystals were transferred to NVH oil (catalog No. HR3-617, Hampton Research, Laguna Niguel, CA, USA) and swished back and forth to remove excess mother liquor on the surface of the crystals. The crystals were picked up in commercially available cryoloops (Hampton Research) with a minimal droplet of the oil. They were then flash-cooled by plunging directly into liquid nitrogen (LN_2; 77 K) at room pressure without using any penetrative cryoprotectants. The absence of cryoprotectants allows a direct comparison with the high-pressure cooling method, which also does not use cryoprotectants.

2.2.1.2 High-pressure cooling

The high-pressure cooling process is shown schematically in Fig. 2.1. Crystals were picked up in oil in cryoloops in the exactly same manner as in preparation for room-pressure flash-cooling. In the high pressure cooling, the oil coating is essential to prevent dehydration of the crystals during the 25 min pressurizing process. The pressure-cooling apparatus is shown in Fig. 2.2. In brief, the cryoloop stud was

inserted into one end of a small length of brass tubing partially filled with a short length of steel piano wire (Fig. 2.2a). This was then inserted into one end of a 30 cm straight length of heavy-wall stainless-steel high-pressure tubing (catalog No. 60-HM4-12, High Pressure Equipment Company, Erie, PA, USA) capped at the other end with an endcap. A strong magnet (rare-earth magnet, Hartville Tool, Hartville, OH, USA) placed on the outside of the high pressure tubing attracted the piano wire inside and held the cryoloop assembly in place. The high-pressure tubing was placed into a special jig in a vertical position with the crystal at the top and the capped end at the bottom of an LN_2 container (Fig. 2.2b). The upper end of the tubing was then connected to a high-pressure He-gas compressor (catalog No. 46-13427-2, Newport Scientific, Jessup, MD, USA) using standard commercial high-pressure cone-seal fittings (High Pressure Equipment Company). A pressure of up to 200 MPa was applied to the crystals. Because stainless-steel tubing is a poor heat conductor, the upper end (crystals) remains above 283 K. The crystals were left under pressure for 25 min to equilibrate and then (while still under high pressure) dropped into the lower part of the tubing under LN_2 by removing the magnet holding the cryoloop assembly. After 10 min, pressure was released and the high-pressure connections to the pump were unscrewed, leaving the crystals with the bottom endcaps in the LN_2 container. Simple homemade fixtures were used to disassemble the remaining tubing in the LN_2 container. The cooled crystals in their cryoloops were then transferred into crystalcaps (Hampton Research) under LN_2 and stored in an LN_2 dewar until data collection at room pressure.

The pressure-cooling apparatus described above consists primarily of a commercially available high-pressure gas compressor and off-the-shelf high-pressure plumbing and gauges. The assembly and disassembly required to freeze crystals is

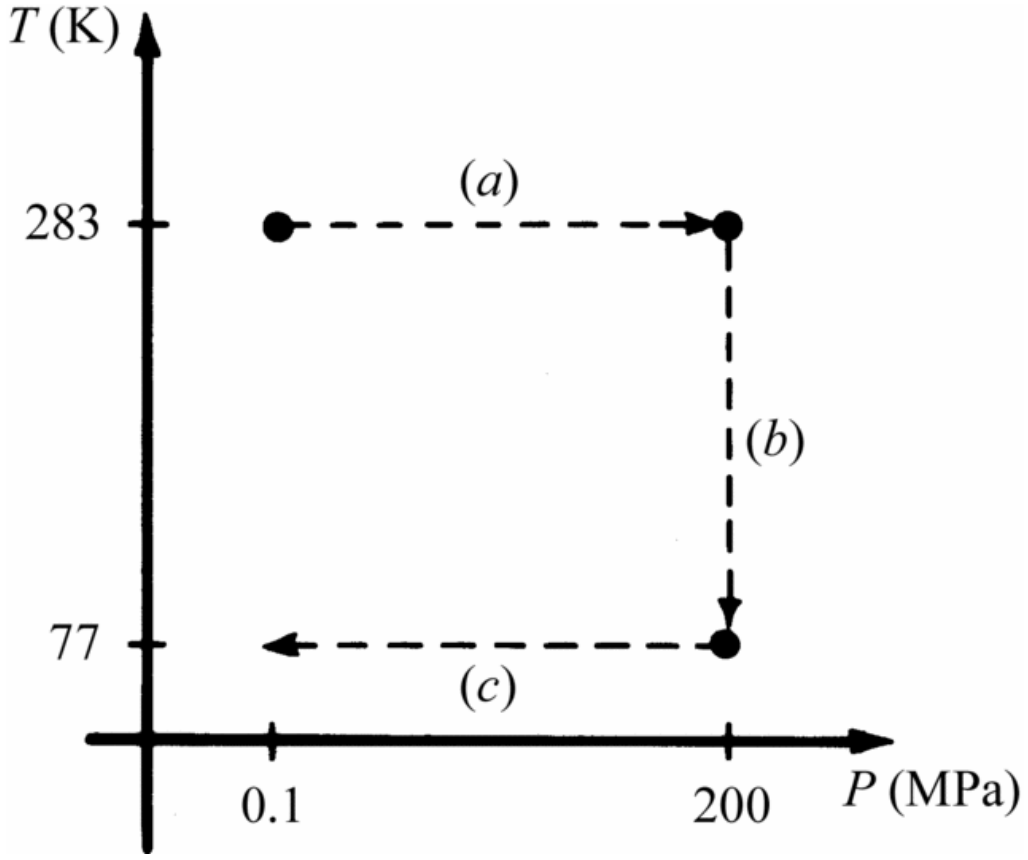

Figure 2.1. Simplified diagram of the high-pressure cooling method. (a) Pressurization to 200 MPa at 283 K using He-gas compressor. Crystals are left under pressure for 25 min to equilibrate. (b) Cooling crystals under pressure by dropping samples to the lower part of pressure tubing immersed in LN_2 (77 K). (c) After 10 min, pressure is released while the samples are kept cooled at 77 K. Crystals are stored in a LN_2 dewar until data collection at low temperature and ambient pressure.

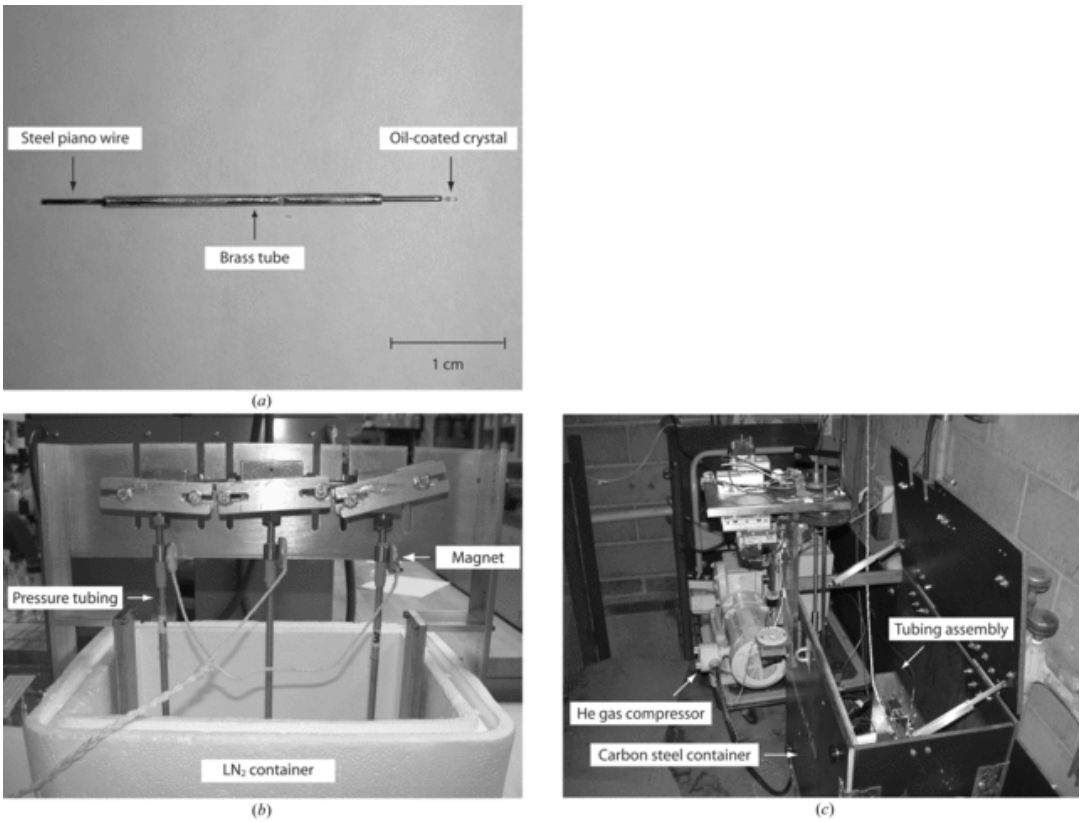

Figure 2.2. High-pressure cooling apparatus. (a) Sample pin. An oil-coated crystal in a cryoloop is inserted into one end (right) of a brass tube (2.5 cm long) and a steel piano wire in the other end (left). (b) High-pressure tubing assembly in a LN_2 container. A sample is loaded into the top of each 30 cm long tube and is held in place by a magnet outside the tube. Three crystals can be pressure-cooled at a time. (c) High-pressure tubing assembly in a carbon-steel container. The assembly is connected to a He-gas compressor (rear). All high-pressure operations are controlled remotely for safety reasons.

performed with simple hand wrenches and homemade jigs. We typically can pressure-freeze several crystals an hour. To date, hundreds of crystals of about a dozen proteins have been successfully cooled. Obviously, with some effort the apparatus can be engineered with quick-disconnect high pressure fittings for more effective throughput.

It is important to note that helium gas expands by almost 2000 times when released into air from 200 MPa. This tremendous explosive power necessitates great caution. For safety reasons, our apparatus is enclosed in a half-inch-thick carbon-steel container. This, in turn, is housed in a cinderblock utility room (Fig. 2.2c). All high-pressure operations are performed without personnel present in the room, via remotely controlled monitors, switches, motors and pulleys.

2.2.2 Materials and data collection

Three kinds of protein crystals were prepared by both flash-cooling at room pressure and high-pressure cooling. Diffraction data were collected at the Cornell High Energy Synchrotron Source (CHESS) on beamline F1 (λ= 0.9186 Å, ADSC Quantum-4 CCD detector) and F2 (λ= 0.9795 Å, ADSC Quantum-210 CCD detector). In all cases the detector face was perpendicular to the incident beam (2θ value of zero). All data were collected at 110 K (N_2-gas stream) and room pressure with oscillation angle ($\Delta\varphi$) 1.0˚.

2.2.2.1 Glucose isomerase

Glucose isomerase from *Streptomyces rubiginosus* (catalog No. HR7-102) was purchased from Hampton Research and dialyzed against pure water before crystallization. Crystals were grown by the hanging-drop method by mixing 2 µl of a reservoir solution containing 1.15 M ammonium sulfate, 1 mM magnesium sulfate and 10 mM HEPES pH 7.5 with 2 µl 25 mg/ml protein solution in pure water (modified

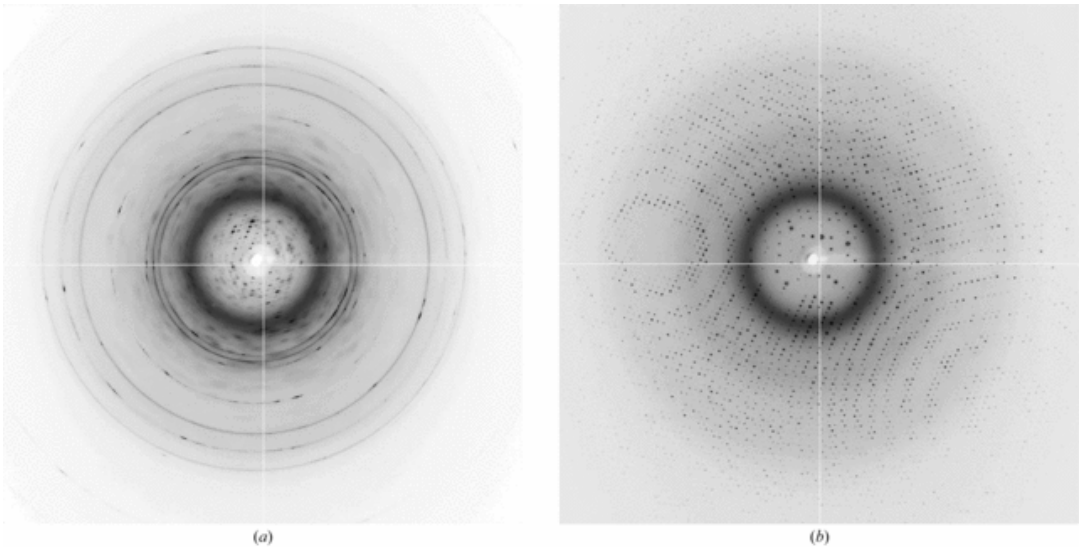

Figure 2.3. Glucose isomerase. (a) Diffraction image of a crystal flash-cooled at ambient pressure (λ= 0.9795 Å, beam diameter= 150 µm, Δφ= 1.0°, d = 150 mm, 60 s). Strong ice rings are seen. The diffraction resolution is 5.0 Å and the mosaicity is very poor. (b) Diffraction image of a crystal pressure-cooled at 130 MPa (λ= 0.9795 Å, beam diameter= 150 µm, Δφ= 1.0°, d= 150 mm, 30 s). The diffraction resolution reaches 1.3 Å and the mosaicity is 0.39°.

from Carrell *et al*., 1989). The crystals appeared in a few days and grew to maximum size (1 × 1 × 1 mm) in a week. Approximately 250 μm sized crystals were used for data collection. Data were collected at CHESS F2 station (beam diameter = 150 μm). The first image (Fig. 2.3a) corresponds to the crystal flash-cooled at room pressure. The distance between the crystal and detector (d) was 150 mm and the exposure time was 60 s. Four consecutive images were collected to estimate resolution and mosaicity. The second image (Fig. 2.3b) corresponds to the crystal pressure-cooled at 130 MPa. The distance was 150 mm and the exposure time was 30 s. A data set containing 155 frames was collected for structure determination.

2.2.2.2 Thaumatin

Thaumatin from *Thaumatococcus daniellii* (catalog No. T7638) was purchased from Sigma (Saint Louis, MO, USA) and used for crystallization without further purification. Crystals were grown by the hanging-drop method by mixing 2 μl of a reservoir solution containing 0.9 M sodium potassium tartrate with 2 μl 25 mg/ml protein solution in 50 mM HEPES buffer pH 7.0 (modified from Ko *et al*., 1994). The crystals appeared in a day and grew to maximum size (150 × 250 × 500 μm, truncated bipyramidal shape) in a week. The first image (Fig. 2.4a) corresponds to the crystal flash-cooled at room pressure and was collected at CHESS F2 station (beam size = 100 μm, d = 200 mm and exposure time= 20 s). Four consecutive images were collected to estimate the resolution and mosaicity. The second image (Fig. 2.4b) corresponds to the crystal pressure-cooled at 185 MPa and was collected at CHESS F1 station (beam size = 100 μm, d = 175 mm and exposure time = 15 s). A data set containing 200 frames was collected.

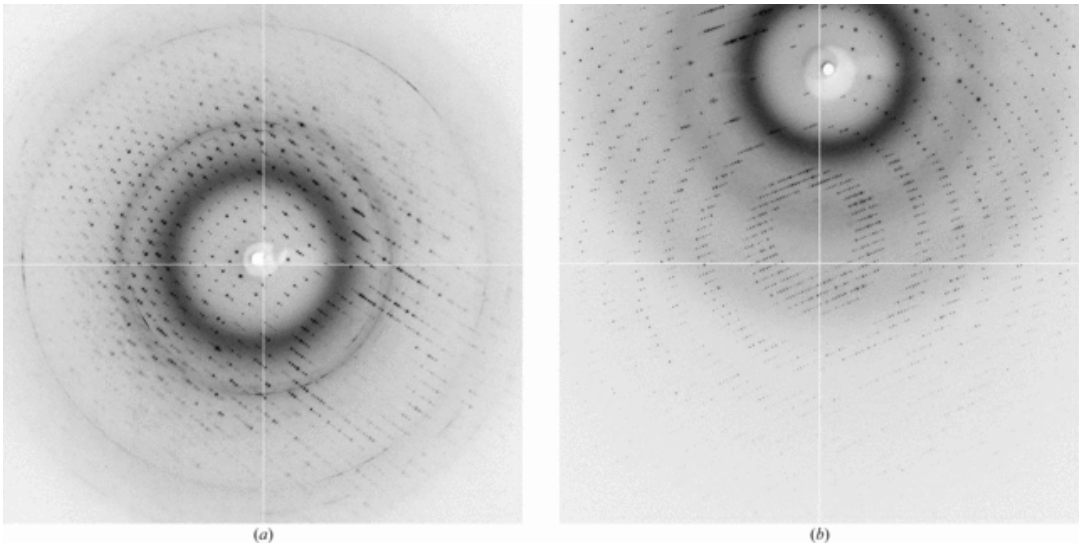

Figure 2.4. Thaumatin. (a) Diffraction image of a crystal flash-cooled at ambient pressure (λ= 0.9795 Å, beam diameter= 100 μm, Δφ= 1.0°, d= 200 mm, 20 s). Ice rings are seen. The diffraction resolution is 1.8 Å and the mosaicity is 1.29°. (b) Diffraction image of a crystal pressure-cooled at 185 MPa (λ= 0.9186 Å, beam diameter = 100 μm, Δφ= 1.0°, d = 175 mm, 15 s). The diffraction resolution reaches 1.15 Å and the mosaicity is 0.11°.

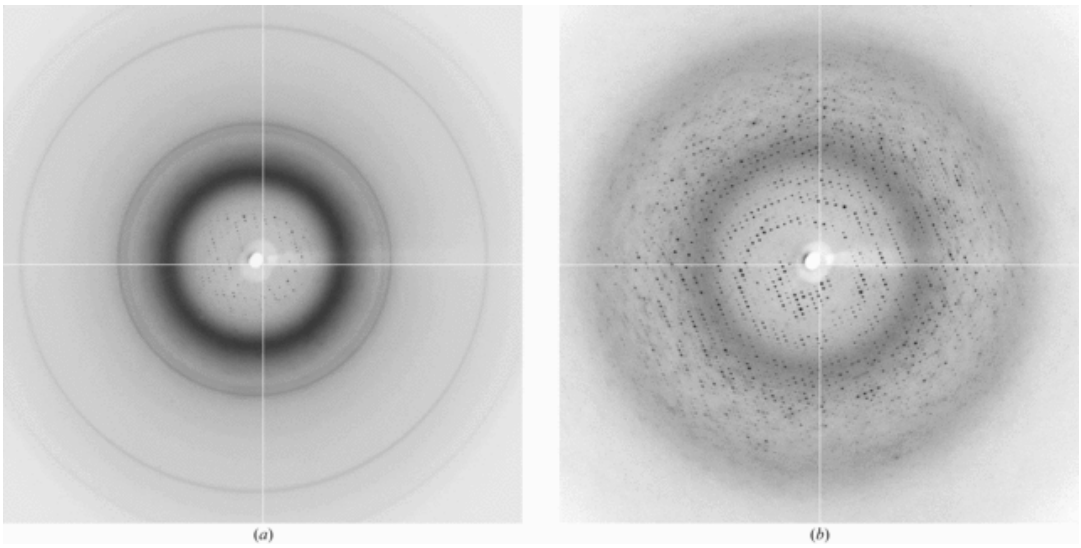

Figure 2.5. AHP-LAAO. (a) Diffraction image of a crystal flash-cooled at ambient pressure (λ= 0.9795 Å, beam diameter= 150 µm, Δφ= 1.0°, d= 200 mm, 60 s). Strong ice rings are seen. The diffraction resolution is only 7.0 Å and the mosaicity is very poor. (b) Diffraction image of a crystal pressure-cooled at 190 MPa (λ= 0.9795 Å, beam diameter= 150 µm, Δφ= 1.0°, d= 250 mm, 60 s). The diffraction resolution reaches 2.7 Å and the mosaicity is 0.56°.

2.2.2.3 AHP-LAAO

AHP-LAAO (L-amino-acid oxidase from *Agkistrodon halys pallas*) protein solution was kindly provided by H. Zhang and L. Niu. Crystals were grown by the hanging-drop method by mixing 1 μl of a reservoir solution containing 2 M ammonium sulfate and 0.1 M sodium citrate pH 5.0 with 2 μl 40 mg/ml protein solution in pure water (modified from Zhang *et al*., 2004). The crystals appeared in two weeks and grew to maximum size (50 × 100 × 100 μm) after one month. Data were collected at CHESS F2 station (beam diameter = 150 μm). The first image (Fig. 2.5a) corresponds to the crystal flash-cooled at room pressure. The distance was 200 mm and the exposure time was 60 s. Four consecutive images were collected to estimate resolution and mosaicity. The second image (Fig. 2.5b) corresponds to the crystal pressure-cooled at 190 MPa. The distance was 250 mm and the exposure time was 60 s. A data set containing 60 frames was collected.

2.2.3 Data processing and structure determination

The data were processed with *DPS/MOSFLM* (Steller *et al*., 1997; Leslie, 1992) and scaled with *SCALA* (Collaborative Computational Project, Number 4, 1994). The mosaicity of each data set was determined in the *MOSFLM* refinement process using four consecutive images. The initial structures were determined by the molecular-replacement method using the program *MOLREP* (Vagin & Teplyakov, 1997) from the *CCP4* program suite (Collaborative Computational Project, Number 4, 1994). The structures were then refined using the data sets with *REFMAC5* (Murshudov *et al*., 1997; Collaborative Computational Project, Number 4, 1994). Water molecules were automatically located and (F_o - F_c) and ($2F_o$ - F_c) maps were generated during the refinement process. The difference maps were displayed with the *Xtalview/Xfit*

program (McRee, 1999) for model corrections. Structural figures were produced using *PyMol* (DeLano, 2002).

2.3 Results

2.3.1 Glucose isomerase

The crystal flash-cooled at room pressure diffracted to only 5.0 Å and spots were severely smeared (Fig. 2.3a). The image was not auto-indexable and mosaicity could not be estimated. The crystal looked entirely white and cloudy in the cold stream and very intense ice rings were seen in the image, indicating that much water had turned into crystalline ice during the flash-cooling process at atmospheric pressure (0.1 MPa). The diffraction images from several crystals prepared by the flash-cooling method at 0.1 MPa were no better than this image. On the other hand, the crystal pressure-cooled at 130 MPa diffracted to 1.3 Å with 0.39˚ mosaicity (Fig. 2.3b). An overexposed snapshot image (90 s) was collected at a closer distance (100 mm) to check the diffraction limit and the diffraction spots reached the maximum resolution area (1.05 Å) of the image (figure not shown). The pressure-cooled crystal looked clear and transparent and no ice rings were observed, indicating that crystalline ice formation was entirely suppressed by pressure without any penetrative cryoprotectants. The average resolution and mosaicity of three different crystals prepared by high-pressure cooling at 130 MPa were 1.3 Å (at least) and 0.48˚, respectively.

The pressure-cooled crystal belonged to the body-centered orthorhombic space group I222, with unit-cell parameters a = 92.9, b = 98.7, c = 102.6 Å. There was one monomer in an asymmetric unit and the solvent content was 54.7 % (Matthews coefficient V_M = 2.7 Å^3 Da^{-1}; Matthews, 1968). The structure (PDB code 8xia) from Carrell *et al*. (1989) was employed as a starting model for molecular replacement. In

Table 2.1. Summary of crystallographic statistics. Values in parentheses are for the last shell.

	Glucose isomerase (130 MPa)	Thaumatin (185 MPa)	AHP-LAAO (190 MPa)
Space group	I222	$P4_12_12$	$I2_13$
Unit-cell parameters (Å)	a = 92.9, b = 98.7, c = 102.6	a = b= 58.0, c = 151.1	a = b = c = 167.9
Solvent content (%)	54.7	56.7	61.8
Resolution range (Å)	30-1.45 (1.53-1.45)	30-1.5 (1.58-1.5)	30-2.9 (3.06-2.9)
No. of observations	437820 (28611)	300340 (35155)	127586 (17208)
No. of unique reflections	82638 (11314)	41519 (5569)	17583 (2535)
Multiplicity	5.3 (2.5)	7.2 (6.3)	7.3 (6.8)
Completeness (%)	99.1 (94.3)	98.1 (92.3)	99.9 (99.9)
R_{sym} (%)	7.2 (20.9)	10.5 (26.0)	12.3 (38.2)
$I/\sigma(I)$	16.5 (4.0)	13.3 (6.6)	14.0 (3.7)
R factor (%)	17.6	17.5	
R_{free} factor (%)	19.8	20.2	
Average B factor ($Å^2$)	13.0	13.7	
No. of water molecules	773	486	
R.m.s. deviation from ideality			
Bond lengths (Å)	0.011	0.013	
Angles (º)	1.331	1.389	

the final model, the crystallographic R factor and R_{free} factor converged to 17.6 and 19.8 %, respectively, at 1.45 Å. Details of the data collection statistics and structure-refinement statistics are listed in Table 2.1.

2.3.2 Thaumatin

The crystal flash-cooled at room pressure diffracted to 1.8 Å with 1.29˚ mosaicity (Fig. 2.4a). Ice rings are seen in the diffraction image and the crystal looked slightly cloudy, indicating that water was not entirely vitrified during the flash cooling process at 0.1 MPa. The average resolution and mosaicity of three different flash-cooled crystals were 1.93 Å and 1.4˚, respectively. On the other hand, the crystal pressure-cooled at 185 MPa diffracted to 1.15 Å with 0.11˚ mosaicity (Fig. 2.4b). Crystalline ice formation was completely suppressed by pressure, as no ice rings appeared in the image. The pressure-cooled crystals looked transparent, unlike the flash-cooled ones. The average resolution and mosaicity of four different crystals prepared by high-pressure cooling at 185–190 MPa were 1.35 Å and 0.3˚, respectively. The crystal flash-cooled at room pressure (Fig. 2.4a) belonged to the primitive tetragonal space group $P4_12_12$, with unit-cell parameters a = b = 58.3, c = 149.8 Å.

The pressure-cooled crystal (Fig. 2.4b) belonged to the same space group, with unit-cell parameters a = b = 58.0, c = 151.1 Å. There was one molecule in an asymmetric unit and the solvent content was 56.7% (Matthews coefficient V_M = 2.9 $Å^3\ Da^{-1}$; Matthews, 1968) for the pressure-cooled crystal. The structure (PDB code 1lxz) from Charron *et al*. (2002) was employed as a starting model for molecular replacement. In the final model, the crystallographic R factor and R_{free} factor converged to 17.5 and 20.2%, respectively, at 1.5 Å. Details of the data-collection statistics and structure refinement statistics are listed in Table 2.1.

2.3.3 AHP-LAAO

The crystal flash-cooled at room pressure diffracted to only 7.0 Å and strong ice rings were produced (Fig. 2.5a). The image was not auto-indexable and mosaicity could not be estimated. Another crystal prepared by flash-cooling gave a diffraction image even poorer than this one. On the other hand, the crystal pressure-cooled at 190 MPa diffracted to 2.7 Å with 0.56˚ mosaicity (Fig. 2.5b). No ice rings were observed and crystalline ice formation was suppressed by pressure, as for the glucose isomerase crystals. The average resolution and mosaicity of three different crystals prepared by high-pressure cooling at 190 MPa were 2.7 Å and 0.59˚, respectively. The pressure-cooled crystal belonged to the body-centered cubic space group $I2_13$, with unit-cell parameters a = b = c = 167.9 Å. There was one molecule in an asymmetric unit and the solvent content was 61.8 % (Matthews coefficient V_M = 3.2 $Å^3$ Da^{-1}; Matthews, 1968). Details of the data collection statistics are listed in Table 2.1.

2.4 Discussion

The suppression of crystalline ice at ambient pressure typically requires either extremely rapid cooling or the addition of cryoprotectants. Pressure cooling appears to suppress the formation of crystalline ice. Indeed, Urayama *et al*. (2002) found that myoglobin crystals were successfully cryocooled without ice formation at high pressure (150 MPa) even when cooled at only a degree or two per second. The reason that the cooling rate appears to be more forgiving at high pressures is not fully understood, but we make the following hypothesis. As shown in the temperature–pressure phase diagram of water (Fig. 2.6), the melting point and the water supercooled region decrease as pressure increases up to 210 MPa. Furthermore, the nucleation and growth of ice I (hexagonal or cubic ice) is suppressed because the higher density of liquid water is favored at high pressure (Le Chatelier's principle).

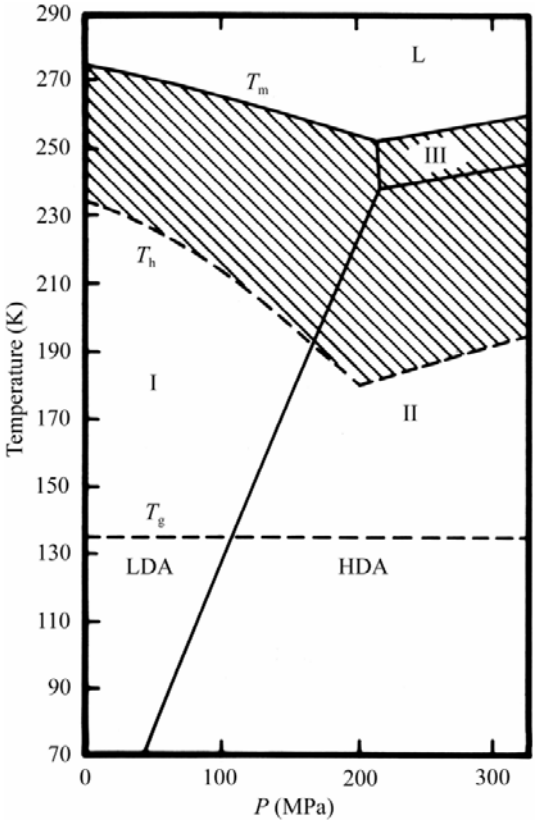

Figure 2.6. The pressure-temperature phase diagram of H_2O [adapted from Kanno et al. (1975), Franks (1985), Garman & Schneider (1997) and Mishima & Stanley (1998)]. Amorphous ices form when liquid water is rapidly cooled below the glass-transition temperature (T_g), preventing the nucleation and growth of crystalline ices. HDA ice may form upon cooling above ~100 MPa. LDA ice is formed below ~100 MPa. The hatched region is the allowed region for supercooled liquid water. The melting point (T_m) and the lowest temperature (T_h) for supercooled water both decrease with pressure up to 210 MPa. The region in which the amorphous phase can exist depends on the thermal/pressure history of the system. HDA ice is metastable at ambient pressure as long as the temperature is kept below 120 K. Note that the glass-transition line (T_g) is very hard to determine exactly experimentally and should be taken as an estimate.

Another type of crystalline ice, ice II, is allowed at high pressure. However, the nucleation and growth rates of ice II at high pressure are initially slower than those of ice I at ambient pressure, even though ice II has a smaller volume than liquid water (Franks, 1982).

Crystal degradation during normal flash-cooling occurs for several reasons. When crystals are cooled, the unit-cell volume usually shrinks by 2–7 % as a result of molecular rearrangement in the protein packing (Juers & Matthews, 2001). The protein molecule itself contracts as well (1–2 %), but much less than the unit cell.

These effects reduce the volume available for water in the crystal. However, normal crystalline ice (ice I) has a larger volume per water molecule (i.e. a lower density) than liquid water. When low-density amorphous (LDA) ice forms at ambient pressure, although it produces no ice-diffraction rings, the amorphous ice also expands relative to liquid water. In fact, the 6.7 % volume expansion of LDA ice (0.94 g/cm^3 at 77 K, 0.1 MPa) is almost the same as that of hexagonal ice I at liquid-nitrogen temperature (Ghormley & Hochanadel, 1971; Röttger *et al*., 1994). These conflicting tendencies (shrinking of the available water volume and the water expansion) lead to crystal disruption. Therefore, at room pressure suitable cryoprotectants must be found not only to suppress crystalline ice formation but also to raise the density of the resultant amorphous water.

We propose that the improvement in diffraction quality during high-pressure cooling involves the formation of high density amorphous (HDA) ice. When cooled at high pressures, liquid water may freeze directly into HDA ice and, once formed, stays metastably in the HDA state when the pressure is removed, as long as the temperature is kept below 120 K (Mishima *et al*., 1984). In contrast to ice I and LDA ice, HDA ice has a significantly higher density (1.17 g/cm^3 at 77 K, 0.1 MPa). As a result, HDA ice at 0.1 MPa occupies less volume per molecule than liquid water at 0.1 MPa. This

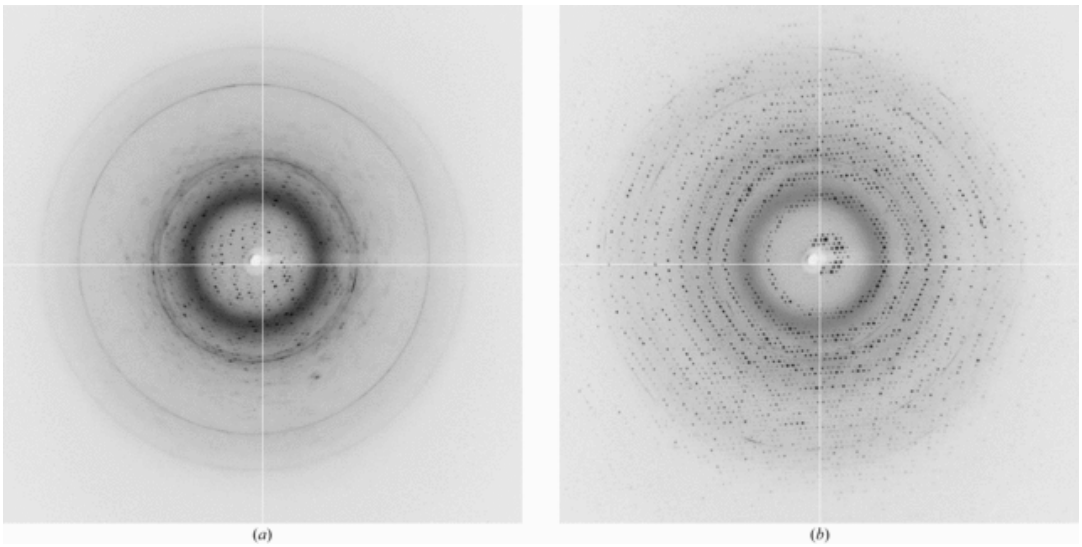

Figure 2.7. Glucose isomerase at different pressures (λ= 0.9795 Å, beam diameter= 150 µm, Δφ= 1.0°, d= 150 mm, 30 s). (a) Diffraction image of a crystal pressure-cooled at 90 MPa. The diffraction resolution is only 3.0 Å. (b) Diffraction image of a crystal pressure-cooled at 110 MPa. The diffraction resolution is 1.3 Å. Note that relatively faint ice rings are seen in both images, indicating that water vitrification is not entirely achieved at these modest pressure levels. See Fig. 2.3(b) for glucose isomerase pressure-cooled at 130 MPa.

helps mitigate crystal disruption. Glucose isomerase crystals pressure-cooled at several different pressures support this explanation. A clue that HDA ice is involved is the observation that crystals pressure-cooled below ~100 MPa, where the LDA ice can form (see Fig. 2.6), consistently diffracted to worse than 3.0 Å resolution (Fig. 2.7a), whereas crystals pressure-cooled above ~100 MPa consistently diffracted to better than 1.3 Å (Fig. 2.7b). Verification of the HDA hypothesis, for example, by neutron-scattering studies of the vitrified water, is beyond the scope of this paper.

This paper reports detailed results of pressure-cooling three different types of protein crystals. The method has also been systematically applied to ten other proteins (data not shown). In all cases except one, water vitrification and acceptable crystal diffraction was achieved without penetrative cryoprotectants. The exceptional case was deoxyhemoglobin, where the pressure-cooled crystals consistently diffracted poorly compared with the crystals flash-cooled at room pressure.

It is interesting to note that most protein crystals readily survive pressurization. It has been reported that tetragonal hen egg-white lysozyme crystals grown at low salt concentration (0.83 M NaCl) cracked when pressurized with mother liquor in a beryllium pressure cell at 30–40 MPa (Kundrot & Richards, 1987). However, in our apparatus, lysozyme crystals grown in 0.8 M NaCl did not crack under pressures up to 200 MPa. Our observations are that crystal cracking is rare during helium high-pressure cooling.

In practice, high-pressure cooling is an effective approach to the cryoprotection of protein crystals without the need for penetrative cryoprotectants. Zhang *et al*. (2004) tried to cryocool AHP-LAAO protein crystals by normal flash-cooling methods with cryoprotectants, but the flash-cooled crystals diffracted to worse than 5 Å. As described earlier, the AHPLAAO crystals pressure-cooled at 190 MPa diffracted to 2.7 Å without any penetrative cryoprotectants.

Structural perturbations in proteins arising from pressure are generally small, but must be kept in mind. Kundrot & Richards (1987) reported very small structural shifts in lysozyme at room temperature and 100 MPa. This small structural change in lysozyme was confirmed by an NMR solution study (Refaee *et al*., 2003). Urayama *et al*. (2002) performed a careful analysis on myoglobin and also measured very small differences at the level of shifts of protein secondary-structure blocks by 0.1–0.4 Å when proteins are either flash-cooled at room pressure or pressure-cooled in liquid isopentane. In order to investigate the perturbation of protein structures by He-gas high-pressure cooling, the initial structures were determined by molecular replacement using the known atmospheric pressure protein coordinates in the PDB and then refined against the diffraction data sets as described in 2.2.3. The results are shown in Fig. 2.8 (AHP-LAAO is not presented in this paper simply because the structural difference might be biased by the relatively low-resolution structures). For glucose isomerase, the superposition of the flash-cooled structure (PDB code 8xia; 285–288 K, 0.1 MPa; Carrell *et al*., 1989) and the pressure-cooled structure (110 K, 130 MPa) shows little difference (Fig. 2.8a). The r.m.s. deviation between the C^{α} backbone atoms in the two models is 0.327 Å and the r.m.s. deviation between all atoms is 0.459 Å. For thaumatin, the superposition of the flash-cooled structure (PDB code 1lxz; 100 K, 0.1 MPa; Charron *et al*., 2002) and the pressure-cooled structure (110 K, 185 MPa) also shows only very small changes (Fig. 2.8b). The r.m.s. deviation between C^{α} atoms in the two models is 0.299 Å and the r.m.s. deviation between all atoms is 0.472 Å. Overall, the evidence so far suggests that the magnitude of structural perturbation upon pressure cooling is typically comparable with the small perturbations that are always observed upon lowering temperature, e.g. upon flash-cooling independent of pressure. The inference, by extension, is that most proteins do not show large-scale structural perturbations under our pressure-cooling conditions.

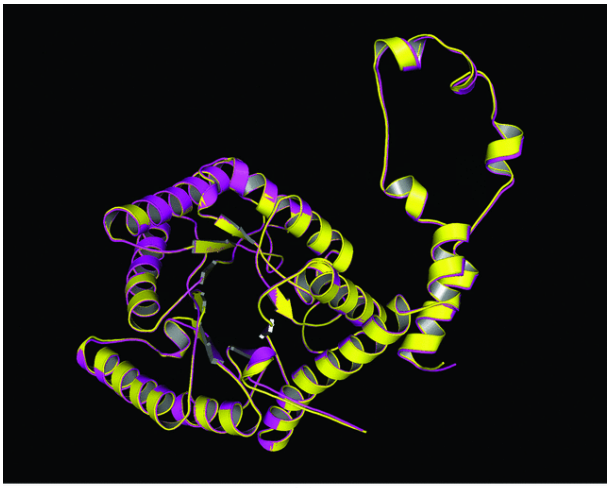

(*a*)

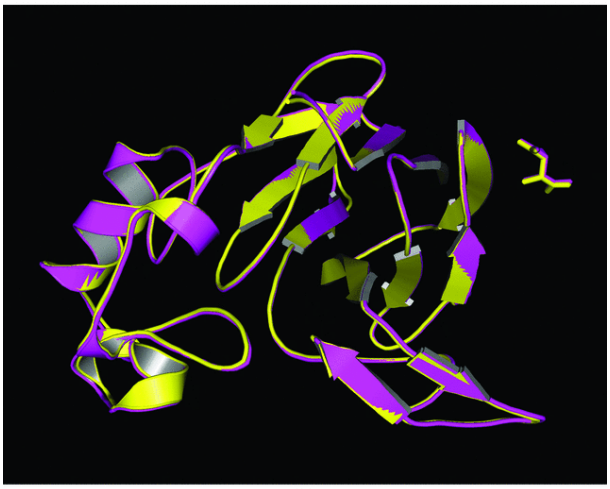

(*b*)

Figure 2.8. (a) Superposition of the room-pressure glucose isomerase structure (yellow) from 8xia (Carrell et al., 1989) and the pressure-cooled structure (magenta). The r.m.s. deviation between C^{α} atoms in the two model is 0.327 Å and the r.m.s. deviation between all atoms is 0.459 Å. (b) Superposition of the room-pressure cooled thaumatin structure (yellow) from 1lxz (Charron et al., 2002) and the pressure-cooled structure (magenta). The r.m.s. deviation between C^{α} atoms in the two model is 0.299 Å and the r.m.s. deviation between all atoms is 0.472 Å. These structural deviations are comparable to the structural change on dropping the temperature.

It is known that pressure certainly perturbs many proteins in solution. There is a large amount of literature demonstrating that pressures encountered in the biosphere (<130 MPa) have large effects on the functioning of many proteins (Unno *et al*., 1990; Moss *et al*., 1991; Jung, 2002; Verkhusha *et al*., 2003). At some level of resolution, these functional perturbations must be manifest as structural perturbations. As mentioned above, in most cases pressures below 200 MPa seem to only slightly perturb protein backbone structures, involving atomic displacements of a few tenths of an angstrom. The fact that a structural perturbation is small does not necessarily mean that the functional effect is also small. For example, recall that the spatial displacements of the heme group upon binding of oxygen in hemoglobin or myoglobin are under 1 Å.

Similarly, the structural perturbations caused by simply cooling to liquid-nitrogen temperature, which are generally of similar magnitude, would likely have enormous consequences for protein function if only these effects were not masked by the cooling of water and the peptide glass transition. This comes as no surprise. The functions of many proteins are dramatically sensitive to temperature changes above 273 K. Yet the corresponding changes in structure may be small and may not be straightforward to understand in functional terms (Weber & Drickamer, 1983).

An analogy is useful here. Imagine that one wanted to understand an automobile gasoline engine but knew nothing about engines other than that they delivered rotary power to a car. Imagine that one had the static three-dimensional structures at 1 mm resolution of two almost identical engines. The only differences between the two engines are that one has a spark-plug gap expanded by a few tenths of a millimetre and the cylinders out of round by a few tenths of a millimetre. Since so little was known a priori about engines, either structure would be greatly and equally helpful in understanding how engines worked, because it would be possible to identify the parts

of the engine, their relative positions and from this perhaps infer how mechanical power were generated. If one now tried to operate the two engines, it would become apparent that one operates very much worse than the other, if it operates at all. Would the two structural maps allow one to understand why one engine functions differently to the other? It can be achieved only with great difficulty, because the level of structural difference is below the observed resolution. Understanding at this level would involve either higher resolution or experimentation of what happens, for instance, when the gaps of the spark plugs are intentionally changed or inferences based on small changes in a relatively large mass (*e.g.* a piston out of round).

In summary, high-pressure cooling is a promising approach for crystals that are difficult to flash-cool by conventional methods; this method is now being used by CHESS users. The level of structural perturbation induced by pressure cooling is small in all cases examined so far, typically a few tenths of an angstrom. In terms of an overall structural determination, which is the object of the majority of crystallographic experiments, this level of perturbation is acceptable and is of the same magnitude as the perturbations induced by cooling to cryogenic temperatures. However, in terms of the detailed structure that might occur, for instance, around active sites, the effect of such small perturbations may not be negligible.

REFERENCES

Carrell, H. L., Glusker, J. P., Burger, V., Manfre, F., Tritsch, D. & Biellmann, J.-F. (1989). *Proc. Natl Acad. Sci*. USA, **86**, 4440–4444.

Charron, C., Kadri, A., Robert, M.-C., Giegé, R. & Lorber, B. (2002). *Acta Cryst*. D**58**, 2060–2065.

Chayen, N. E., Boggon, T. J., Cassetta, A., Deacon, A., Gleichmann, T., Habash, J., Harrop, S. J., Helliwell, J. R., Nieh, Y. P., Peterson, M. R., Raftery, J., Snell, E. H., Hadener, A., Niemann, A. C., Siddons, D. P., Stojanoff, V., Thompson, A. W., Ursby, T. & Wulff, M. (1996). *Q. Rev. Biophys*. **29**, 227–278.

Collaborative Computational Project, Number 4 (1994). *Acta Cryst*. D**50**, 760–763.

DeLano, W. (2002). *PyMol*. DeLano Scientific, San Carlos, CA, USA.

Franks, F. (1982). Editor. *Water – A Comprehensive Treatise*, Vol. 7, pp. 215–338. New York: Plenum.

Franks, F. (1985). *Biophysics and Biochemistry at Low Temperature*. Cambridge University Press.

Garman, E. (1999). *Acta Cryst*. D**55**, 1641–1653.

Garman, E. F. & Schneider, T. R. (1997). *J. Appl. Cryst*. **30**, 211–237.

Ghormley, J. A. & Hochanadel, C. J. (1971). *Science*, **171**, 62–64.

Hope, H. (1988). *Acta Cryst*. B**44**, 22–26.

Hope, H. (1990). *Annu. Rev. Biophys. Biophys. Chem*. **19**, 107–126.

Juers, D. H. & Matthews, B. W. (2001). *J. Mol. Biol.* **311**, 851–862.

Juers, D. H. & Matthews, B. W. (2004). *Q. Rev. Biophys*. **37**, 1–15.

Jung, C. (2002). *Biochem. Biophys. Acta*, **1595**, 309–328.

Kanno, H., Speedy, R. J. & Angell, C. A. (1975). *Science*, **189**, 880–881.

Ko, T.-P., Day, J., Greenwood, A. &McPherson, A. (1994). *Acta Cryst*. D**50**, 813–825.

Kriminski, S., Caylor, C. L., Nonato, M. C., Finkelstein, K. D. & Thorne, R. E. (2002). *Acta Cryst*. D**58**, 459–471.

Kriminski, S., Kazmierczak, M. & Thorne, R. E. (2003). *Acta Cryst*. D**59**, 697–708.

Kundrot, C. E. & Richards, F. M. (1987). *J. Mol. Biol.* **193**, 157–170.

Leslie, A. G. W. (1992). *Jnt CCP4–ESRF/EACBM Newsl. Protein Crystallogr*. **26**.

McRee, D. (1999). *J. Struct. Biol*. **125**, 156–165.

Matthews, B. W. (1968). *J. Mol. Biol.* **33**, 491–497.

Mishima, O., Calvert, L. D. & Whalley, E. (1984). *Nature* (London), **310**, 393–395.

Mishima, O. & Stanley, H. E. (1998). *Nature* (London), **396**, 329–335.

Moss, G. W., Lieb, W. R. & Franks, N. P. (1991). *Biophys. J*. **60**, 1309– 1314.

Murshudov, G. N., Vagin, A. A. & Dodson, E. J. (1997). *Acta Cryst*. D**53**, 240–255.

Refaee, M., Tezuka, T., Akasaka, K. & Williamson, M. P. (2003). *J. Mol. Biol.* **327**, 857–865.

Rodgers, D. W. (1994). *Structure*, **2**, 1135–1140.

Röttger, K., Endriss, A., Ihringer, J., Doyle, S. & Kuhs, W. F. (1994). *Acta Cryst*. B**50**, 644–648.

Steller, I., Bolotovsky, R. & Rossman, M. G. (1997). *J. Appl. Cryst*. **30**, 1036–1040.

Thomanek, U. F., Parak, F., Mössbauer, R. L., Formanek, H., Schwager, P. & Hoppe, W. (1973). *Acta Cryst*. A**29**, 263–265.

Unno, M., Ishimori, K. & Morishima, I. (1990). *Biochemistry*, **29**, 10199–10205.

Urayama, P., George, N. P. & Gruner, S. M. (2002). *Structure*, **10**, 51–60.

Vagin, A. & Teplyakov, A. (1997). *J. Appl. Cryst*. **30**, 1022–1025.

Verkhusha, V. V., Pozhitkov, A. E., Smirnov, S. A., Borst, J. W., Hoek, A., Klyachko, N. L., Levashov, A. V. & Visser, A. J. W. G. (2003). *Biochim. Biophys. Acta*, **1622**, 192–195.

Watowich, S. J., Skehel, J. J. & Wiley, D. C. (1995). *Acta Cryst*. D**51**, 7–12.

Weber, G. & Drickamer, H. G. (1983). *Q. Rev. Biophys*. **16**, 89–112.

Young, A. C.M., Dewan, J. C., Nave, C. & Tilton, R. F. (1993). *J. Appl. Cryst*. **26**, 309–319.

Zhang, H., Teng, M., Niu, L., Wang, Y., Wang, Y., Liu, Q., Huang, Q., Hao, Q., Dong, Y. & Liu, P. (2004). *Acta Cryst*. D**60**, 974–977.

CHAPTER THREE
SOLUTION OF PROTEIN CRYSTALLOGRAPHIC STRUCTURES BY HIGH-PRESSURE CRYOCOOLING AND NOBLE-GAS PHASING*

3.1 Introduction

In X-ray crystallography, only the intensities of the diffraction reflections can directly be measured and the relative phase information is lost. This is the well known phase problem of X-ray crystallography. Various methods have been developed over the years to solve the phase problem (Dauter, 2006). The multiple isomorphous replacement (MIR) method was used to solve the first protein structures. However, it requires multiple crystals which have different kinds of heavy atoms as isomorphous derivatives. Furthermore, nonisomorphism between the crystals is very often a limitation. With the advent of intense and tunable synchrotron-radiation sources, methods based on the anomalous scattering that occurs when the scattered X-ray energy is near an absorption edge have become very popular. The multiple-wavelength anomalous diffraction (MAD; Hendrickson, 1999) method requires the collection of several complete sets of data at different carefully tuned energies spanning the absorption edge of incorporated resonant scattering atoms. The multiple passes increase the likelihood that radiation damage degrades the quality of the crystal and limits the accuracy of the intensity measurements. In some cases, the protein has naturally occurring suitable resonant atoms such as Fe. In more common cases, the atom has to be added to the protein; for example, during expression by replacement of S-methionine with Se-methionine. Alternatively, the crystal may have unique sites for

* Reproduced with permission from Kim, C. U., Hao, Q & Gruner, S. M. (2006). *Acta Cryst*. D**62**, 687-694. Copyright 2006 International Union of Crystallography.

binding of specific resonant scatterers, as for example with soaks in heavy-atom solutions or by exposure to pressurized xenon gas.

More recently, single-wavelength anomalous diffraction (SAD) has been utilized to solve structures (Shen *et al*., 2006). SAD is an experimentally simpler version of MAD. SAD does not require accurate X-ray wavelength tuning and the radiation damage is less problematic because only a single complete data set is required. The phase ambiguity that naturally arises in SAD phasing can be successfully broken using the Sim distribution (Hendrickson & Teeter, 1981), density modification (Wang, 1985) or direct methods (Fan *et al*., 1984; Harvey *et al*., 1998). Structures are increasingly being solved by SAD phasing, which is now of interest for high-throughput crystallography.

Since SAD phasing relies on a single data set, accurate and highly redundant intensity measurements are required, especially when weak anomalous scatterers such as sulfur are used (Ramagopal *et al*., 2003). Assuming that a high-quality protein crystal is available, the next important step for accurate data collection is to find a suitable way to cryocool the crystal in order to minimize radiation damage. Protein crystals have most commonly been frozen by flash-cryocooling to near liquid-nitrogen temperatures by immersion in cold gas or liquid at ambient pressure (Garman & Owen, 2006). There are two challenges with this procedure. Firstly, there is usually a requirement to find cryoprotectants to facilitate amorphous ice formation and reduce damage upon cryocooling. Finding suitable cryoprotectants is a trial-and-error process that is sometimes unsuccessful. Secondly, even if acceptable cryoprotectants can be found, the crystal quality is often degraded upon flash-cryocooling. This is manifested as an increase in the mosaic spread and a decrease in the observable diffraction resolution. This degradation in crystal quality limits the ability to phase the structure.

Recently, we have reported an alternative procedure, high-pressure cryocooling, for protein-crystal cryoprotection that does not require penetrative cryoprotectants (Kim *et al*., 2005). Using high-pressure cryocooling, exceptionally high quality diffraction data were collected from several different kinds of protein crystals. Since this method involves the use of helium gas as a pressurizing medium, it is of interest to see whether the method could be extended to diffraction phasing by the incorporation of heavy noble gases such as krypton or xenon.

It has been reported that the noble gases krypton and xenon bind to several crystallized proteins (Schoenborn *et al*., 1965; Tilton *et al*., 1984; Schiltz *et al*., 1994; Prangé *et al*., 1998) and they have been used to solve protein structures (for a review, see Fourme *et al*., 1999). Krypton (atomic number Z = 36) is lighter than xenon (Z = 54), but its *K* edge (14.3 keV, 0.87Å) is readily accessible on most synchrotron beamlines, so krypton derivatization provides an opportunity to conduct anomalous diffraction experiments. Schiltz *et al*. (1997) reported that porcine pancreas elastase (PPE; 26 kDa) was successfully phased with a single half-occupied krypton by single isomorphous replacement with anomalous scattering (SIRAS). In the study, the anomalous signal was treated as an auxiliary source to improve the initial phase obtained by the isomorphous replacement signal. Later, krypton MAD phasing was successfully applied to the relatively small proteins myoglobin (17 kDa) and SP18 (18 kDa) (Cohen *et al*., 2001). Those crystals were incubated in 2.76 MPa krypton gas for 2 min; the krypton pressure was then released and the crystals were flash-cryocooled in a nitrogen cold stream (100 K) at ambient pressure with the help of cyroprotectants (25% sucrose for myoglobin, 25% ethylene glycol for SP18). Four krypton binding sites were found in myoglobin (occupancies of 0.68, 0.28, 0.17 and 0.08, respectively) and one krypton site was found in SP18 (occupancy of 0.42).

In this paper, porcine pancreas elastase (PPE) was selected as a test case for krypton SAD phasing. A half-occupied krypton in the PPE protein (Schiltz *et al*., 1997) has an anomalous scattering strength of 1.9 e at its *K* absorption peak (14.3 keV). This anomalous strength in PPE (240 residues, 26 kDa) is predicted to give a small Bijvoet amplitude ratio ($<|\Delta F|>/<F>$, 380 water molecules in the PPE protein hydration layer were included in the calculation) of 0.86 % (Hendrickson & Teeter, 1981). The solvent content of a PPE crystal is relatively low (35–40 %), which makes density modification by solvent flattening less efficient (Ramagopal *et al*., 2003). Here, we report a successful case of krypton SAD phasing of a PPE crystal, which had a single 0.31 occupied krypton site (estimated Bijvoet ratio of 0.53 %) and 35 % solvent content. The key feature that allowed this challenging PPE system to be phased was the very high quality diffraction obtained by the high-pressure cryocooling of the crystal.

3.2 Experimental

3.2.1 Materials and sample preparation

3.2.1.1 Crystallization of porcine pancreas elastase (PPE)

Lyophilized PPE (catalog No. 20929) purchased from SERVA (Heidelberg, Germany) was used without further purification. Crystals were grown by the hanging-drop method by mixing 2 µl reservoir solution containing 30 mM sodium sulfate and 50 mM sodium acetate pH 5.0 with 2 µl of a 25 mg/ml protein solution in pure water (modified from Shotton *et al*., 1968). Crystals appeared in a few days and crystals of dimensions 0.1 × 0.1 × 0.2 mm were used for the Kr flash cryocooling and Kr–He high-pressure cryocooling as described below.

3.2.1.2 Kr flash-cryocooling at ambient pressure

To study the krypton association/dissociation kinetics of PPE, crystal samples were prepared using a Xenon Chamber (Hampton Research, Laguna Niguel, CA, USA). Crystals were first coated with oil to remove excess mother liquor on the surface of the crystals and to prevent dehydration during gas pressurization. We previously investigated various oils and found that NVH oil (Hampton Research) works well with many proteins and protects against dehydration during gas processing. Hence, NVH oil was used in this study. Three NVH oil-coated crystals were pressurized to the maximum pressure level of the gas chamber (4 MPa). After 10 min, the pressure was released in 20 s and the crystals were left in air for 5 s, 3 min and 9 min (named Kr10m_5s, Kr10m_3m and Kr10m_9m, respectively). The crystals were then flash-cryocooled at ambient pressure by plunging directly into liquid nitrogen. In parallel, an additional four crystals were pressurized to 4 MPa for 45 min, left in air for 5 s, 10 s, 3 min and 9 min and then flash-cryocooled in the same way (named Kr45m_5s, Kr45m_10s, Kr45m_3m and Kr45m_9m, respectively). The flash-cryocooling was carried out without adding penetrative cryoprotectants to compare the diffraction with that of the Kr–He high-pressure cryocooled crystals, which also do not contain additional penetrative cryoprotectants.

3.2.1.3 Kr–He high-pressure cryocooling

Details of the He high-pressure cryocooling process are described in Kim *et al*. (2005). Briefly, crystals are picked up in a cryoloop in a droplet of Hampton NVH oil. The purpose of the oil is to prevent dehydration of the crystal during the pressurization manipulations. As shown in Kim *et al*. (2005), crystals that are oil-coated and flash-cryocooled, as opposed to pressure-cryocooled, suffer considerably more cooling damage, i.e. the oil alone is not an adequate cryoprotectant. Although crystals with

penetrative cryoprotectants can also be pressure-cryocooled, in our experience penetrative cryoprotectants are usually not needed with pressure cryocooling, so they were not used. The oil-coated crystals are loaded into the high-pressure cryocooling apparatus, which is then pressurized with helium gas to pressures in the 100–200 MPa range. Once at high pressure, a magnetic constraint is released and the crystals fall down a length of high-pressure tubing into a cold zone kept at liquid-nitrogen temperature. The helium pressure is released and the crystals are thereafter handled at ambient pressure, just as normal flash-cryocooled crystals for cryocrystallographic data collection. The process for Kr–He high-pressure cryocooling is similar, but a little more complex. Firstly, three PPE crystals were carefully coated with NVH oil and loaded into the three pressure tubes of the apparatus, which were then connected to the gas compressor. The crystals were then pressurized with krypton gas to 10 MPa. After 1 h, the compressed krypton gas was released, liquid nitrogen was poured into the liquid nitrogen bath of the pressure cryocooling apparatus and the crystals were re-pressurized with helium. After 90 s the helium pressure reached 155 MPa and the crystals were dropped into their respective tubes and cryocooled to liquid-nitrogen temperature at 155 MPa pressure. Overall, the time from krypton pressure release to cryocooling was about 200 s. The helium pressure was released 6 min after cryocooling and the crystals were transferred into cryocaps under liquid nitrogen for data collection. The three samples were named KrHe_1, KrHe_2 and KrHe_3, respectively.

3.2.2 Data collection

Diffraction data were collected at the Cornell High Energy Synchrotron Source (CHESS) on beamline F2 (beam diameter= 150 μm, ADSC Quantum 210 CCD detector). In all cases the detector face was perpendicular to the incident beam (2θ

value of zero). All data were collected at 110 K (N_2- gas stream) and ambient pressure with an oscillation angle ($\Delta\varphi$) of 1.0˚ per image.

3.2.2.1 Data collection for Kr flash-cryocooled crystals

Diffraction data from seven Kr flash-cryocooled crystals were collected at 12.6 keV (0.9796 Å). The exposure time was 20– 40 s and the distance between the crystal and detector (d) was 150–200 mm. A data set containing 100–120 frames was collected for structure determination from each crystal.

3.2.2.2 Data collection for Kr–He high-pressure cryocooled crystals

Diffraction data from three Kr–He high-pressure cryocooled crystals were collected at the absorption peak. In order to locate the 14.324 keV *K* edge of krypton, the monochromator crystals [Si (111)] were moved into the 14 keV region and calibrated using the L_I edge of gold at 14.353 keV. The PPE sample was then loaded onto a goniometer and a fluorescence scan was performed to find the absorption peak energy. Data were collected at the peak energy, 14.324 keV for the first two crystals (KrHe_1, KrHe_2) and 14.326 keV for the last one (KrHe_3), by the inverse-beam mode with a wedge of ten frames. The distance between the crystal and detector was 153–180 mm. The exposure time for each frame was 50–60 s. A total of 360 frames were collected from each crystal.

3.2.3 Data processing, phasing and model building

3.2.3.1 Kr flash-cryocooled crystals

Data were indexed, pre-refined, integrated, post-refined, scaled and merged with *HKL2000* (Otwinowski & Minor, 1997). The initial structures were determined by the

molecular-replacement method using *MOLREP* (Vagin & Teplyakov, 1997) from the *CCP4* program suite (Collaborative Computational Project, Number 4, 1994) using the known protein coordinates 1c1m (Prangé *et al*., 1998) from the PDB. The structures were then refined against the data sets with *REFMAC5* (Murshudov *et al*., 1997). As krypton occupancies and thermal *B* factors are highly correlated, the krypton occupancy was manually adjusted so that the refined thermal *B* factor of the Kr atom was close to the average thermal *B* factor of the crystallographically refined main-chain atoms.

3.2.3.2 Kr–He high-pressure cryocooled crystals

Data were indexed, pre-refined, integrated, post-refined, scaled and merged with *HKL2000* (Otwinowski & Minor, 1997) as above but with the 'scale anomalous' flag to keep Bijvoet pairs separate. In the SAD phasing, the anomalous scattering substructure was initially solved and refined using the program *SAPI* (Hao *et al*., 2003). The absolute configuration of the substructure was determined with *ABS* (Hao, 2004). The heavy-atom position was then input into *OASIS-2004* (Wang *et al*., 2004) for SAD phasing. Afterwards, density modification was performed using *DM* (Cowtan, 1994). Auto model building was performed with *ARP/wARP* (Perrakis *et al*., 1999) and *REFMAC5* (Murshudov *et al*., 1997) was used for refinement.

3.3 Results

3.3.1 Kr flash-cryocooled crystals and preliminary krypton occupancy study

The crystallographic data statistics for the Kr flash-cryocooled crystals are summarized in Table 3.1. The fact that crystal Kr45m_5s had almost the same

Table 3.1. Summary of crystallographic statistics for the Kr flash cryocooled crystals at ambient pressure. Values in parentheses are for the last shell.

	Kr10m_ 5s	Kr10m_ 3m	Kr10m_ 9m	Kr45m_ 5s	Kr45m_ 10s	Kr45m_ 3m	Kr45m_ 9m
Wavelength (Å)	0.9796	0.9796	0.9796	0.9796	0.9796	0.9796	0.9796
Space group	$P2_12_12_1$	$P2_12_12_1$	$P2_12_12_1$	$P2_12_12_1$	$P2_12_12_1$	$P2_12_12_1$	$P2_12_12_1$
Unit-cell parameters (Å)	a= 50.4, b=58.1, c= 74.9	a= 50.5, b=58.2, c= 74.8	a= 50.2, b=57.9, c= 74.8	a= 49.3, b=57.3, c= 74.1	a=50.0, b=57.7, c= 74.5	a= 50.3, b=57.8, c= 74.4	a= 50.4, b=58.1, c= 75.0
Solvent content (%)	41	41	41	39	40	40	41
Mosaicity (°)	0.87	0.84	0.96	1.27	0.46	1.56	0.80
Resolution range (Å)	30-1.9 (1.97-1.9)	30-1.8 (1.86-1.8)	30-1.8 (1.86-1.8)	30-1.8 (1.86-1.8)	30-1.6 (1.66-1.6)	30-2.0 (2.07-2.0)	30-1.8 (1.86-1.8)
No. of observations	77092	93308	93121	89297	129576	51588	95105
No. of unique reflections	17551	20803	20973	19559	28401	14552	21175
Multiplicity	4.4 (2.7)	4.5 (3.9)	4.4 (3.7)	4.6 (4.2)	4.6 (3.6)	3.5 (2.6)	4.5 (4.0)
Completeness (%)	97.5 (93.2)	98.4 (95.5)	99.4 (97.0)	96.4 (95.7)	98.6 (99.9)	95.2 (89.4)	99.4 (95.6)
Rsym (%)	8.4 (27.3)	9.1 (40.6)	7.8 (28.8)	13.7 (42.9)	7.8 (24.4)	5.2 (20.5)	8.6 (23.7)
I/σ(I)	18.6 (3.7)	17.7 (2.9)	20.6 (3.3)	12.5 (2.5)	21.7 (4.8)	25.8 (5.0)	19.7 (4.5)
R value (%)	17.8	18.7	18.7	18.1	18.5	18.1	18.3
R_{free} value (%)	24.3	24.2	23.3	22.8	21.9	26.6	23.4
Average B factor ($Å^2$)	18.2	16.8	15.8	19.1	14.0	17.6	16.4
No. of water molecules	230	275	275	274	395	239	315
R.m.s. deviation from ideality							
Bond lengths (Å)	0.016	0.016	0.015	0.014	0.011	0.020	0.014
Angles (°)	1.5	1.5	1.5	1.5	1.3	1.8	1.4
Kr occupancy	0.47	0.13	0.09	0.43	0.32	0.20	0.05
Kr B factor ($Å^2$)	16.4	14.8	13.7	16.6	10.9	16.2	14.1

occupancy (0.43) as crystal Kr10m_5s (0.47) confirms that the krypton binding to the PPE crystal under our experimental arrangement was complete within 10 min. The average krypton occupancy of crystal Kr10m_5s and Kr45m_5s was 0.45 and it appeared to be reasonable compared with the previously reported value of 0.49 at 5.6 MPa (Schiltz *et al*., 1997). This occupancy (0.45) and the applied pressure (P = 4 MPa) were used to estimate the equilibrium constant (λ) of the krypton-binding reaction to PPE in the Langmuir isotherm: occupancy = λP/ (1 + λP) (Schiltz *et al*., 1997). The calculated value (λ) was approximately 0.2 (MPa^{-1}). The Kr10m and Kr45m time series suggest that the krypton occupancy depends on the time for which crystals are left in a krypton-free environment: up to about 3 min, krypton diffused out from crystals relatively quickly. With longer times (from 3 to 9 min) the occupancy decreased more slowly.

These preliminary results were used to estimate the krypton occupancy in PPE crystals prepared by the Kr–He high-pressure cryocooling process described in 3.2.1.3. Firstly, the krypton pressurization of PPE crystals was long enough for saturation of the krypton-binding site. The maximum krypton occupancy at 10 MPa was estimated to be 0.67 using the Langmuir isotherm with the binding equilibrium constant λ = 0.2 MPa^{-1}. The ratio (0.37) of average krypton occupancy (0.165) of Kr10m_3m and Kr45m_3m to that (0.45) of Kr10m_5s and Kr45m_5s was used to roughly calculate the expected occupancy for the crystals left for 200 s before being high-pressure cryocooled. The estimated occupancy was approximately 0.25 or less.

3.3.2 Kr–He high-pressure cryocooled crystals and krypton SAD phasing

The crystallographic data statistics of the Kr–He high pressure cryocooled crystals are summarized in Table 3.2. Since the anomalous scattering substructure was

Table 3.2. Summary of crystallographic statistics for the Kr-He high pressure cryocooled crystals. Values in parentheses are for the last shell.

	KrHe_1	KrHe_2	KrHe_3
Wavelength (Å)	0.8656	0.8656	0.8654
Space group	$P2_12_12_1$	$P2_12_12_1$	$P2_12_12_1$
Unit-cell parameters (Å)	a= 50.2, b=58.2, c= 74.6	a= 46.7, b=57.9, c= 73.9	a= 46.6, b=57.7, c= 73.7
Solvent content (%)	41	35	35
Mosaicity (º)	0.39	0.26	0.32
Resolution range (Å)	30-1.5 (1.55-1.5)	30-1.5 (1.55-1.5)	30-1.3 (1.35-1.3)
No. of observations	433653	428805	614816
No. of unique reflections *	67826	61882	92573
Multiplicity *	6.4 (2.7)	6.9 (4.2)	6.6 (3.2)
Completeness (%)	99.9 (98.8)	99.5 (95.1)	98.0 (84.7)
Rsym (%)	7.6 (18.2)	6.7 (12.4)	5.3 (27.8)
I/σ(I)	28.2 (4.0)	35.7 (10.8)	42.7 (3.9)
$\langle\lvert\Delta F\rvert\rangle/\langle F\rangle$ (%)	2.44	2.20	3.19
$\langle\lvert\Delta F\rvert\rangle/\langle\sigma(\Delta F)\rangle$	0.57	0.84	0.84
R value (%)	18.7	20.7	21.6
R_{free} value (%)	22.5	24.3	23.5
Average B factor (Å^2)	14.1	13.5	14.0
No. of water molecules	435	361	387
R.m.s. deviation from ideality			
Bond lengths (Å)	0.009	0.010	0.008
Angles (º)	1.2	1.5	1.4
Kr occupancy	0.14	0.22	0.31
Kr B factor (Å^2)	10.5	10.06	10.15

* The Bijvoet pairs are kept separate in the statistics.

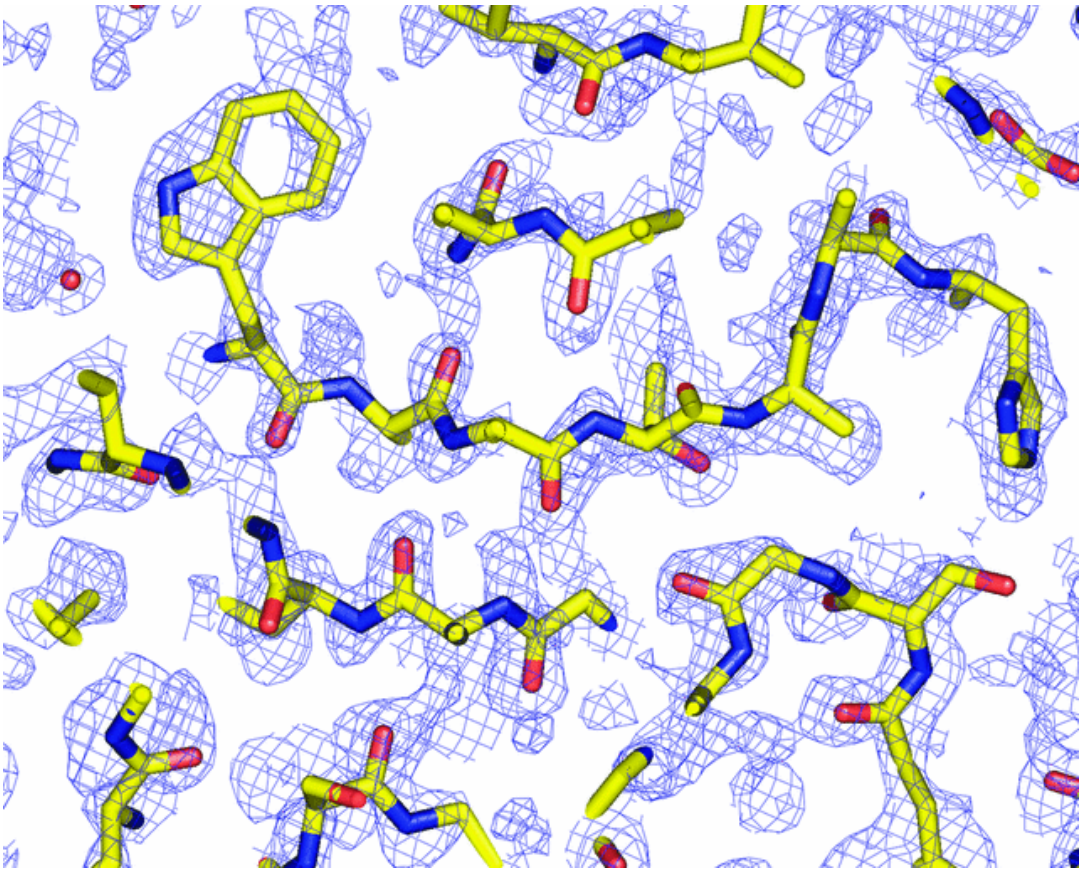

Figure 3.1. Electron-density map before density modification at 1.3 Å resolution. The final refined model solved by molecular replacement was superimposed for the map evaluation. The figure of merit is 0.5 and the map correlation coefficient calculated with the final refined density map is 0.58 for the main chain and 0.42 for side chains. The density map, contoured at the 1σ level, was prepared using *PyMOL* (DeLano, 2002)

not clearly located in the KrHe_1 and KrHe_2 data, the krypton SAD phasing was performed with the KrHe_3 data set.

A single Kr-atom position was found and refined by *SAPI* using anomalous differences at 2.5 Å resolution with an *R* value of 30.1 %. The absolute configuration of the substructure was determined with *ABS* and then the position was input into *OASIS-2004* for SAD phasing at 1.3 Å. To evaluate the phase quality, an electron-density map (Fig. 3.1) was generated using *PyMol* (DeLano, 2002). Density modification was performed using *DM* and the overall figure of merit increased from 0.5 to 0.695. Although the crystal KrHe_3 had very low solvent content (35 %), density modification by solvent flattening seemed to improve the map quality.

Therefore, the phases after *SAPI/ABS/OASIS-2004/DM* were used for model autobuilding in *ARP/wARP* with the default mode. After ten cycles of autobuilding, 219 residues out of 240 were found and docked in the electron density. The final *R* value was 27.0 % with a connectivity index of 0.93. It was noticed in the electron-density map that most of the unassigned residues were distributed in the highly disordered regions adjacent to the solvent layer.

In order to investigate the effect of resolution on the SAD phasing power, the 1.3 Å data set was cut off at resolutions of 1.5, 1.7, 1.8, 1.9, 2.0 and 2.5 Å and each data set was input into *OASIS-2004* for SAD phasing. Although the figure-of-merit values at the cutoff resolutions were higher than the value at 1.3 Å, it turned out that the high-resolution data were essential for successful model autobuilding in *ARP/wARP*. At better resolution than 1.7 Å, *ARP/wARP* was able to find approximately 220 residues. However, *ARP/wARP* had difficulty in finding residues when the cutoff was raised to 1.8 Å and no residues were properly found with lower resolution data sets. Details of the results are summarized in Table 3.3.

Table 3.3. SAD phasing of KrHe_3 at different resolutions. The map correlation coefficient was calculated with the $2F_o$- F_c map of the final refined structure solved by molecular replacement.

	30-1.3 Å	30-1.5 Å	30-1.7 Å	30-1.8 Å	30-1.9 Å	30-2.0 Å	30-2.5 Å
No. of unique reflections *	48640	32478	22469	18970	16203	13933	7252
<|ΔF|>/<F> (%)	3.19	2.11	1.74	1.64	1.56	1.52	1.38
<|ΔF|>/ <σ (ΔF)>	0.84	1.07	1.25	1.34	1.40	1.45	1.59
F.O.M. after *DM*	0.695	0.817	0.803	0.784	0.743	0.777	0.742
No. of residues found	219	224	227	34	0	9	0
No. of residues docked in sequence	219	224	227	9	0	0	0
Map correlation coefficient for main chain	0.71	0.79	0.74	0.70	0.64	0.60	0.40
Map correlation coefficient for side chain	0.56	0.66	0.59	0.56	0.51	0.47	0.32
R value (%)	27.0	21.8	21.5	23.7	23.0	19.7	18.5
Connectivity index	0.93	0.95	0.96	0.77	0.60	0.80	0.50

* The Bijvoet pairs are merged in the statistics.

To estimate the krypton occupancy by the same standard that was applied for the Kr flash-cryocooled crystals, the final refined structures of the Kr–He high-pressure cryocooled crystals were solved by the molecular-replacement method as described in 3.2.3.1. Since the anomalous signals were very weak in all cases, the signals were ignored in the model construction process. As predicted, KrHe_1 and KrHe_2 had lower krypton occupancy (0.14 and 0.22, respectively) than KrHe_3 (0.31). Details of the refined structures are summarized in Table 3.2.

3.4 Discussion

It was shown that a single 0.31 occupied krypton site could successfully phase the PPE structure, which contains 240 residues (26 kDa). Since the estimated Bijvoet amplitude ratio ($<|\Delta F|>/<F>$) was only 0.53 % and the solvent content was low (35 %), the high-quality data obtained by Kr–He high-pressure cryocooling were essential for successful SAD phasing. The diffraction quality of PPE crystals prepared by Kr flash cryocooling at ambient pressure and Kr–He high-pressure cryocooling was compared in terms of resolution limit and mosaicity (Fig. 3.2). The average resolution [cutoff $I/\sigma(I) \sim 3.0$] and mosaicity of seven Kr flash-cryocooled crystals at ambient pressure (Table 1) were 1.7 Å and 0.97˚, respectively. The average resolution [cutoff $I/\sigma(I) \sim 3.0$] and mosaicity of three Kr–He high-pressure cryocooled crystals (Table 2) were 1.3 Å and 0.32˚, respectively. This superior diffraction obtained by Kr–He high-pressure cryocooling was comparable to that of the PPE crystals prepared by successful flash-cryocooling at ambient pressure with 20% glycerol as a cryoprotecting agent (Mueller-Dieckmann *et al*., 2004): the average resolution and mosaicity of nine PPE crystals prepared by the flash cryocooling method with the cryoprotectant were 1.5 Å (or better) and 0.41˚, respectively.

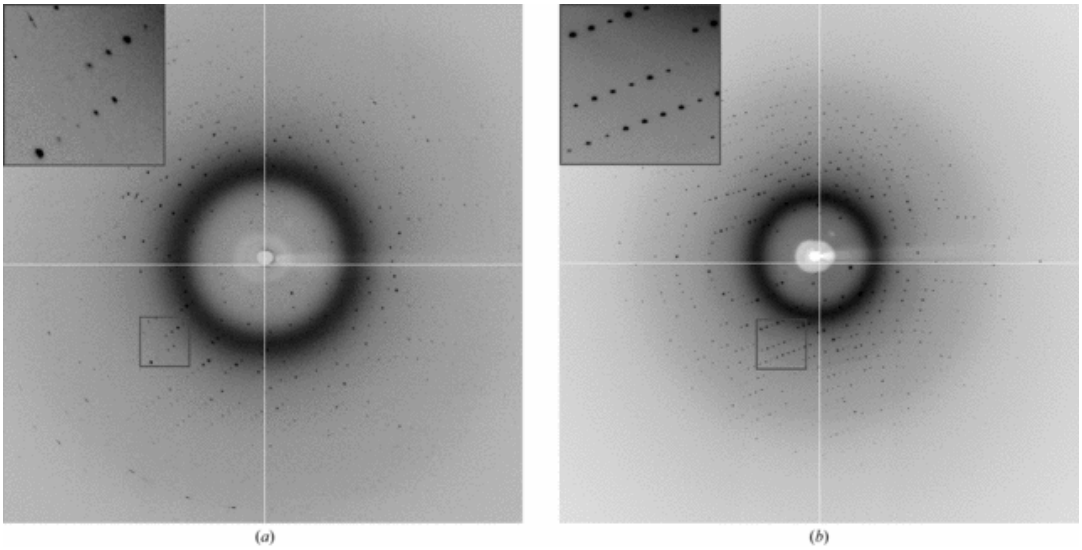

Figure 3.2. Diffraction images of PPE crystals. (a) Diffraction image of the crystal Kr10m_5s prepared by Kr flash-cryocooling at ambient pressure. The resolution limit [I/σ(I) ~ 3.0] is around 1.8 Å and the mosaicity is 0.87°. The diffraction spots in the enlarged region look smeared. (b) Diffraction image of the crystal KrHe_3 prepared by Kr-He high-pressure cryocooling. The resolution limit [I/σ(I) ~ 3.0] is around 1.2 Å and the mosaicity is 0.32°. The diffraction spots in the enlarged region look compact. This high-quality diffraction was obtained without adding any penetrative cryoprotectants.

When very weak anomalous signals are involved, special efforts are often required in data collection to minimize the background scattering (Schiltz *et al*., 1997). However, it should be mentioned that no such special efforts were taken during data collection for this study. Prior to the data collection, there was concern that the oil around the crystals might produce a significant background and hamper accurate signal measurement. However, accurate diffraction measurement was possible even in the presence of the oil background. We believe that the superior crystal diffraction achieved using high-pressure cryocooling compensated for the background produced by the oil. Furthermore, it turned out that the oil coating is actually very useful in the krypton SAD phasing. As the interaction between noble gases and other materials is the result of low-energy interactions (*e.g.* van der Waals forces), the solubility of xenon or krypton is significantly higher in oil than in pure water (Wilhelm *et al*., 1977; Pollack *et al*., 1989). The captured krypton in the oil during the Kr–He high-pressure cryocooling process produced a strong krypton fluorescence signal in the crystal scan step, which dramatically helped to locate the X-ray wavelength precisely at the krypton absorption peak. Moreover, owing to the higher affinity of krypton for oil than pure water, it is likely that krypton can stay in oil longer than in water. Therefore, oil may act as a krypton-buffering medium for the enclosed protein crystals when the outside compressed krypton gas is released. Indeed, the preliminary krypton occupancy study described in 3.3.1 showed that the krypton occupancy in PPE decreased relatively slowly over 9 min.

Capturing sufficient krypton during Kr–He high-pressure cryocooling seemed to be challenging. Since bulk krypton is in a solid phase at liquid-nitrogen temperature and solid krypton in the apparatus would hamper removal of the pressure-cryocooled crystals from the pressure tubings, the krypton pressure was released before filling the liquid-nitrogen bath. Limitations with the existing apparatus regarding the time it took

to vent krypton and then pressure with helium meant that the crystals were exposed to low krypton partial pressure (0.1 MPa or less) for about 200 s before being high-pressure cryocooled. Even with the buffering effect of the oil, considerable krypton seemed to escape as soon as the krypton pressure was vented. The 200 s time interval was limited by the time required to cryocool the sample assembly to liquid nitrogen temperature (about 80 s) and the time to increase the helium pressure to over 100 MPa for the cryoprotection effect (about 80 s). With our existing apparatus, these two processes could not be performed at the same time. However, simple machine modifications would allow the entire pressurization and cryocooling process to occur in less than about 90 s. In this case, the krypton occupancy in PPE would be likely to be higher than the current estimated value of 0.25.

It should be emphasized that the estimated occupancy value is not the upper limit of the actual krypton occupancy. In the Kr flash-cryocooling, the krypton-containing crystals are exposed to air, i.e. a krypton-free environment. In contrast, in the Kr–He high-pressure cryocooling process, crystals are left in the pressure tubings that are partially filled with krypton gas even after the krypton pressure is released. In addition, although the solubility of helium in pure water is seven times smaller than that of krypton (Wilhelm *et al*., 1977), considerable helium dissolves in water at 155 MPa. We have not explored this quantitatively, but it might affect krypton solubility in water and its kinetics of protein association/dissociation. Indeed, one of the three Kr–He high-pressure cryocooled crystals showed higher occupancy (0.31) than the predicted upper limit value (0.25), suggesting some variability in our experimental setup.

In Kim *et al*. (2005), crystals were left under a high helium pressure for 25 min to be equilibrated. However, in this study the crystal was cryocooled within a few moments of application of a high helium pressure to limit the escape of krypton inside

the crystals. In order to investigate the structural perturbation caused by the Kr–He high-pressure cryocooling, the KrHe_3 structure solved by molecular replacement was compared with the room-temperature structure (PDB code 1c1m). The superposition of the two structures shows little difference: the r.m.s. deviation between the C^{α} backbone atoms in the two structures is 0.413 Å and the r.m.s. deviation between all atoms is 0.458 Å. The major structural deviation was observed in the floppy loop regions. Therefore, it is believed that in this case Kr–He high-pressure cryocooling resulted in relatively little perturbation of the structure.

Although the structural changes of PPE were small, significant differences in unit-cell parameters, especially along the *a* axis, were observed in KrHe_2 and KrHe_3 data. This unit-cell parameter variation contributed to the relatively lower solvent content (35%) of these two data sets. The reduced unit-cell volume of KrHe_2 and KrHe_3 might indicate that repacking of PPE molecules in the crystals occurred during high-pressure cryocooling. Further careful investigation will be required to reveal the correlation between this molecular rearrangement and the resultant diffraction quality.

Since Kr SAD phasing has been successful, our intention is to extend this method to the use of xenon gas. Xenon has many superior aspects for macromolecular crystallography compared with krypton. First, xenon has stronger protein binding (the polarizability of xenon is about twice as large as that of krypton; Schiltz *et al*., 1997) so the occupancy of xenon in a protein is usually higher even when equilibrated at lower partial pressures. For example, the occupancy of xenon in PPE at 0.4 and 0.8 MPa are 0.71 and 0.93, respectively, whereas the occupancy of krypton in PPE at 5.6 MPa is only about 0.5 (Schiltz *et al*., 1994, 1997). Another advantage is the fact that xenon seems to bind to proteins more slowly and in reverse diffuses out more slowly than krypton (Schiltz *et al*., 1997; Cohen *et al*., 2001). This suggests that it would be

possible to obtain higher xenon occupancy during the high-pressure cryocooling process. Finally, xenon has much stronger anomalous signals even far from its K absorption edge (34.56 keV). For comparison, the $\Delta f''$ values of xenon at Cu K_α (8 keV) and Cr K_α (5.4 keV) are 7.4 and 11.8 e, respectively, whereas the $\Delta f''$ of krypton at its *K* absorption peak (14.3 keV) is only 3.8 e. Assuming the diffraction quality of a protein crystal is the same as that of the PPE used for SAD phasing in this study, a single 0.5 occupied xenon can phase a protein as large as 250 kDa at Cu K_α (8 keV) and 650 kDa at Cr K_α (5.4 keV).

At longer wavelengths, the increasing anomalous strength of xenon competes with the accompanying increasing absorption and background, both of which limit the accuracy of the measurement of the anomalous signals. Therefore, the wavelength would have to be carefully selected to maximize the anomalous signal-to-noise. Mueller-Dieckmann *et al*. (2004) tested a xenon–PPE complex in the 0.80–2.65 Å wavelength range. They concluded that the optimal wavelength or anomalous signal data collection was between 2.1 and 2.4 Å, which indicates that xenon SAD phasing at longer wavelengths following high-pressure cryocooling might be generally applicable.

There is another factor that might enhance the benefits of data collection at longer wavelengths: the anomalous signal from S atoms originally present in proteins becomes more meaningful. The $\Delta f''$ of sulfur is 0.56 e at Cu K_α (1.54 Å) and 1.14 e at Cr K_α (2.29 Å) wavelengths. Indeed, sulfur anomalous signals have recently been used for SAD phasing (Hendrickson & Teeter, 1981; Wang, 1985; Dauter *et al*., 1999; Liu *et al*., 2000). In case the xenon anomalous signal itself is insufficiently strong for phasing, the native amino-acid sulfur anomalous signal at longer wavelengths can help the phasing process, where the xenon signal helps locate the S atoms as in the present krypton SAD phasing. As a trial to find additional potential anomalous scatterers, an anomalous difference map was created using *FFT* (Ten Eyck, 1973) with the phases

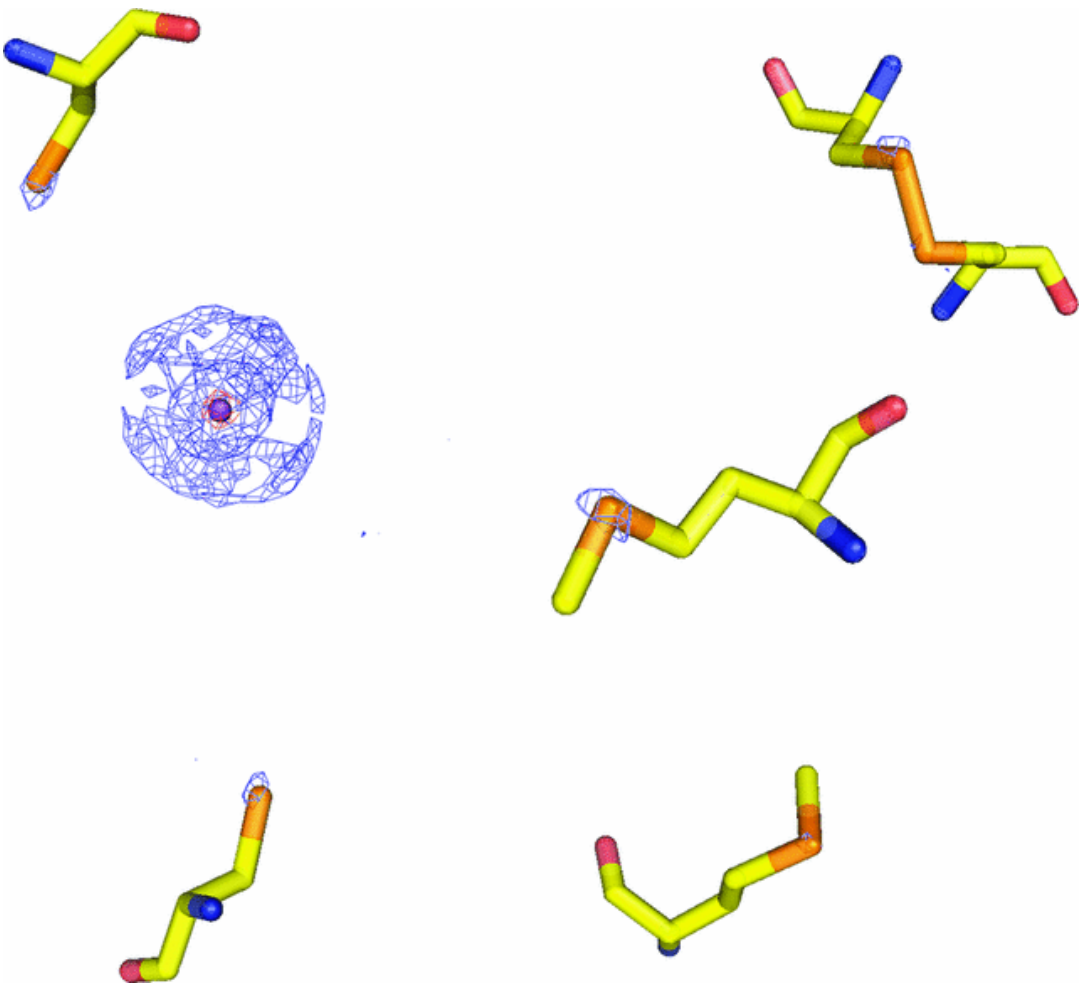

Figure 3.3. Anomalous difference map contoured at the 3.6σ level (blue) generated with the phases calculated from a single 0.31 occupied krypton. The final refined model obtained in the molecular replacement was superimposed to specify the origin of the peaks. Very strong density [central peak (red) contoured at 100σ] is found at the krypton site and six additional peaks are assigned to S atoms that are present in PPE. Two of them form a disulfide bond and their density peaks are clearly distinguished. The anomalous strength of sulfur at the krypton peak energy (14.3 keV) is only 0.18 e. The map was prepared using *PyMOL* (DeLano, 2002).

calculated from the single 0.31 occupied krypton. As shown in Fig. 3.3, very strong density was found at the krypton site (the central density is higher than 100σ) and seven additional well confined sites were found around krypton at 3.6σ. To investigate the origin of these signals, the final refined model solved by the molecular replacement was superimposed on the density. We were able to assign six peaks out of the seven to S atoms (there are a total of 11 S atoms in the PPE structure). Two atoms out of six made a disulfide bond and their electron density peaks were clearly distinguished. Since the anomalous strength of sulfur at the krypton peak (14.3 keV) is only 0.18 e, this is a remarkable result and reflects the quality of the diffraction produced by the high-pressure cryocooling.

In summary, it has been shown that high-pressure cryocooling opens promising approaches for phasing. In Kr–He high-pressure cryocooling, crystals were successfully cryocooled without adding any penetrating cryoprotectants. The diffraction was of sufficiently high quality that the weak anomalous signal from a single 0.31 occupied Kr atom was sufficient for SAD phasing of the protein PPE, which has 240 residues (26 kDa). Since 30–50 % of all proteins are expected to have binding sites for noble gases such as krypton and xenon (Stowell *et al*., 1996; Fourme *et al*., 1999), we believe that this method might become a very useful tool in many cases, eliminating the need for selenomethionine incorporation and the search for cryoprotectant conditions. This would be especially useful in cases where selenomethionine incorporation is difficult (*e.g.* many eukaryotic proteins) and for high-throughput crystallography.

REFERENCES

Cohen, A., Ellis, P., Kresge, N. & Soltis, S. M. (2001). *Acta Cryst*. D**57**, 233–238.

Collaborative Computational Project, Number 4 (1994). *Acta Cryst*. D**50**, 760–763.

Cowtan, K. (1994). *Jnt CCP4/ESF–EACBM Newsl. Protein Crystallogr*. **31**, 34–38.

Dauter, Z. (2006). *Acta Cryst*. D**62**, 1–11.

Dauter, Z., Dauter, M., de La Fortelle, E., Bricogne, G. & Sheldrick, G. M. (1999). *J. Mol. Biol.* **289**, 83–92.

DeLano, W. (2002). *PyMOL*. DeLano Scientific, San Carlos, CA, USA.

Fan, H. F., Han, F. S., Qian, J. Z. & Yao, J. X. (1984). *Acta Cryst*. A**40**, 489–495.

Fourme, R., Shepard, W., Schiltz, M., Prangé, T., Ramin,M., Kahn, R., de La Fortelle, E. & Bricogne, G. (1999). *J. Synchrotron Rad*. **6**, 834–844.

Garman, E. F. & Owen, R. L. (2006). *Acta Cryst*. D**62**, 32–47.

Hao, Q. (2004). *J. Appl. Cryst*. **37**, 498–499.

Hao, Q., Gu, Y. X., Yao, J. X., Zheng, C. D. & Fan, H. F. (2003). *J. Appl. Cryst*. **36**, 1274–1276.

Harvey, I., Hao, Q., Duke, E. M. H., Ingledew, W. J. & Hasnain, S. S. (1998). *Acta Cryst*. D**54**, 629–635.

Hendrickson, W. A. & Teeter, M. M. (1981). *Nature (London)*, **290**, 107–113.

Hendrickson, W. A. (1999). *J. Synchrotron Rad*. **6**, 845–851.

Kim, C. U., Kapfer, R. & Gruner, S. M. (2005). *Acta Cryst*. D**61**, 881–890.

Liu, Z.-J., Vysotski, E. S., Chen, C.-J., Rose, J. P., Lee, J. &Wang, B.-C. (2000). *Protein Sci*. **9**, 2085–2093.

Mueller-Dieckmann, C., Polentarutti, M., Djinovic Carugo, K., Panjikar, S., Tucker, P. A. & Weiss, M. (2004). *Acta Cryst*. D**60**, 28–38.

Murshudov, G. N., Vagin, A. A. & Dodson, E. J. (1997). *Acta Cryst*. D**53**, 240–255.

Otwinowski, Z. & Minor,W. (1997). *Methods Enzymol*. **276**, 307–326.

Perrakis, A., Morris, R. & Lamzin, V. S. (1999). *Nature Struct. Biol.* **6**, 458–463.

Pollack, G. L., Kennan, R. P., Himm, J. F. & Carr, P. W. (1989). *J.Chem. Phys.* **90**, 6569–6579.

Prangé, T., Schiltz, M., Pernot, L., Colloc'h, N., Longhi, S., Bourguet, W. & Fourme, R. (1998). *Proteins*, **30**, 61–73.

Ramagopal, U. A., Dauter, M. & Dauter, Z. (2003). *Acta Cryst*. D**59**, 1020–1027.

Schiltz, M., Prangé, T. & Fourme, R. (1994). *J. Appl. Cryst*. **27**, 950–960.

Schiltz, M., Shepard, W., Fourme, R., Prange, T., de La Fortelle, E. & Bricogne, G. (1997). *Acta Cryst*. D**53**, 78–92.

Schoenborn, B. P., Watson, H. C. & Kendrew, J. C. (1965). *Nature* (London), **207**, 28–30.

Shen, Q., Hao, Q. & Gruner, S. M. (2006). *Physics Today*, March, pp. 46–52.

Shotton, D. M., Hartley, B. S., Camerman, N., Hofman, T., Nyburg, S. C. & Rao, L. (1968). *J. Mol. Biol.* **32**, 155–156.

Stowell, M. H. B., Soltis, M., Kisker, C., Peters, J. W., Schindelin, H., Rees, D. C., Cascio, D., Beamer, L., Hart, P. J., Wiener, M. C. & Whitby, F. G. (1996). *J. Appl. Cryst*. **29**, 608–613.

Ten Eyck, L. F. (1973). *Acta Cryst*. A**29**, 183–184.

Tilton, R. F., Kuntz, I. D. & Petsko, G. A. (1984). *Biochemistry*, **23**, 2849–2857.

Vagin, A. & Teplyakov, A. (1997). *J. Appl. Cryst*. **30**, 1022–1025.

Wang, B.-C. (1985). *Methods Enzymol*. **115**, 90–112.

Wang, J.-W., Chen, J.-R., Gu, Y.-X., Zheng, C.-D., Jiang, F. & Fan, H.-F. (2004). *Acta Cryst*. D**60**, 1987–1990.

Wilhelm, E., Battino, R. & Wilcock, R. J. (1977). *Chem. Rev.* **77**, 219–259.

CHAPTER FOUR
HIGH-PRESSURE CRYOCOOLING FOR CAPILLARY SAMPLE CRYOPROTECTION AND DIFFRACTION PHASING AT LONG WAVELENGTHS*

4.1 Introduction

Radiation damage, which often limits the room-temperature collection of complete macromolecular diffraction data sets, is conventionally mitigated by crystal cryocooling. The goal of cryoprotection is to lower the temperature of the crystal to below the protein glass-transition temperature with as little degradation of the crystal diffraction quality as possible. This often requires the incorporation of chemical cryoprotectants (Garman & Schneider, 1997). Practically, cryoprotectants that work well with one protein often do not work with another, requiring a trial-and-error search. Even when a suitable cryoprotectant is found, care has to be taken to avoid unwanted chemical reactions between the cyroprotectant and the protein, such as the binding of cryoprotectant to protein active sites.

Recently, Kim *et al*. (2005) reported an alternative procedure, high-pressure cryocooling, in which the use of penetrating cryoprotectants could be avoided by cryocooling protein crystals under high pressure. Exceptionally high quality diffraction data were obtained in terms of both diffraction resolution and crystal mosaicity. This method was successfully used in the study of the RCK domain of the KtrAB K+ transporter (Albright *et al*., 2006). High-pressure cryocooling was especially useful in this case since crystal cryoprotection and better quality diffraction could be achieved without perturbation of the ligand-binding site by cryoprotectants.

---

* Reproduced with permission from Kim, C. U., Hao, Q. & Gruner, S. M. (2007). *Acta Cryst*. D**63**, 653-659. Copyright 2007 International Union of Crystallgraphy.

The high quality of the diffraction data from high-pressure cryocooled crystals enables a variety of diffraction-phasing procedures. High-pressure cryocooling was successfully extended to diffraction phasing of porcine pancreatic elastase (PPE) by incorporating krypton during the cryocooling process (Kim *et al*., 2006). Even though the single Kr-binding site was only 31 % occupied, the quality of the diffraction allowed successful Kr SAD phasing. Intriguingly, the anomalous difference map created using the experimental PPE phases showed electron density (3.6σ level) at the S atoms naturally present in the protein, even though sulfur has an anomalous strength of only 0.18 electrons at the data collection wavelength (0.86 Å). Since krypton SAD phasing was successful, the use of xenon in high-pressure cryocooling was of particular interest. Xenon has a stronger anomalous signal than krypton in the typical wavelength range for diffraction data collection (Schiltz *et al*., 1994, 1997; Cohen *et al*., 2001). Furthermore, it was estimated that xenon might be captured with higher occupancy in the high-pressure cryocooling, which would be very useful for SAD phasing (Kim *et al*., 2006).

Here, we present three new results. (i) Xe–He high-pressure cryocooling followed by xenon SAD phasing was successfully demonstrated on PPE. (ii) Of greater interest is the demonstration of SAD phasing using the native sulfurs (Hendrickson & Teeter, 1981; Wang, 1985; Dauter *et al*., 1999; Micossi *et al*., 2002) of a thaumatin crystal prepared with He high-pressure cryocooling. (iii) Conventional wisdom holds that it is difficult to cryocool crystals in capillaries because the slow cooling rate leads to ice crystals. However, we demonstrated native sulfur phasing of a thaumatin crystal that was grown and the diffraction data were obtained in a thick-walled polycarbonate capillary. The entire capillary containing the crystal and mother liquor (no additional cryoprotectants) was successfully high-pressure cryocooled. Although the thermal mass of the capillary and surrounding bulk mother liquor

resulted in relatively slow cryocooling of the sample, no ice rings were observed in the diffraction pattern. These results open new possibilities for high-throughput protein crystallography.

4.2 Experimental

4.2.1 Materials and sample preparation

4.2.1.1 Crystallization

Lyophilized PPE (catalog No. 20929) was purchased from SERVA (Heidelberg, Germany) and used without further purification. Crystallization experiments were carried out at 293 K using the hanging-drop vapor-diffusion technique. As described in Kim *et al*. (2006), 2 µl of a 25 mg/ml protein solution in pure water was mixed with 2 µl of a reservoir solution containing 30 mM sodium sulfate and 50 mM sodium acetate pH 5.0. Crystals (space group $P2_12_12_1$) appeared within a few days and crystals of dimensions 0.2 × 0.2 × 0.3 mm were used for Xe–He high-pressure cryocooling.

Thaumatin from *Thaumatococcus daniellii* was purchased from Sigma (Saint Louis, MO, USA; catalog No. T7638) and used for crystallization without further purification. Thaumatin crystallization was carried out at 293 K in a polycarbonate capillary with an inside diameter of 300 µm and a wall thickness of 300 µm (Gilero, Raleigh, NC, USA). Robust plastic capillaries were used to minimize capillary breakage, since this experiment was initiated as a study for high throughput methodologies. Equal amounts of protein solution (25 mg/ml in 50 mM HEPES buffer pH 7.0) and reservoir solution containing 0.9 M sodium potassium tartrate were mixed. The mixed solution was then inserted into the polycarbonate capillary and the capillary was placed into a larger tube containing 0.9 M sodium potassium tartrate

solution at the bottom. The large tube was carefully sealed with Parafilm to minimize evaporation of the crystallizing solution. The equilibrium between the capillary and the reservoir solution in the larger tube was reached by vapor diffusion. Crystals (space group $P4_12_12$) appeared within a few days and grew on the capillary inner surface (150 × 150 × 200 μm, truncated bipyramidal shape) in a few weeks.

4.2.1.2 High-pressure cryocooling

PPE crystals were prepared by Xe–He high-pressure cryocooling, which was modified from Kr–He high-pressure cryocooling as described in Kim *et al*. (2006). PPE crystals were first coated with NVH oil (Hampton Research) to prevent crystal dehydration and loaded into high-pressure tubes, which were then connected to the gas compressor. High-pressure cryocooling could not be carried out in a single step with the Xe–He mixture gas because Xe would solidify in the liquid-nitrogen-cooled bottom of the pressure tube and prevent the sample from falling (Sauer *et al*., 1997; Schiltz *et al*., 1997; Soltis *et al*., 1997). Therefore, the crystals were initially pressurized with xenon gas to 1.0 MPa. After 15 min, the compressed xenon gas was released, liquid nitrogen (LN_2) was poured into the LN_2 bath of the cryocooling apparatus and the crystals were re-pressurized with helium. After 60 s, the helium pressure reached 145 MPa and the crystals were cryocooled to LN_2 temperature at 145 MPa pressure. Overall, the time from xenon-pressure release to cryocooling was about 150 s. The helium pressure was released 2 min after cryocooling and the crystals were transferred into a cryocap under liquid nitrogen for data collection.

Thaumatin crystals were prepared by the He high-pressure cryocooling process described in Kim *et al*. (2005). Briefly, the polycarbonate capillary containing crystals was cut into 2 cm lengths and loaded into the high-pressure cryocooling apparatus, which was then pressurized with helium gas to 170 MPa. The mother liquor around

the crystals in the capillary was not removed so that the crystals were left fully hydrated; hence, oil coating to prevent crystal hydration was not needed. The capillary ends were left open under pressure, but water evaporation from the capillary during the brief process was negligible. No additional penetrating cryoprotectants were added to the mother liquor for high-pressure cryocooling. Once at high pressure, a magnetic constraint was released and the crystals fell down a length of high-pressure tubing into a zone kept at LN_2 temperature. The helium pressure was released and the crystals were subsequently handled at low temperature and ambient pressure for cryocrystallographic data collection.

As described in Kim *et al*. (2005), high-pressure cryocooling requires a minimum pressure of ~100 MPa for crystal cryoprotection. Pressures higher than 100 MPa seem to have no significant effect on the crystal diffraction quality, at least for PPE and thaumatin. Therefore, the pressures of 145 and 170 MPa used for PPE and thaumatin sample preparations, respectively, were not controlled intentionally.

4.2.2 Data collection

Diffraction data were collected at the Cornell High Energy Synchrotron Source (CHESS) on beamline F2 (150 μm beam diameter, ADSC Quantum-210 CCD detector). In all cases, the detector face was perpendicular to the incident beam (2θ value of zero). All data were collected at 110 K (N_2 gas stream) and ambient pressure with an oscillation angle (Δφ) of 1.0˚ per image. In order to obtain useful anomalous signals from xenon and sulfur, the X-ray energy was located and calibrated at the Fe K edge (7.11 keV), where the anomalous strengths of xenon and sulfur are 9.0 and 0.7 e, respectively. Diffraction data were collected by the inverse-beam mode with a wedge of ten frames. The distance between the crystal and the detector was 65 mm for PPE

and 95 mm for thaumatin. The exposure time for each frame was 2 min for PPE and 5 min for thaumatin. A total of 360 frames were collected from each crystal.

4.2.3 Data processing, phasing and model building

Data were indexed, pre-refined, integrated, post-refined, scaled and merged with HKL-2000 (Otwinowski & Minor, 1997) using the 'scale anomalous' flag to keep Bijvoet pairs separate. The initial structures were determined by the molecular-replacement method using *MOLREP* (Vagin & Teplyakov, 1997) from the *CCP4* program suite (Collaborative Computational Project, Number 4, 1994). The structures were then refined against the data set with *REFMAC5* (Murshudov *et al*., 1997). In the PPE structure refinement, as the xenon occupancy and thermal *B* factor are highly correlated, the xenon occupancy was manually adjusted so that the refined thermal *B* factor of the Xe atom was close to the average thermal *B* factor of the crystallographically refined main-chain atoms. In SAD phasing, the anomalous scattering substructure was initially solved and refined using the programs *SAPI* (Hao *et al*., 2003) and *ABS* (Hao, 2004). In PPE, one Xe atom was found in the previously reported site (Schiltz *et al*., 1997; Mueller-Dieckmann *et al*., 2004). All 17 sulfur sites in thaumatin (eight disulfide pairs and one S atom of a methionine residue) were located. The heavy-atom positions were then input into *OASIS-2004* (Wang *et al*., 2004) for SAD phasing. Afterwards, density modification was performed using *DM* (Cowtan, 1994). Auto model building was performed with ARP/wARP (Perrakis *et al*., 1999) and *REFMAC5* (Murshudov *et al*., 1997) was used for refinement. The electron density maps and structural images were generated using *PyMOL* (DeLano, 2002).

4.3 Results

4.3.1 Porcine pancreas elastase

The crystallographic data statistics of the PPE crystal prepared by Xe–He high-pressure cryocooling are summarized in Table 4.1. The mosaicity of the Xe–He high-pressure cryocooled PPE crystal was 0.33˚, whereas the mosaicity of conventionally (ambient pressure) flash-cryocooled PPE crystals without penetrating cryoprotectants was approximately 1˚ (Kim *et al*., 2006). This indicates that crystal cryoprotection was successfully achieved by Xe–He high-pressure cryocooling. The resolution limit (1.8 Å) seemed to be poorer than that of Kr–He high-pressure cryocooled crystals (1.3 Å), but this was mainly a consequence of the increased absorption and relatively weak beam intensity at the longer data collection wavelength (1.7463 Å). The crystallographic structure was solved by the molecular-replacement method using the known structure 1c1m (Prangé *et al*., 1998). In the final refined model the occupancy of xenon was refined to be 0.70, which is much higher than the occupancy of krypton (0.31) reported by Kim *et al*. (2006). Since the anomalous strength of xenon at 1.7463 Å is 9.0 e, a single 0.70 occupancy xenon site in PPE (240 residues, 26 kDa) gave an estimated Bijvoet amplitude ratio ($<|\Delta F|>/<F>$) of 2.8%.

Xe SAD phasing was then carried out without the use of the known protein structure. The F_o map (Fig. 4.1a) was generated at 1.8 Å resolution and the final refined model solved using the molecular-replacement method was superimposed to visually evaluate the map quality. The map correlation coefficients between the F_o map and the $2F_o$ - F_c map from the final refined model for the main chain and side chains were 0.83 and 0.74, respectively. In the auto model-building process, 97 % of the total residues (232 out of 240) could be found and docked in the electron density. In order to investigate the effect of resolution on the SAD phasing, the 1.8 Å data set

Table 4.1. Data collection and refinement statistics for PPE and thaumatin. Numbers in parentheses refer to the highest-resolution shell.

	PPE	Thaumatin
High pressure cryocooling	Xenon / Helium	Helium
Wavelength (Å)	1.7463	1.7433
Space group	$P2_12_12_1$	$P4_12_12$
Unit-cell parameters (Å)		
a (Å)	50.153	57.968
b (Å)	58.166	57.968
c (Å)	74.658	150.716
Solvent content (%)	40.8	56.9
Mosaicity (º)	0.33	0.34
Resolution range (Å)	30 - 1.8 (1.86 - 1.8)	30 - 1.9 (1.97 - 1.9)
No. of observations	281537	469249
No. of unique reflections *	38238	38263
Multiplicity *	7.4 (6.6)	12.3 (3.5)
Completeness (%)*	97.7 (94.8)	99.4 (93.9)
R_{sym} (%)*	11.2 (26.8)	8.9 (17.5)
I/σ(I)	19.5 (4.6)	32.0 (5.0)
R value (%)	17.8	17.6
R_{free} value (%)	22.6	21.6
Average B factor (Å^2)	14.6	17.1
No. of water molecules	327	401
R.m.s. deviation from ideality		
Bond lengths (Å)	0.014	0.014
Angles (º)	1.387	1.322
Xenon occupancy	0.70	N/A
Xenon B factor (Å^2)	11.8	N/A

* The Bijvoet pairs are kept separate in the statistics.

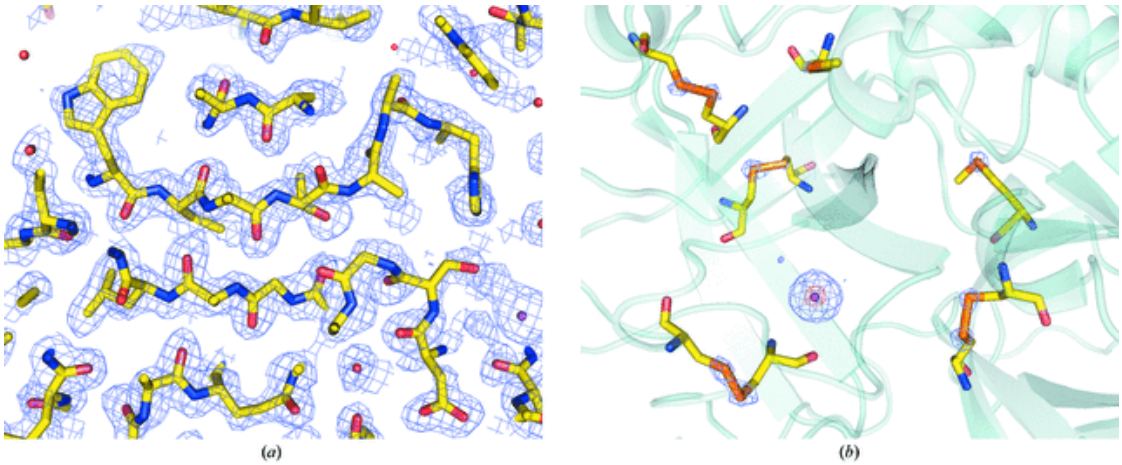

Figure 4.1. Xe SAD phasing of PPE. (a) F_o electron-density map (1σ level) after Xe SAD phasing and density modification at 1.8 Å resolution. The final refined model solved by molecular replacement was superimposed for visual map evaluation. The figure of merit is 0.807 and the map correlation coefficient calculated with the final refined $2F_o$ - F_c density map is 0.83 for the main chain and 0.74 for side chains. (b) Anomalous difference map, contoured at the 4.5σ level, generated with the phases calculated from a single 0.70 occupancy xenon. The final refined model obtained using molecular replacement was superimposed to specify the origin of the peaks. Very strong density (red central peak contoured at 80σ) is found at the xenon site and ten additional peaks are assigned to S atoms that are naturally present in PPE. The electron-density peaks in a disulfide bond can be clearly distinguished. The anomalous strength of sulfur at the data-collection wavelength (1.7643 Å) is 0.70 e.

was cut off at resolutions of 1.9, 2.0, 2.1 and 2.2 Å. Auto model building was straightforward up to 1.9 Å and a partial structure could be found and docked at 2.0 Å. In the anomalous difference map (Fig. 4.1b), a very strong peak (central peak >80σ) was observed at the xenon site. Additionally, all ten sulfurs (anomalous strength of 0.7 e at 1.7643 Å) that are naturally present in PPE were visible at 4.5σ, with peak heights ranging up to 7σ. These S atoms were included for SAD phasing and Xe–S SAD phasing was carried out at various resolution limits. Overall, the phase quality was slightly improved compared with Xe SAD phasing, so that auto model building was straightforward up to 2.0 Å and a partial structure could be found and docked at 2.1 Å. Details of Xe SAD phasing and Xe–S SAD phasing are summarized in Table 4.2.

4.3.2 Thaumatin

As shown in Fig. 4.2(a), the entire cryocooled sample looked clear, including a crystal and mother liquor in the capillary. The crystal diffraction (Fig. 4.2b) showed no crystalline ice rings, which confirms that amorphous ice formed inside the capillary on He high-pressure cryocooling. In contrast, ambient pressure flash-cryocooling of capillary samples resulted in crystalline ice rings.

The crystallographic data statistics of the thaumatin crystal are summarized in Table 4.1. The refined crystallographic structure was solved by the molecular-replacement method using the known structure 1lxz (Charron *et al*., 2002). Using the calculated phases, the anomalous difference map (Fig. 4.2c) was generated at 1.9 Å to check the anomalous signals from S atoms. In the map, all 17 sulfurs could be clearly distinguished and the maximum peak height was higher than 10σ at most of the sulfur sites.

S SAD phasing was then carried out to see if the diffraction could be phased without a known structure. In the anomalous substructure, all 17 S-atom positions

Table 4.2. SAD phasing statistics for PPE.

	Xe SAD phasing					Xe-S SAD phasing				
Resolution range (Å)	30-1.8	30-1.9	30-2.0	30-2.1	30-2.2	30-1.8	30-1.9	30-2.0	30-2.1	30-2.2
No. of unique reflections *	20337	17447	15040	13076	11434	20337	17447	15040	13076	11434
Estimated <|ΔF|>/<F> (%)	2.8	2.8	2.8	2.8	2.8	3.0	3.0	3.0	3.0	3.0
Experimental <|ΔF|>/<F> (%)	4.6	4.4	4.2	4.1	4.0	4.60	4.4	4.2	4.1	4.0
Experimental <|ΔF|>/<σ (ΔF)>	0.89	1.01	1.09	1.15	1.20	0.89	1.01	1.09	1.15	1.20
F.O.M. after *DM*	0.807	0.821	0.800	0.775	0.767	0.824	0.837	0.809	0.797	0.807
No. of residues found	232	230	178	35	8	234	235	228	122	51
No. of residues docked in sequence	232	230	133	0	0	234	235	228	21	0
Map correlation coefficient for main chain	0.83	0.81	0.78	0.74	0.70	0.85	0.83	0.80	0.76	0.71
Map correlation coefficient for side chain	0.74	0.71	0.68	0.64	0.61	0.76	0.74	0.71	0.67	0.63
R value (%)	22.5	22.3	24.3	20.7	18.8	21.6	21.8	23.0	21.8	19.0
Connectivity index	0.97	0.97	0.91	0.75	0.57	0.97	0.98	0.95	0.86	0.74

* The Bijvoet pairs are merged in the statistics.

Figure 4.2. He high-pressure cryocooling and S SAD phasing of thaumatin. (*a*) Thaumatin crystal in a polycarbonate capillary at 110 K. The entire sample, the crystal and mother liquor in the capillary, was He high-pressure cryocooled without adding penetrative cryoprotectants. This clear sample could not be obtained by conventional (room-pressure) flash-cryocooling when cryoprotectants were not added. (*b*) Diffraction image of the thaumatin crystal grown in a polycarbonate capillary that was He high-pressure cryocooled at 170 MPa. The diffuse background scatter from the capillary ranges from 4.5 to 5.5 Å. The lack of ice rings on the image confirms that water vitrification was successfully achieved under high pressure. The resolution limit [$I/\sigma(I) \sim 5.0$] is approximately 1.9 Å and the crystal mosaicity is 0.34°. The diffraction spots in the enlarged region look compact. (*c*) Anomalous difference map (5σ level) generated with the refined phases. All 17 sulfurs that naturally present in thaumatin are clearly visible. The shape of the electron density at disulfide bonds is dumbbell-shaped, so two-sulfur positions could be easily distinguished. The peak height was over the 10σ level (red) for most of the sulfur sites and the peak at Met112 was even visible at the 15σ level. (*d*) F_o electron-density map (1σ level) after S SAD phasing and density modification at 1.9 Å resolution. The final refined model solved by molecular replacement was superimposed for visual map evaluation. The figure of merit is 0.824 and the map correlation coefficient calculated with the final refined $2F_o - F_c$ density map is 0.85 for the main chain and 0.76 for side chains.

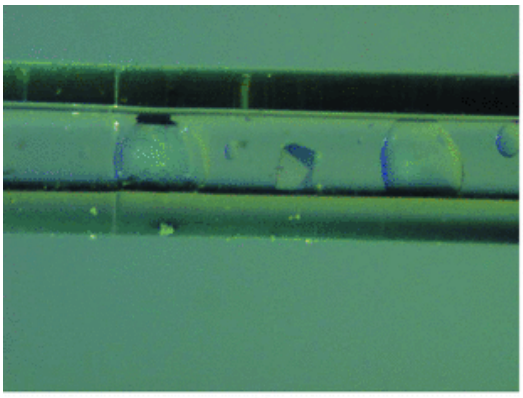

(a)

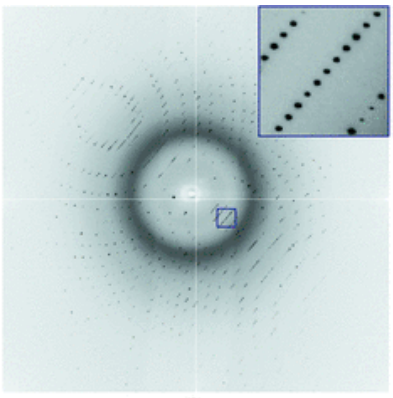

(b)

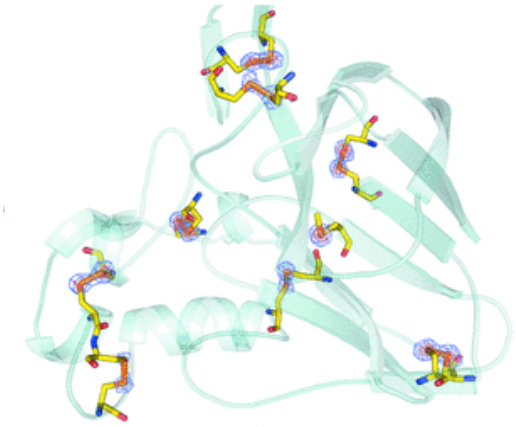

(c)

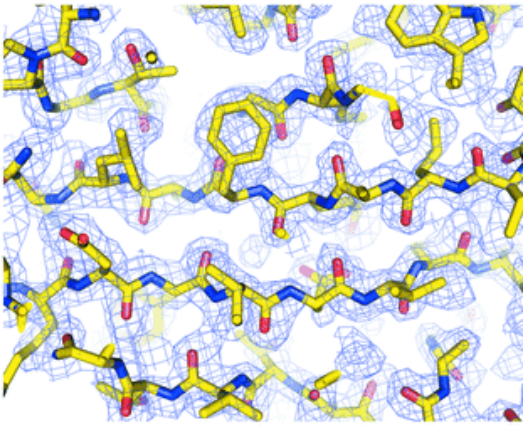

(d)

could be resolved at 1.9 Å resolution. The map correlation coefficients between the F_o map (Fig. 4.2d) at 1.9 Å and the $2F_o$ - F_c map from the final refined model were 0.82 for the main chain and 0.75 for the side chains. In the auto model-building process, 95 % of the total residues (197 out of 207) could be found and docked in the electron density. S SAD phasing at different resolutions was straightforward up to 2.1 Å and a partial structure could be found and docked at 2.2 and 2.3 Å. Details of S SAD phasing are summarized in Table 4.3.

4.4 Discussion

To date, high-pressure cryocooling without added penetrative cryoprotectants has been applied to various protein crystals, resulting in high-quality diffraction. It should be emphasized that high-pressure cryocooling mainly mitigates damage during the cryocooling process. The resultant diffraction quality is limited by the initial crystal quality prior to being frozen.

In high-pressure cryocooling, oil coating was an important step to prevent crystal dehydration in the high-pressure gas prior to cooling. However, in some cases it has been observed that crystals are degraded by the oil itself before the completion of high-pressure cryocooling. In this case, crystal encapsulation in a capillary is an alternative way to prevent crystal dehydration, as shown in the case of thaumatin. This result is surprising because vitrification of the capillary sample was impossible by flash-cryocooling at ambient pressure, regardless of the precipitant concentration at least up to 1.5 M, when no cryoprotectants were added. For comparison, several capillary samples were made with various amount of glycerol as a cryoprotectant agent, keeping the sodium potassium tartrate concentration constant at 0.9 M. It was observed that more than 13% (v/v) glycerol was required to make a visually transparent capillary sample upon plunging into an LN_2 bath at ambient pressure.

Table 4.3. SAD phasing statistics for thaumatin.

	Thaumatin S SAD phasing					
Resolution range (Å)	30-1.9	30-2.0	30-2.1	30-2.2	30-2.3	30-2.4
No. of unique reflections *	20909	18143	15756	13764	12099	10680
Estimated <|ΔF|>/<F> (%)	1.4	1.4	1.4	1.4	1.4	1.4
Experimental <|ΔF|>/<F> (%)	2.1	1.7	1.5	1.5	1.4	1.4
Experimental <|ΔF|>/<σ (ΔF)>	0.64	0.70	0.75	0.78	0.81	0.84
F.O.M. after *DM*	0.794	0.747	0.785	0.756	0.780	0.783
No. of residues found	197	194	192	175	166	60
No. of residues docked in sequence	197	194	192	121	93	0
Map correlation coefficient for main chain	0.82	0.79	0.78	0.75	0.74	0.71
Map correlation coefficient for side chain	0.75	0.73	0.72	0.70	0.69	0.68
R value (%)	23.9	24.6	23.6	22.0	23.2	22.3
Connectivity index	0.96	0.96	0.95	0.92	0.91	0.76

* The Bijvoet pairs are merged in the statistics.

This result may have a significant impact on high-throughput crystallography. Although huge efforts are being expended to automate the screening/crystallization steps and data collection, the process of harvesting crystals and cryocooling is still performed manually. High-pressure cryocooling may play a key role in these steps by allowing a completely automated crystallography pipeline where crystals are screened and grown in capillaries, the capillaries are high-pressure cryocooled for cryoprotection, the vitrified samples are auto-mounted and complete data sets are collected.

For this purpose, the physical constraints for high-pressure cryocooling capillary samples need to be carefully investigated. It was observed that crystalline ice in the surrounding mother liquor was sometimes not suppressed under pressure: in experiments on thaumatin, some capillaries prepared by high-pressure cryocooling were not successfully vitrified. Pure water in a polycarbonate capillary was not vitrified by high-pressure cryocooling, suggesting that an appropriate precipitant concentration was required to facilitate amorphous ice formation. It is known that the formation of amorphous ice generally requires a very fast cooling rate (Kriminski *et al*., 2003). However, the cooling rate of a capillary sample is limited by the large thermal mass of the thick-walled capillary and the mother liquor inside the capillary. Use of thinner, lower thermal mass capillaries such as polyethylene terephthalate tubing (Kalinin & Thorne, 2005) would increase the cooling rate and may result in a higher percentage of successfully high-pressure cryocooled samples. On the other hand, adding a minimal amount of cryoprotecting agents to the capillary samples should also be carefully tested to determine whether combining chemical cryoprotectants and high-pressure cryocooling would produce better results for capillary samples.

Compared with Kr–He high-pressure cryocooling (Kim *et al*., 2006), Xe–He high-pressure cryocooling has additional benefits for diffraction phasing. This report shows that a higher occupancy of Xe was obtained for PPE at a lower applied Xe pressure (a Kr pressure of 10 MPa resulting in 0.31 occupancy compared with a Xe pressure of 1 MPa resulting in 0.70 occupancy). These results are consistent with the estimation from previous reports (Schiltz *et al*., 1994, 1997). Additionally, xenon has stronger anomalous signals than krypton in most of the practical data-collection wavelength range: the anomalous scattering strength of xenon gradually increases from 3.4 e at the Se *K* absorption peak (0.98 Å) to 11.8 e at Cr K_α (2.29 A), whereas that of krypton at its *K* absorption peak (0.87 Å) is only 3.8 e. For PPE, the anomalous signal used for Xe SAD phasing was approximately five times stronger than that used for Kr SAD phasing. Therefore, partial auto model building was possible with a lower cutoff resolution data set (30–2.0 Å) in Xe SAD phasing. In Kr SAD phasing, model autobuilding had difficulty in finding residues using a 30–1.8 Å resolution data set.

If there are no noble gas binding sites, then high-pressure cryocooling can simply be used for crystal cryoprotection and S SAD phasing can be tried if high-quality diffraction is available and the anomalous signal from S atoms is sufficient, as in the thaumatin case. Alternatively, high-pressure cryocooling can be combined with most other existing methods for experimental phasing such as SeMet synthesis and heavy-atom solution soaks.

In summary, Xe–He high-pressure cryocooling was applied to PPE and Xe SAD phasing was successfully carried out. The anomalous signal from xenon captured by Xe–He high-pressure cryocooling was stronger than that of krypton captured by Kr–He high-pressure cryocooling. He high-pressure cryocooling was applied to successfully cryocool a thaumatin crystal and mother liquor in a capillary. Surprisingly, the entire system could be vitrified, although the cooling rate was

relatively slow. The diffraction quality was sufficiently good that S SAD phasing could successfully be achieved. These results demonstrate that high-pressure cryocooling opens novel possibilities in specimen preparation for macromolecular crystallography.

REFERENCES

Albright, R. A., Vazquez Ibar, J.-L., Kim, C. U., Gruner, S. M. & Morais Cabral, J. H. (2006). *Cell*, **126**, 1147–1159.

Charron, C., Kadri, A., Robert, M.-C., Giegé, R. & Lorber, B. (2002). *Acta Cryst*. D**58**, 2060–2065.

Cohen, A., Ellis, P., Kresge, N. & Soltis, S. M. (2001). *Acta Cryst*. D**57**, 233–238.

Collaborative Computational Project, Number 4 (1994). *Acta Cryst*. D**50**, 760–763.

Cowtan, K. (1994). *Jnt CCP4/ESF–EACBM Newsl. Protein Crystallogr*. **31**, 34–38.

Dauter, Z., Dauter, M., de La Fortelle, E., Bricogne, G. & Sheldrick, G. M. (1999). *J. Mol. Biol.* **289**, 83–92.

DeLano, W. L. (2002). *PyMOL*. DeLano Scientific, San Carlos, CA, USA.

Garman, E. F. & Schneider, T. R. (1997). *J. Appl. Cryst*. **30**, 211–237.

Hao, Q. (2004). *J. Appl. Cryst*. **37**, 498–499.

Hao, Q., Gu, Y.-X., Yao, J.-X., Zheng, C.-D. & Fan, H.-F. (2003). *J. Appl. Cryst*. **36**, 1274–1276.

Hendrickson, W. A. & Teeter, M. M. (1981). *Nature (London)*, **290**, 107–113.

Kalinin, Y. & Thorne, R. (2005). *Acta Cryst*. D**61**, 1528–1532.

Kim, C. U., Hao, Q. & Gruner, S. M. (2006). *Acta Cryst*. D**62**, 687–694.

Kim, C. U., Kapfer, R. & Gruner, S. M. (2005). *Acta Cryst*. D**61**, 881–890.

Kriminski, S., Kazmierczak, M. & Thorne, R. E. (2003). *Acta Cryst*.D**59**, 697–708.

Micossi, E., Hunter, W. N. & Leonard, A. G. (2002). *Acta Cryst*. D**58**, 21–28.

Mueller-Dieckmann, C., Polentarutti, M., Djinovic Carugo, K., Panjikar, S., Tucker, P. A. & Weiss, M. (2004). *Acta Cryst*. D**60**, 28–38.

Murshudov, G. N., Vagin, A. A. & Dodson, E. J. (1997). *Acta Cryst*. D**53**, 240–255.

Otwinowski, Z. & Minor,W. (1997). *Methods Enzymol*. **276**, 307–326.

Perrakis, A., Morris, R. & Lamzin, V. S. (1999). *Nature Struct. Biol*. **6**, 458–463.

Prangé, T., Schiltz, M., Pernot, L., Colloc'h, N., Longhi, S., Bourguet, W. & Fourme, R. (1998). *Proteins*, **30**, 61–73.

Sauer, O., Schmidt, A. & Kratky, C. (1997). *J. Appl. Cryst*. **30**, 476–486.

Schiltz, M., Prangé, T. & Fourme, R. (1994). *J. Appl. Cryst*. **27**, 950–960.

Schiltz, M., Shepard, W., Fourme, R., Prangé, T., de La Fortelle, E. & Bricogne, G. (1997). *Acta Cryst*. D**53**, 78–92.

Soltis, S. M., Stowell, M. H. B., Wiener, M. C., Phillips, G. N. Jr & Rees, D. C. (1997). *J. Appl. Cryst*. **30**, 190–194.

Vagin, A. & Teplyakov, A. (1997). *J. Appl. Cryst*. **30**, 1022–1025.

Wang, B.-C. (1985). *Methods Enzymol*. **115**, 90–112.

Wang, J.-W., Chen, J.-R., Gu, Y.-X., Zheng, C.-D., Jiang, F. & Fan, H.-F. (2004). *Acta Cryst*. D**60**, 1987–1990.

CHAPTER FIVE
PRESSURE INDUCED HIGH-DENSITY AMORPHOUS ICE IN PROTEIN CRYSTALS

5.1 Introduction

In X-ray protein crystallography, a typical protein crystal at room temperature only survives a fraction of the total x-ray dose needed for a complete high-resolution data set before it is destroyed by X-ray radiation damage (Ravelli & Garman, 2006). Over the past two decades, cryocrystallography techniques, whereby a protein crystal is flash-cryocooled and the crystal diffraction data are collected at cryogenic temperatures, have played a key role in mitigating radiation damage (Garman & Schneider, 1997). However, crystal cryocooling typically requires finding suitable cryoprotectants, which is not always successful, and most commonly results in crystals with significantly increased mosaic spreads (Garman & Owen, 2006).

An alternative crystal cryocooling method, high pressure cryocooling, was developed by Kim *et al*. (2005), where use of penetrating cryoprotectacts could be avoided by cryocooling protein crystals in helium gas at high pressures. This method was tested with various protein crystals and commonly resulted in exceptionally high quality crystal diffraction. It also has proven useful in improving diffraction from protein ligand complexes. For example, it was successfully used in the study of the RCK domain of the KtrAB K+ transporter, not only to obtain excellent diffraction but also to limit the perturbation of ligand binding site by cryoprotectants (Albright *et al*., 2006). More recently, the high pressure cryocooling method was extended to the crystal diffraction phasing by the incorporation of heavy noble gases, Krypton and Xenon (Kim *et al*., 2006; Kim *et al*., 2007). It was also shown that the method can be

used to cryoprotect an entire capillary sample consisting of crystals and crystallization solution in a thick-walled polycarbonate capillary (Kim *et al*., 2007).

Kim *et al*. (2005) proposed a mechanism for high pressure cryocooling involving the formation of high density amorphous (HDA) ice for the solution internal to the protein crystals. In contrast to low density amorphous (LDA) ice, which forms at ambient pressure by hyperquenched cryocooling with a density of 0.94 g/cm^3 at 77 K and 0.1 MPa (Ghormley & Hochanadel, 1971), HDA ice has significantly higher density: 1.17 g/cm^3 at 77 K, 0.1 MPa (Mishima *et al*., 1984). The volume expansion of water upon the formation of LDA has been suggested as the cause for the increased crystal mosaicity observed with conventional cryocooling (Kriminski *et al.*, 2002; Juers & Matthews, 2004). It has been suggested that the density difference between LDA and HDA, may account for the lower mosaicity observed with high pressure cryocooling (Kim *et al*., 2005).

Conventionally, HDA ice of pure water has been prepared by pressure-inducing amorphization in which hexagonal ice at liquid nitrogen temperature is subject to high pressure of 1.2 – 2.0 GPa and undergoes a collapse-transition to HDA ice (see Mishima & Stanley, 1998, for a review). In contrast, high pressure cryocooling of protein crystals has been performed at considerably lower pressures, 100 ~ 200 MPa, albeit not with pure water. Therefore, it has been of considerable interest to see if HDA ice forms inside protein crystals by high pressure cryocooling.

Below, we describe the use of X-ray diffraction to study water phases in both the solution used for protein crystallization and in protein crystals prepared by high pressure cryocooling. The results support the existence of HDA ice produced by high pressure cryocooling both in bulk solution and within protein crystals. As each sample was warmed from 80 K to 270 K, phase transitions from HDA ice to LDA ice, cubic

ice and hexagonal ice could be observed, which correlated to the diffraction quality of crystals.

5.2 Experimental details

5.2.1 Sample preparation

The crystallization solution of 0.9 M sodium potassium tartrate in pure water, which was used in the preparation of the thaumatin crystals, was used without thaumatin protein for the bulk solution study. The sample in a capillary was prepared by centrifuging the solution for 20 seconds to the bottom of a 15mm long glass X-ray capillary (catalog no. 05-SG, Charles Supper Company, Natick, MA) having a diameter of 0.5 mm and a wall thickness of 10 μm. A 12 mm length MicroTube (catalog no. HR4-917, Hampton Research, Laguna Niguel, CA) was press-fitted into the open end of the capillary to facilitate sample manipulation.

Lyophilized thaumatin powder from *Thaumatococcus daniell* (catalog no. T7638, Sigma, Saint Louis, MO) was used for crystallization without further purification. Crystals were grown at room temperature by the hanging-drop method with 25 mg/ml thaumatin solution in 50 mM HEPES buffer at pH = 7 and crystallization solution containing 0.9 M sodium potassium tartrate as a precipitant (modified from Ko *et al*., 1994). The crystal space group was determined to be $P4_12_12$, having a solvent content of ~ 55 %.

Glucose isomerase from *Streptomyces rubiginosus* (catalog No. HR7-102, Hampton Research, Laguna Niguel, CA) was dialyzed against pure water before crystallization. Crystals were grown by the hanging drop method by mixing a reservoir solution containing 1.15 M ammonium sulfate, 1 mM magnesium sulfate and 10 mM HEPES pH 7.5 with 25mg/ml protein solution in pure water (modified from Carrell *et*

al., 1989). The crystal space group was determined to be I222, having a solvent content of ~ 55 %.

Lyophilized porcine pancreas elastase (catalog No. 20929, SERVA, Heidelberg, Germany) was used for crystallization without further purification. Crystals were grown by the hanging drop method by mixing a reservoir solution containing 30 mM sodium sulfate and 50 mM sodium acetate pH 5.0 with a 25 mg/ml protein solution in pure water (modified from Shotton *et al*., 1968). The crystal space group was determined to be $P2_12_12_1$, having a solvent content of ~ 40 %.

Prior to high pressure cryocooling, protein crystals were mounted on 0.3 - 0.4 mm mounted-cryoloops. To avoid crystal dehydration, the crystals were coated with NVH oil (catalog no. HR3-611, Hampton Research). Excess crystallization solution around crystals was very carefully removed during the oil coating process by swishing the crystals back and forth in the oil. The amount of crystallization solution surrounding a protein crystal was negligible relative to the amount of solvent inside of the crystal.

5.2.2 High-pressure cryocooling

Samples were high pressure cryocooled as described in Kim *et al.* (2005). Briefly, samples were loaded into the high pressure cryocooling apparatus which was then pressurized with helium gas to 200 MPa. Once at high pressure, the samples were allowed to fall into a zone at liquid nitrogen temperature. Helium pressure was then released. Thereafter samples were handled/stored at ambient pressure and near liquid nitrogen temperatures prior to X-ray diffraction measurements.

5.2.3 X-ray diffraction measurement

The X-ray diffraction data were collected at macromolecular crystallography stations A1 (λ = 0.9771 Å, ADSC Quantum 210 CCD detector, beam size of 100 μm) and F1 (λ = 0.9179 Å, ADSC Quantum 270 CCD detector, beam size of 100 μm) at the Cornell High Energy Synchrotron Source (CHESS). To prevent sample warming, a cryotong (Hampton Research) was used to transfer samples rapidly from liquid nitrogen to a goniometer. During data collection, samples were kept cold under a flow of cryogenic nitrogen gas which was controlled through the control panel of a Cryostream 700 series cryocooler from Oxford Cryosystems (Devens, MA). During the warming studies, sample temperature was increased at the rate of 2 K/min. After reaching a desired temperature, samples were left at the temperature for 5 to 10 min for sample equilibration. The X-ray diffraction data of the crystallization solution were collected with temperature steps of 0.5 to 10 K and the data of protein crystals were collected with steps of 2 to 10 K, with the smaller temperature steps taken in the vicinity of the phase transition. To get the unit cell parameters and crystal mosaicity, 5 consecutive images were collected at each temperature, with an oscillation angle of 1□starting at the same crystal orientation. The X-ray exposure time was 15-30 sec for the solution samples and 3- 5 sec for protein crystal samples. The magnitude of the scattering vector, Q, is given by $Q = 4\pi \sin(\theta) / \lambda$, where λ is the x-ray wavelength and 2θ is the angle between the incident beam and the diffracted x-rays. The corresponding d-spacing in real space, d, is given by $d = 2\pi / Q$.

5.2.4 Data analysis

The diffraction from the protein crystals consists of Bragg peaks from the protein molecules in the crystal superimposed on the diffuse rings arising from the oil external to the crystal and water internal to the crystal. Recall that care was taken to remove

most of the water external to the crystal during the oil-coating step. The underlying diffuse diffraction was isolated from the Bragg spots by applying a polar-coordinate median filter to the intensity values of the image. Here, the median value of all intensity values at a given scattering vector magnitude, Q, is taken to be the intensity of the diffuse scattering at that value of Q. The sample-to-detector distance was calibrated based on the reported Bragg peaks of the hexagonal ice (Blackman & Lisgarten, 1957).

Peak positions of the broad amorphous ice diffraction from the pressure-cryocooled crystallization solution were determined by fitting a quadratic function into the vicinity of the diffraction intensity maxima. The diffuse scattering from the amorphous ice phases within the protein crystal samples was found to be weaker than the nearby scattering peak from the oil used for coating the crystal. The oil and ice peaks were fit to 3 Voigt functions plus a linear background. Voigt functions were used simply because they readily fit the experimental diffraction profile. The width and position of the cubic ice peaks were fit using Gaussian lineshapes.

The 5 consecutive crystal diffraction images were processed with *HKL*-2000 (Otwinowski & Minor, 1997) to refine unit cell parameters and crystal mosaicity at each temperature.

5.3 Results and discussion

5.3.1 High-pressure cryocooled crystallization solution

X-ray diffraction measurements were conducted on a high-pressure cryocooled sample consisting of the bulk protein crystallization solution in the absence of protein. Fig. 5.1(a) and Fig. 5.2(a) show the scattering from this crystallization solution as temperature was increased. The position of the innermost peak of the ice scattering is

graphed from 80 K to 170 K in Fig. 5.3. This peak was at $Q = 2.10$ Å^{-1} ($d = 2.99$ Å) at 80 K, in good agreement with the value found for HDA ice prepared at much higher pressures (Mishima *et al*., 1984; Tulk *et al*., 2002). The peak position shifts only slightly at temperatures up to 130 K. However, between 130 K to 140 K, the peak shifts from 2.08 Å^{-1} ($d = 3.02$ Å) at 130 K to 1.77 Å^{-1} ($d = 3.55$ Å) at 140 K. As seen in Fig. 5.2(a), the peak at 135 K is considerably broadened. The observed peak width is consistent with phase coexistence of HDA and LDA ice within the sample (Klotz *et al*., 2005).

Note that distinct intermediate states of amorphous ice have been reported with relaxation times on the order of many hours (Tulk *et al*., 2002). These states are not observed distinctly in this case if they are present since the temperature was increased much more quickly in this study. From 140 to 170 K, the peak position shifts toward the bulk LDA ice value of 1.71 Å^{-1} ($d = 3.67$ Å) (Dowell & Rinfret, 1960) and narrows in width to that expected for LDA ice. Note that the sample consisted of 0.9 M sodium potassium tartrate as a protein crystallization agent. It was observed that the high pressure cryocooling of pure water resulted in crystalline ice. This means that the solutes in the crystallization solution facilitated formation of the amorphous phase, likely by perturbing homogeneous nucleation (Kanno & Angell, 1977; Kanno, 1987). However, the X-ray scattering profiles of the crystallization solution still reflect the characteristic features of the HDA ice phase of pure water. The observed peak position and the shape of the scattering profile of the crystallization solution at 80 K ~ 130 K are consistent with the reported scattering from HDA ice formed from pure water (Mishima *et al*, 1984; Mishima *et al*, 1985; Bosio *et al*, 1986). Since the peak position of the diffuse scattering is given by the inter-oxygen spacing of the scattering water, the amorphous ice phase formed in the crystallization solution is at the similar density

Figure 5.1. (a) X-ray diffraction images of the high-pressure cryocooled crystallization solution at different temperatures. The peak positions of amorphous ices at 80 K and 150 K are clearly distinguishable, indicating the density difference between HDA ice and LDA ice. The diffraction peaks of cubic ice and hexagonal ice are shown at 180 K and 230 K, respectively. Note that the peak position at 150 K, which is at around 3.65 Å, matches the positions of the main sharp peaks at 180 K and 230 K. (b) X-ray diffraction images of the high-pressure cryocooled thaumatin crystal at different temperatures. Crystal diffraction spots are seen superimposed on diffuse rings. These diffuse rings are due to oil (innermost ring) around the crystal and ice (second ring) inside the crystal. The broad ice peak is located at the Q value of 2.03 Å-1 (d= 3.10 Å) at 80 K, confirming that HDA ice formed inside of the crystal by high pressure cryocooling. The HDA ice transformed into LDA ice, cubic ice and hexagonal ice upon crystal warming.

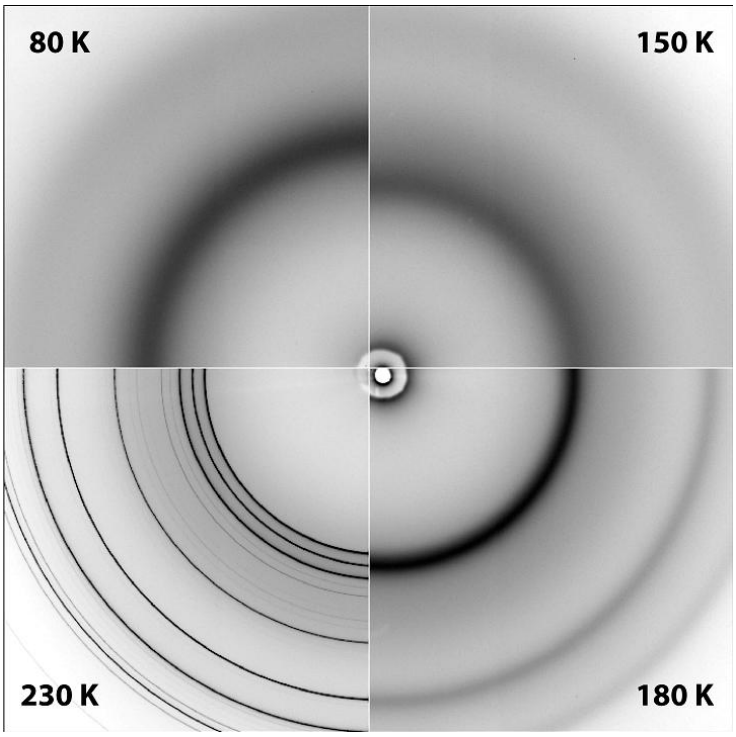

(a)

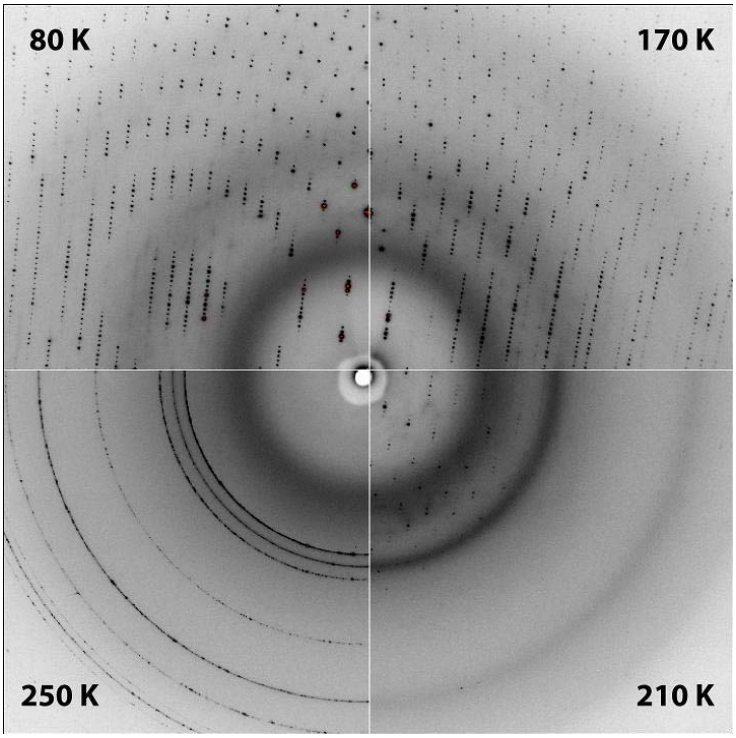

(b)

Figure 5.2. (a) X-ray diffraction intensity profiles of the high-pressure cryocooled crystallization solution upon warming. The profiles show the features characteristic of HDA ice in the 80 K and 130 K curves, with a broad peak located at around 2.1 Å-1 (*d* = 3.0 Å). A significant change in the diffraction has occurred by 140 K, indicative of a phase transition from HDA to LDA ice. Around 170 K, the sample starts to crystallize and transform into cubic ice and finally to hexagonal ice at 230 K. (b) Median filtered (to remove the sharp protein Bragg spots) x-ray diffraction intensity profiles of a high-pressure cryocooled thaumatin crystal upon warming. The scattering peak near 1.1 Å-1 (*d*= 5.7 Å) is due to oil coating the crystal. The second peak moves from 2.03 Å-1 (*d*= 3.10 Å) at 80 K to 1.72 Å-1 (*d*= 3.65 Å) at 170 K, indicating a transformation from HDA to LDA ice. The broad phase transition is indicative of confined water as opposed to the sharp transition seen for the bulk sample in (a).

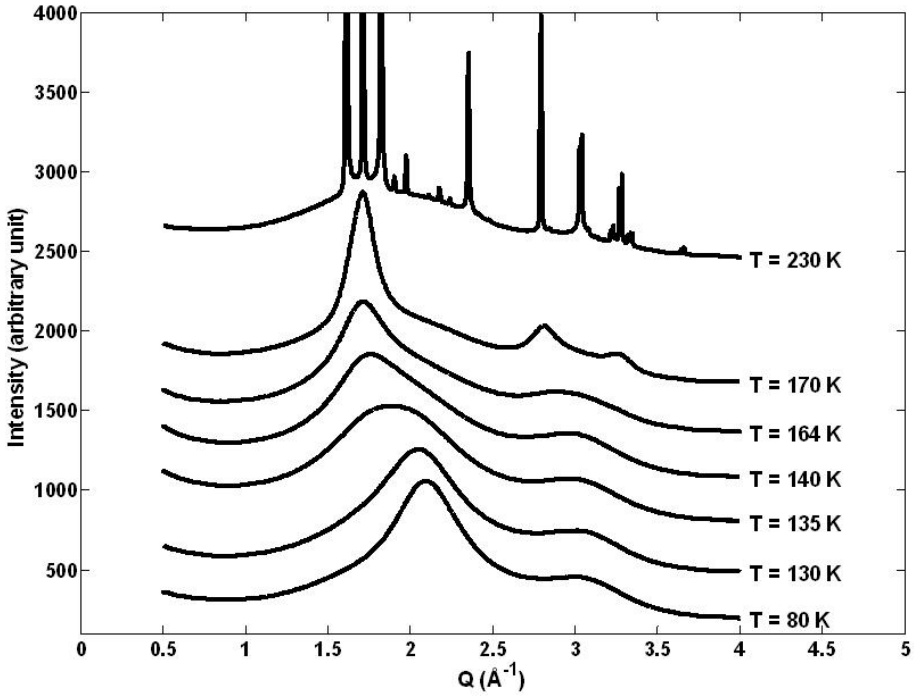
Intensity (arbitrary unit)
Q (Å^{-1})
T = 230 K
T = 170 K
T = 164 K
T = 140 K
T = 135 K
T = 130 K
T = 80 K

(a)

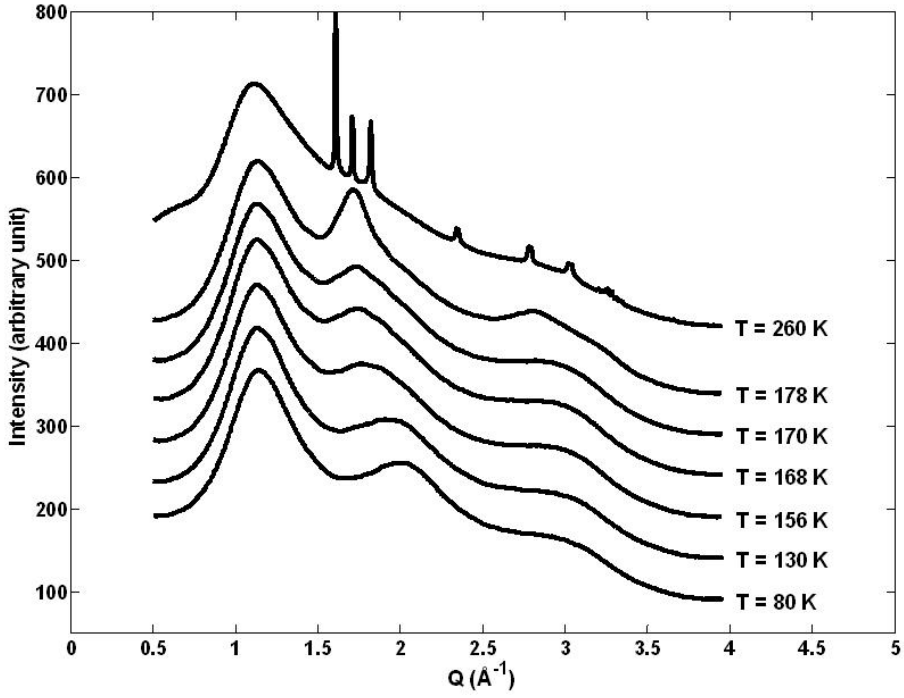
Intensity (arbitrary unit)
Q (Å^{-1})
T = 260 K
T = 178 K
T = 170 K
T = 168 K
T = 156 K
T = 130 K
T = 80 K

(b)

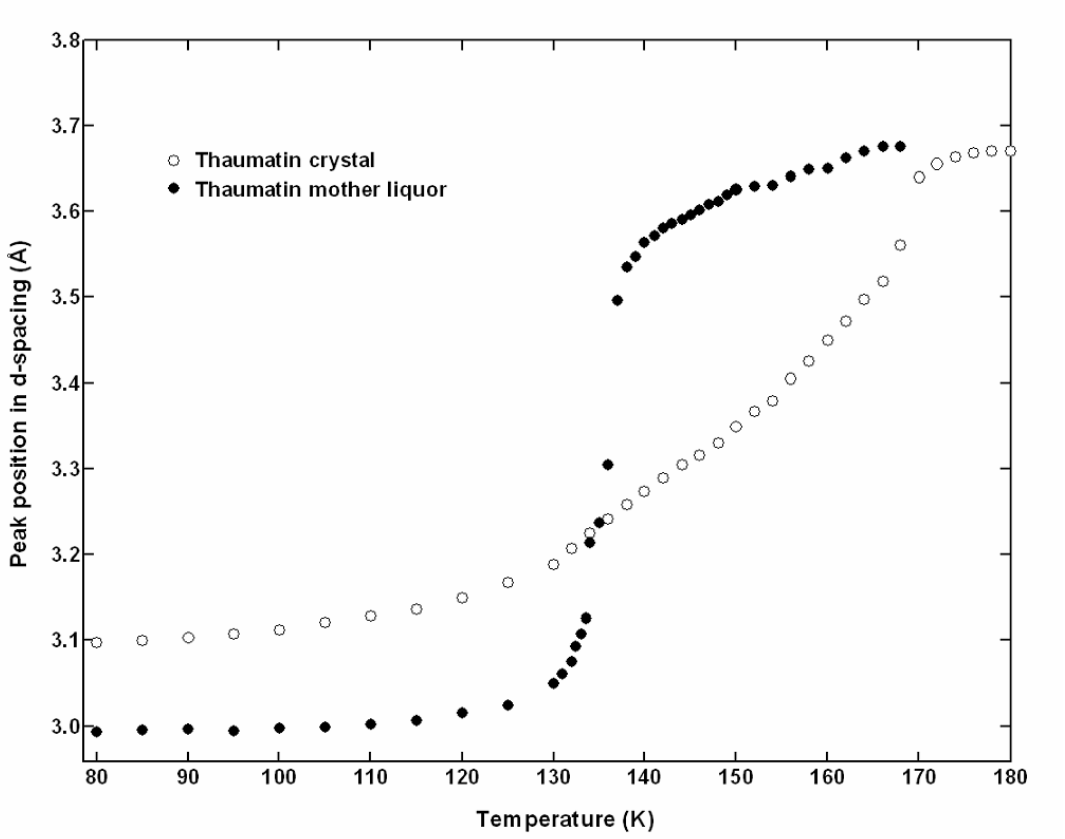

Figure 5.3. Ice peak position of the thaumatin crystallization solution and thaumatin crystal prepared by high-pressure cryocooling. The position of the scattering from the solution shows a dramatic shift between 130 K and 140 K, indicative of phase transition from HDA ice to LDA ice. Above 170 K, the solution has transformed to cubic ice. The scattering from water within the crystal is located at higher *d* at low temperatures and shows a wider phase transition between 130 K and 170 K. This implies that the water inside the crystal behaves differently than bulk water due to its local environment and confined geometry.

as that of HDA ice of pure water. Beyond ~ 140 K, the diffraction begins to exhibit the characteristic peaks of LDA ice located at around 1.71 $Å^{-1}$ (d = 3.67 Å), a value typical of LDA ice (Dowell & Rinfret, 1960), indicating that the phase transition from HDA ice to LDA ice occurred as observed in pure water (Mishima *et al*, 1984; Mishima *et al*., 1985).

As temperature increased further, additional ice phases emerged (Fig. 5.1(a) and Fig. 5.2(a)). Between 165 K and 170 K, somewhat sharper peaks began to appear in the distance ratio √3: √8: √11, indicative of cubic ice (Blackman & Lisgarten, 1957). These peaks are much broader than those typical of crystalline phases, indicating microcrystalline ice. A Debye-Shearer analysis of the peak widths suggests a crystallite size of 170 Å. The broad cubic ice lines became slightly sharper and eventually transformed to hexagonal ice around 210 K. Upon the phase transformation, the diffraction peaks became noticeably sharper with peak widths limited by the size of the x-ray beam. One can place a lower limit of 3000 Å on the domain size of the crystalline ice. Fig. 5.1(a) shows the representative diffraction patterns of each crystalline ice phase: cubic ice at 180 K and hexagonal ice at 230 K, respectively. Note that the peak scattering position of LDA ice at around 1.71 $Å^{-1}$ (d = 3.67 Å) is located at the position of the main crystalline diffraction peaks of cubic and hexagonal ice, consistent with the fact that crystalline ice and LDA ice have comparable densities (Ghormley & Hochanadel, 1971). The peak of the HDA ice scattering at 80 K in Fig. 5.1(a) is at a distinctly larger scattering angle. This indicates a smaller waterwater distance and, hence, a higher density.

5.3.2 High-pressure cryocooled protein crystals

Fig. 5.1(b) shows the diffraction images of the high-pressure cryocooled thaumatin crystal at 4 different temperatures: 80 K, 170 K, 210 K and 250 K. The

scattering underlying the Bragg diffraction is due to the ice within the crystal plus the oil surrounding the crystal and is shown in Fig. 5.2(b). Upon warming, the solvent inside the high pressure cryocooled crystal showed the characteristic diffraction peaks of all the ice phases observed in the bulk crystallization solution study. The position of the scattering peak due to the ice is plotted from 80 K to 180 K in Fig. 5.3. At 80 K, the ice peak was located at Q = 2.03 $Å^{-1}$ (d = 3.10 Å). This indicates an ice density well above that of LDA ice and near that of the HDA phase in bulk solution. A phase transition from HDA ice to LDA ice was observed between 130 K and 170 K. Note that the phase transition occurred over a wide temperature range, indicating that the scattering arises from water confined within the protein crystal unit cell or within small inclusions between crystalline mosaic blocks rather than from bulk water. One expects this confined water to behave differently than bulk water due to its local environment and confined geometry (Mayer, 1994). Above 170 K, cubic ice began to form. As with the bulk solution sample, the peak widths indicate small crystalline ice domains on the order of 160 Å in size. Note this domain size is on the order of the unit cell size of the protein (thaumatin space group of $P4_12_12$, having a= b= ~ 58 Å and c= ~ 150 Å). In addition to the cubic ice, there appears to be a weak amorphous scattering peak remaining under the cubic ice peak. Due to the presence of the larger oil scattering peak and the uncertainties in its line shape, however, it is not possible to give an accurate measure of the scattering intensity of this amorphous peak. As the temperature is increased further, hexagonal ice is formed with the ice domain size greater than 3000 Å, along with further reduction in the amorphous water scattering peak.

During crystal warming, we noticed that the quality of crystal diffraction from the protein was correlated with the ice phase of the water inside the crystal as seen in Fig 5.1(b). Upon transition from HDA ice to LDA ice, the resolution limit of crystal

diffraction slightly decreased and the crystal mosaicity increased by ~ 150 %. This result seems reasonable given that ice expands by ~ 24 % in volume during the phase transition from HDA (density of 1.17 g/cm^3) to LDA ice (density of 0.94 g/cm^3) which can lead to disruption of the crystal. Since the thaumatin crystal consists of ~ 55 % solvent, the simplest estimate would yield a roughly 13 % increase in the unit cell volume upon the formation of LDA ice. Interestingly, however, only a 2.5 % unit cell volume expansion was observed from 130 K to 170 K. Furthermore, in the temperature range of 80 K to 200 K, the unit cell volume was linear with temperature with little change in slope, even during the HDA to LDA ice phase transition. While this is less than the simple estimate, it is 5 times greater than the unit cell expansion observed for a crystal flash-frozen at room pressure then warmed over the same temperature range, indicating the effects of the high pressure cryocooling are being released in a continuous fashion as the crystal is warmed. Similar behavior has also been reported in protein crystals high-pressure frozen within liquid pentane (Urayama, 2001).

The estimate of 13% volume change assumes the ice retains the properties of bulk water and that all the water remains in the unit cell. The packing of water in the hydration shell around the protein is highly disrupted from the bulk state and will reduce the amount of water that undergoes the full volume change at the phase transition. Furthermore, the number of water molecules within the unit cell does not have to remain constant with temperature. As water is excluded from the unit cell, it can gather into inclusions between the mosaic blocks of the protein crystal. Changes in this inclusion neighborhood can affect the mosaicity without changing the volume of the unit cell. The total fraction of water in these inclusions is difficult to estimate, although we know from the broad phase transition that most of the water begins in highly confined surroundings. Furthermore, we know that the scattering from water in

the cubic and hexagonal ice phases comes from domains too large to fit within the unit cell of the protein. While the cubic phase domains are quite small, the ice domains have been refined to considerable size in the hexagonal phase. Each of these implies that considerable water migration is occurring within the crystal even at low temperatures.

Upon formation of crystalline cubic ice from LDA ice, the crystal diffraction from the protein became even more degraded with a continuous reduction in the resolution limit as the crystal warmed through the cubic ice region. Interestingly, the mosaic spread of the crystal is roughly the same as for the LDA ice phase. The protein crystal diffraction entirely disappeared upon the formation of hexagonal ice. We calculated that the total absorbed dose for the high pressure cryocooled crystal up to the formation of hexagonal ice is about 10^7 Gy, which is less than the Henderson dose limit of 2×10^7 Gy (Henderson, 1990), where crystals lose roughly half of its diffraction power. Furthermore, it was observed that crystal diffraction degraded by similar amounts during the crystalline ice formation for thaumatin crystals irradiated by considerably different X-ray doses. Therefore, we conclude that the crystal degradation is mostly due to the formation of crystalline ice, not radiation damage. This observation is somewhat unexpected based on the previously proposed mechanism for the crystal damage upon cooling involving the solvent volume expansion (Kriminski *et al.*, 2002; Juers & Matthews, 2004) because the volume expansion during the formation of cubic or hexagonal ice from LDA ice is negligible (Ghormley & Hochanadel, 1971). It is likely that water initially associated within the unit cell of the high-pressure cryocooled sample is expelled upon the formation of LDA ice and becomes refined into sequentially larger ice domains included among the protein crystal mosaic blocks upon the formation of cubic and hexagonal ice, which seems to lead a drastic degradation of the crystal diffraction. The microcrystal size of

the crystalline ice (about 160 Å for cubic ice and greater than 3000 Å for hexagonal ice) supports this hypothesis. However, revealing the detailed mechanism of crystal disruption during the growth of crystalline ice domain is beyond the scope of this paper.

The formation of HDA ice within other protein crystal systems by high pressure cryocooling was also investigated. The underlying diffuse scattering profiles from glucose isomerase and elastase crystals are shown in Fig. 5.4(a) and Fig. 5.4(b), respectively. Phase transitions from HDA ice to LDA ice, cubic ice and hexagonal ice were observed in these protein crystals as well. Interestingly, the phase transition from HDA to LDA ice was found to be sharper for glucose isomerase than for thaumatin. At 80 K, the glucose isomerase crystal showed an ice scattering peak at 2.04 $Å^{-1}$ (d = 3.08 Å) whereas the elastase crystal showed scattering at 1.84 $Å^{-1}$ (d = 3.41 Å). While the glucose isomerase is near that of the bulk HDA value, the value from elastase indicates a density intermediate to HDA and LDA ice phases. The elastase has the lowest solvent content of any of the crystals studied. One would expect that the water in this crystal to be the most constrained, and hence, the most perturbed from the bulk HDA value. While the formation of HDA ice appears to be a general feature of high pressure cryocooling, the degree to which the water is free to arrange seems to be a function of the solvent content. As in the case of the high pressure cryocooled thaumatin crystal, the crystal diffraction of glucose isomerase and elastase was slightly degraded during the phase transition from HDA ice to LDA ice and drastically deteriorated upon the formation of cubic and hexagonal ice. This observation confirms that the quality of crystal diffraction is closely related with the ice phase inside protein crystal, independent of protein.

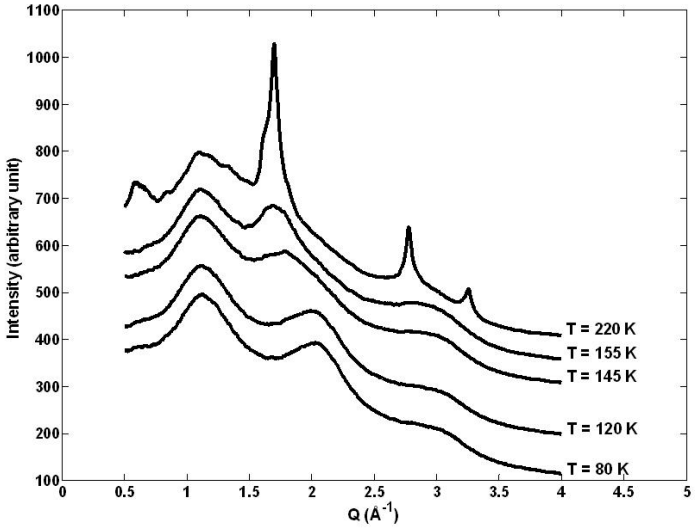

(a)

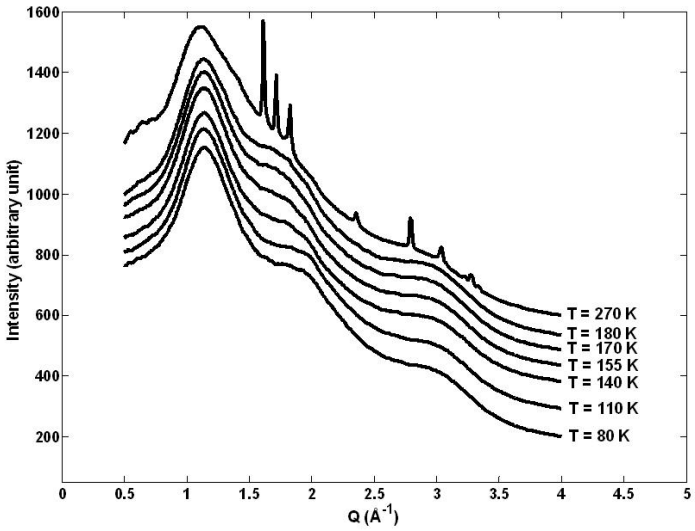

(b)

Figure 5.4. Median-filtered x-ray diffraction profiles of (a) glucose isomerase and (b) elastase crystals upon warming. The scattering peak near 1.1 Å-1 (d= 5.7 Å) is due to oil surrounding the crystal. The second peak is due to water within the crystal and shows a position indicative of HDA ice at low temperatures. Both peaks shift to lower Q at higher temperature, indicating a transition to LDA ice.

5.4 Conclusions

It has been demonstrated that high pressure cryocooling induces HDA ice both in a bulk solution used in protein crystallization and in the water included within protein crystals. X-ray diffraction studies clearly showed features characteristic of amorphous ice at densities near those of HDA ice at low temperatures. Upon warming of the high pressure cryocooled crystallization solution, phase transitions from HDA ice to LDA ice, cubic ice and hexagonal ice could be clearly observed. The same phase transitions were observed in the high-pressure cryocooled protein crystals, which was closely related with the diffraction quality of the crystals. This observation supports the proposed mechanism of high pressure cryocooling.

Our results may have implications for the biological applications of the method and its technical modification for high throughput crystallography. As suggested by Kim *et al*. (2007), high pressure cryocooling in capillaries opens novel routes for high throughput protein crystallography. High pressure cryocooling at up to 200 MPa of pure water in capillaries always resulted in crystalline ice (data not shown). In the case of the thaumatin crystallization solution, the salts in the solution appear sufficient to prevent ice crystal formation upon high pressure cryocooling. Similarly, relatively low concentrations of glycerol and other common cryoprotectants were successfully high pressure cryocooled in capillaries. This suggests a straight-forward strategy for the preparation of high pressure cryocooled protein crystals in capillaries: Identify minimum concentrations of relatively innocuous cryoprotectant solutions that yield HDA when high pressure cryocooled in capillaries. These may then be added to the mother liquor used to crystallize proteins. In this way one is assured that the protein crystals may be high pressure cryocooled in their crystallization solutions.

REFERENCES

Albright, R. A., Vazquez Ibar, J.-L., Kim, C. U., Gruner, S. M. & Morais Cabral, J. H. (2006). *Cell*, **126**, 1147-1159.

Blackman, M. & Lisgarten, N. D. (1957). *Proc. R. Soc. London*, Ser. A **239**, 93.

Bosio, L., Johari G. P. & Teixeira J. (1986), *Phys. Rev. Lett*. **56**, 460-463.

Carrell, H. L., Glusker, J. P., Burger, V., Manfre, F., Tritsch, D. & Biellmann, J.-F. (1989). *Proc. Natl Acad. Sci*. USA, **86**, 4440-4444.

Dowell, L. G. & Rinfret, A. P. (1960). *Nature* **188**, 1144 -1148.

Garman, E. F. & Schneider, T. R. (1997). *J. Appl. Cryst*. **30**, 211-237.

Garman, E. F. & Owen, R. L. (2006). *Acta Cryst*. D**62**, 32-47.

Ghormley, J. A. & Hochanadel, C. J. (1971). *Science*, **171**, 62-64.

Henderson, R. (1990). *Proc. R. Soc. London*, B**241**, 6–8.

Juers, D. H. & Matthews, B. W. (2004). *Q. Rev. Biophys.* **37**, 1-15.

Kanno, H. & Angell, C. A. (1977). *J. Phys. Chem*.. **81**, 2639-2643.

Kanno, H. (1987). *J. Phys. Chem*. **91**, 1967-1971.

Kim, C. U., Kapfer, R. & Gruner, S. M. (2005). *Acta Cryst*. D**61**, 881-890.

Kim, C. U., Hao, Q. & Gruner, S. M. (2006). *Acta Cryst*. D**62**, 687-694.

Kim, C. U., Hao, Q. & Gruner, S. M. (2007). *Acta Cryst*. D**63**, 653-659.

Klotz, S., Strässle, Th., Nelmes, R. J., Loveday, J. S., Hamel, G., Rousse, G., Canny, B., Chervin, J. C. & Saitta, A. M. (2005). *Phys. Rev. Lett*. **94**, 025506.

Ko, T.-P., Day, J., Greenwood, A. & McPherson, A. (1994). *Acta Cryst*. D**50**, 813-825.

Kriminski, S., Caylor, C. L., Nonato, M. C., Finkelstein, K. D. & Thorne, R. E. (2002). *Acta Cryst.* D**58**, 459-471.

Mayer, E. (1994). Hydrogen Bonded Networks, edited by M.-C. Bellissent-Funel & J. C. Dore, pp. 355-372. Dordrecht: Kluwer Academic Publishers.

Mishima, O., Calvert, L. D. & Whalley, E. (1984). *Nature (London)*, **310**, 393-395.

Mishima, O. & Stanley, H. E. (1998). *Nature (London)*, **396**, 329-335.

Mishima, O., Calvert, L. D. & Whalley, E. (1985). *Nature* 314, 76-78.

Otwinowski, Z. & Minor,W. (1997). *Methods Enzymol*. **276**, 307–326.

Ravelli, R. B. & Garman, E. F. (2006). *Curr. Opin. Struct. Biol.* **16**, 624-629.

Shotton, D. M., Hartley, B. S., Camerman, N., Hofman, T., Nyburg, S. C. & Rao, L. (1968). *J. Mol. Biol.* **32**, 155-156.

Tulk, C. A., Benmore, C. J., Urquidi, J., Klug, D. D., Neuefeind, J., Tomberli, B. & Egelstaff, P. A. (2002). *Science* **297**, 1320-1323.

Urayama, P. (2001). PhD thesis, Cornell University, USA.

CHAPTER SIX
APPLICATIONS & CONCLUSIONS

6.1 Challenging cases in high pressure cryocooling

Although high pressure cryocooling has been successfully applied to several different kinds of macromolecular crystals, there have been cases where high pressure cryocooling resulted in failure. These failures seem to be caused by one or more of the following reasons: (A) crystal disruption due to macromolecular conformational change by high pressure, (B) crystal damage by the oil around crystals and (C) unsuccessful sample vitrification by high pressure cryocooling. Examples follow.

An example of reason (A) is human deoxy-hemoglobin. It was repeatedly observed that the high pressure cryocooling of deoxy-hemoglobin (T state) crystals resulted in a deteriorated crystal diffraction. Interestingly, CO-hemoglobin (R state) crystals diffracted better after high pressure cryocooling. As in the case of deoxy-hemoglobin, if pressure itself damages a macromolecular crystal, high pressure cryocooling cannot be simply applied for the purpose of crystal cryoprotection and diffraction improvement. However, it should be emphasized that this case is scientifically very intriguing. Because the deteriorated crystal diffraction includes the pressure effects on the molecule, a careful data collection and data analysis may lead us to a deeper understanding of effect of high pressure on the protein. For example, by applying relatively low pressures (5 MPa to 50 MPa), where the crystal diffraction is not severely deteriorated, it may be possible to capture the intermediate states between the R and T states of hemoglobin. Furthermore, a careful data analysis on the diffuse scattering in the deoxy-hemoglobin crystal diffraction may reveal the protein's molecular dynamics under pressure. Also, it is well-known by spectroscopic studies of hemoglobin in solution [Unno *et al*., 1990] that pressure biases the R-T transition. The

change in the conformational state of the protein may be involved in the crystal damage.

The crystal of Kv1.2 K+ ion channel (Long *et al*., 2005) is an example for (B). It was observed that the membrane crystals began to dissolve in NVH oil in about 10 - 20 min. To avoid this problem, it is always wise to test crystal stability in several mineral oils, including paratone-N, paraffin oil and NVH oil. If the crystals are unstable in all types of mineral oils, then the crystals may have to be prepared in a plastic capillary for high pressure cryocooling, where the oil coating can be avoided, as described in chapter 4.

When it comes to the reason (C), it has been observed that the crystals having a very high solvent content (higher than 70 %) sometimes produced crystalline ice rings after high pressure cryocooling treatment. It means that high pressure alone may not be enough to suppress crystalline ice in some cases. This observation is consistent with the fact that pure water in a capillary could not be vitrified by the high pressure cryocooling as described in chapter 4. In order to successfully high pressure cryocool these challenging examples, the method need to be optimized as suggested in the following section.

6.2 Optimization of high pressure cryocooling

The success rate of high pressure cryocooling is affected by several experimental parameters. One of the most important parameters would be the freezing rate under pressure: a higher freezing rate is generally favorable. Although we have estimated that the freezing rate under pressure in our apparatus might be comparable to that for the room pressure flash cooling, it is very difficult to directly measure the freezing rate of a protein crystal under high pressure. Therefore, the experimental freezing rate of crystal samples in our high pressure cryocooling method is still not well known. More

importantly, even if the freezing rate under pressure were known, it is not trivial to control the freezing rate in our current high pressure cryocooling apparatus.

Another efficient way to increase the success rate of high pressure cryocooling is to combine the method with the conventional chemical crystal cryoprotection. Although finding an optimized concentration of cryoprotectants is generally tedious and challenging, adding low concentrations of cryoprotectants (~ 5 – 10 %) may be straightforward and innocuous for most of the macromolecular crystals. Therefore, if a crystal has a high solvent content, it would be beneficial to add small amount of cryoprotectants to crystals prior to the application of high pressure cryocooling. Another advantage of adding chemical cryoprotectants is that it may reduce the volume-reduction related damage which may arise when a large volume of water in a crystal transforms to HDA ice, which otherwise contracts too much, therefore results in crystal collapse.

To find a lowest concentration required to vitrify pure water by high pressure cryocooling, a preliminary experiment was carried out with a plastic polycarbonate capillary (I.D. = 300 μm, O.D. = 900 μm). Deionized pure water was mixed with various concentrations of glycerol (v/v) and ~ 2 μl of the mixed solution was inserted into the plastic capillary. It was observed that at least 23~ 24 % of glycerol concentration was required to optically vitrify the sample by the conventional room pressure flash cryocooling (i.e., directly plunging into a liquid nitrogen bath). On the other hand, the minimum glycerol concentration for the sample vitrification by high pressure cryocooling was reduced to be about 10 %. Because 10 % glycerol was sufficient to vitrify pure water, this result suggests that crystallization solutions and macromolecular crystals can be vitrified by high pressure cryocooling in the plastic capillary with the glycerol concentration of ~ 10 % or less. By extension, it is likely that simply adding a small amount of various cryoprotectants would be sufficient to

vitrify samples under high pressure. The precise measurement of the lowest concentration for each cryoprotectant would be very useful for challenging crystal samples. It would also be worth measuring the lowest required concentration of a cryoprotectant as a function of the applied high pressure. This information would be useful for the successful high pressure cryocooling of a crystal sample, whose diffraction quality is strongly influenced on the applied high pressures.

6.3 Application for protein structural studies

Our studies on the protein structures indicate that the structural perturbation by the high pressure cryocooling is generally small, in the order of a few tenths of an angstrom. However, since it is known that pressure strongly affects the function of many proteins, this small structural change may be crucial to understand protein activity. Therefore, the high pressure cryocooling has great potential to be a very useful tool for delicate structural studies, which may elucidate the pressure effects on proteins.

For the purpose, it should be answered whether the pressure effects can be successfully extracted from the high pressure cryocooled structures or not. The results in chapter 5 suggest that the pressure effects are locked inside a high pressure cryocooled protein crystal as long as HDA ice is retained. However, it should be noticed that the solved structure contains the effects of both the high pressure and low temperature.

An experiment can be proposed to clarify if the pressure effects can be separated from the temperature effects or not. In the experiment, a protein crystal is first prepared by the high pressure cryocooling and its diffraction data set (data set A) is collected at 100 K, where high pressure effects are still captured with HDA ice. Then the crystal is slowly warmed to 170 K, where pressure effects are released along with

the phase transition from HDA to LDA ice. After that, the crystal is cooled back to 100 K and another diffraction data set (data set B) is collected. By comparing the structures from data set A and B, it may be possible to subtract the structural deviation induced by merely high pressure captured during the high pressure cryocooling. This subtracted structural information needs to be compared with the one on the same protein which are prepared by the pressurization at room temperature. This assumes that the crystals still diffract well after warming to 170 K and recooling to 100 K. Whether or not, the case would have to be investigated.

For this study, T4 lysozyme studied by Collins *et al* (2007) is a potential candidate protein. In the study, T4 lysozyme crystals were pressurized in a Beryllium cell up to 200 MPa and its diffraction data sets were collected under pressure at room temperature. The comparison of the structures obtained by high pressure cryocooling and Beryllium cell pressurization might make it clear if the pressure effects on protein structures captured by the high pressure cryocooling are successfully decoupled from the low temperature effects.

6.4 Advantages of gas high pressure cryocooling and its implications to other fields

Our experiences on the high pressure cryocooling indicate that there are some variations between the liquid and gas pressurization. It was reported in Kundrot & Richards (1987) that lysozyme crystals cracked when they were pressurized in mother liquor at 30 - 40 MPa. In order to increase the crystal stability under high pressures up to 150 MPa, the precipitant (NaCl) concentration had to be increased from 0.8 M to 1.3 M. On the other hand, it was observed that the lysozyme crystals which had a lower salt concentration (0.7 M) were stable and could be successfully pressurized without crystal cracking under helium high pressure cryocooling. The same trend was

observed in citrine, a yellow fluorescence protein that Buz Barstow has been studying. When citrine was pressurized in mother liquor at room temperature in a beryllium cell, it was observed that the crystal cracked, resulting in poor crystal diffraction (personal communication with Buz Barstow and Elizabeth). On the other hand, the citrine crystals prepared by helium high pressure cryocooling diffracted well without signs of crystal cracking even up to 500 MPa. Although it is unclear what factors make the difference between liquid and gas pressurization, it is obvious that the gas pressurization is beneficial for crystal cryopreservation.

Another potential advantage of helium high pressure cryocooling is as follows: A considerable amount of helium dissolves in water at high pressure. The partial pressure of helium in water at 100 MPa is approximately 0.7 MPa (Wiebe & Gaddy, 1935). It may be the case that that the dissolved hydrophobic atoms in pure water may suppress the nucleation or growth of the crystalline ice by perturbing the hydrogen bonding network. If this hypothesis is valid, helium pressurization may reduce the concentrations of a cryoprotectant required for the sample vitrification in the liquid high pressure cryocooling. This remains to be verified and explored.

By extension, it will be very interesting to see if the helium high pressure cryocooling can be more beneficial in preparing samples for cryo-electron microscopy than conventional liquid high pressure freezing technique (Dahl & Staehelin, 1989; Costello, 2006; McDonald & Auer, 2006). Studies of helium high pressure cryocooling for cryopreservations of living cells and tissues, such as spermatozoa, oocytes and embryonic stem cells, would be an exciting research area.

6.5 Conclusions

In this dissertation, it has been demonstrated that high pressure cryocooling is a useful tool for macromolecular crystallography. Further optimization and development

of the technique has great promise for structure determination of macromolecules and for high throughput macromolecular crystallography. The technique can be an important tool for studies of macromolecules at extreme condition, i.e., at high pressure. Finally, high pressure cryocooling has great potential for cryo-EM and tissue cryopreservation. The successful extension of the technique to these new fields suggests many exciting biophysical experiments.

REFERENCES

Collins, M.D., Quillin, M. L., Hummer, G., Matthews, B. W. & Gruner, S. M. (2007). *J. Mol. Biol*. **367**, 752-763.

Costello, M. J. (2006). *Ultrastruct Pathol.* **30**, 361-371.

Dahl, R & Staehelin, L. A. (1989). *J Electron Microsc Tech*. **13**, 165-174.

Kundrot, C. E. & Richards, F. M. (1987). *J. Mol. Biol.* **193**, 157–170.

Long, S. B., Campbell, E. B. & MacKinnon R. (2005). *Science* **309**, 897-903.

McDonald, K. L. & Auer, M. (2006). *Biotechniques*. **41**, 137, 139, 141 passim.

Unno, M., Ishimori, K & Morishima, I. (1990). *Biochemistry* **29**, 10199-10205.

Wiebe, R. & Gaddy, V. L. (1935). *J. Am. Chem. Soc.* **57**, 847.